2000-06

A boundary-layer model of thermocapillary flow in a cold corner

Huber, Michael R.

Monterey, California. Naval Postgraduate School

NAVAL POSTGRADUATE SCHOOL
Monterey, California

DISSERTATION

A BOUNDARY-LAYER MODEL OF THERMOCAPILLARY FLOW IN A COLD CORNER

by

Michael R. Huber

June 2000

Dissertation Supervisor: David Canright

Approved for public release; distribution is unlimited.

REPORT DOCUMENTATION PAGE

Form Approved OMB No. 0704-0188

1. AGENCY USE ONLY (*Leave blank*)	2. REPORT DATE	3. REPORT TYPE AND DATES COVERED
	June, 2000	Doctoral Dissertation

4. TITLE AND SUBTITLE A BOUNDARY-LAYER MODEL OF THERMOCAPILLARY FLOW IN A COLD CORNER

5. FUNDING NUMBERS

6. AUTHORS Huber, Michael R.

7. PERFORMING ORGANIZATION NAME(S) AND ADDRESS(ES)
Naval Postgraduate School
Monterey CA 93943-5000

8. PERFORMING ORGANIZATION REPORT NUMBER

9. SPONSORING/MONITORING AGENCY NAME(S) AND ADDRESS(ES)

10. SPONSORING/MONITORING AGENCY REPORT NUMBER

11. SUPPLEMENTARY NOTES The views expressed in this thesis are those of the author and do not reflect the official policy or position of the Department of Defense or the U.S. Government.

12a. DISTRIBUTION/AVAILABILITY STATEMENT
Approved for public release; distribution is unlimited.

12b. DISTRIBUTION CODE

13. ABSTRACT(*maximum 200 words*)

A pool of liquid with a horizontal free surface is bounded on one side by a vertical solid wall, which is maintained at a cold temperature relative to the core flow region. Strong temperature gradients along the surface give rise to surface tension variations (thermocapillary stress), which drives flow. Thin viscous boundary layers form along the surface and wall. A boundary-layer model is designed which captures the dynamics of the cold corner, applicable for any Marangoni number M and Prandtl number P in the convective inertial regime. Analytical expressions for the velocity and boundary-layer thicknesses are developed, which allow accurate prediction of the flow field. The core flow region (outside the viscous boundary layers) is treated as irrotational flow and Laplace's equation is solved using both a Green's function approach and a complex variables approach in the quarter-plane. The flow along the wall is treated as a plane wall jet.

The two-dimensional unsteady heat equation is solved using an alternating direction implicit method. Results show that the flow into the corner is strong enough to contain the thermal field, compressing the isotherms along the wall after steady-state is reached. Additionally, a uniform stream function prediction is developed, by matching the inner and outer flows, giving a relatively accurate depiction of the flow.

14. SUBJECT TERMS Thermocapillary flow, Marangoni number, Prandtl number, Boundary layer

15. NUMBER OF PAGES 135

16. PRICE CODE

17. SECURITY CLASSIFICATION OF REPORT	18. SECURITY CLASSIFICATION OF THIS PAGE	19. SECURITY CLASSIFICATION OF ABSTRACT	20. LIMITATION OF ABSTRACT
Unclassified	Unclassified	Unclassified	UL

NSN 7540-01-280-5500

Standard Form 298 (Rev. 2-89)
Prescribed by ANSI Std. 239-18 298-102

THIS PAGE INTENTIONALLY LEFT BLANK

Approved for public release; distribution is unlimited

A BOUNDARY-LAYER MODEL OF THERMOCAPILLARY FLOW IN A COLD CORNER

Michael R. Huber
Major, Corps of Engineers, United States Army
Bachelor of Science Degree, Loyola College, 1982
Master of Science in Engineering Degree, The Johns Hopkins University, 1984
Master of Science Degree, The Naval Postgraduate School, 1993

Submitted in partial fulfillment of the
requirements for the degree of

DOCTOR OF PHILOSOPHY IN APPLIED MATHEMATICS

from the

NAVAL POSTGRADUATE SCHOOL
June 2000

Author: [redacted]
Michael R. Huber

Approved by:

[redacted]
David Canright
Associate Professor of Mathematics
Dissertation Supervisor

[redacted]
C. L. Frenzen
Associate Professor of Mathematics
Dissertation Committee Chairman

[redacted]
Guillermo Owen
Professor of Mathematics

[redacted]
Indranath Dutta
Associate Professor of Mechanical Engineering

[redacted]
Wei Kang
Associate Professor of Mathematics

Approved by: [redacted]
Michael A. Morgan, Chairman, Department of Mathematics

Approved by: [redacted]
Anthony P. Ciavarelli, Associate Provost for Instruction

THIS PAGE INTENTIONALLY LEFT BLANK

ABSTRACT

A pool of liquid with a horizontal free surface is bounded on one side by a vertical solid wall, which is maintained at a cold temperature relative to the core flow region. Strong temperature gradients along the surface give rise to surface tension variations (thermocapillary stress), which drives flow. Thin viscous boundary layers form along the surface and wall. A boundary-layer model is designed which captures the dynamics of the cold corner, applicable for any Marangoni number M and Prandtl number P in the convective inertial regime.

Analytical expressions for the velocity and boundary-layer thicknesses are developed, which allow accurate prediction of the flow field. The core flow region (outside the viscous boundary layers) is treated as irrotational flow and Laplace's equation is solved using both a Green's function approach and a complex variables approach in the quarter-plane. The flow along the wall is treated as a plane wall jet.

The two-dimensional unsteady heat equation is solved using an alternating direction implicit method. Results show that the flow into the corner is strong enough to contain the thermal field, compressing the isotherms along the wall after steady-state is reached. Additionally, a uniform stream function prediction is developed, by matching the inner and outer flows, giving a relatively accurate depiction of the flow.

THIS PAGE INTENTIONALLY LEFT BLANK

DISCLAIMER

The computer programs in Appendix E are supplied on an "as is" basis, with no warrantees of any kind. The author bears no responsibility for any consequences of using these programs.

THIS PAGE INTENTIONALLY LEFT BLANK

TABLE OF CONTENTS

LIST OF FIGURES

THIS PAGE INTENTIONALLY LEFT BLANK

SYMBOL LIST

English letter symbols

$a(x)$	coefficient function of velocity profile used in approximate methods
A	aspect ratio (ratio of depth to width)
c_p	specific heat at constant pressure
d	length scale
f, $f(\eta)$	velocity profile function used in approximate methods
F	flux of exterior momentum flux
$F(z)$	complex potential
$G(\vec{x}, \vec{x_0})$	Green's function used in solving Laplace's equation
k	thermal conductivity
l	horizontal length of free surface viscous boundary layer
L	vertical length of rigid cold wall viscous boundary layer
M	Marangoni number
p	pressure (force per unit area)
P	Prandtl number
Q	heat flux
R	Reynolds number
t	nondimensional boundary-layer temperature
T	temperature
T_c	temperature of cold wall
T_h	temperature of core flow region
$\vec{u}$, $\vec{U}$	velocity vector
u	horizontal component of velocity in the free surface boundary layer
U	horizontal component of velocity in the core (free-stream) region
U	velocity scaling used in approximate method
v	vertical component of velocity in the free surface boundary layer
V	vertical component of velocity in the core (free-stream) region
V	velocity scaling used in approximate method
x	horizontal cartesian coordinate; distance from cold wall
y	vertical cartesian coordinate; distance from free surface
Y_0	vertical offset used in uniform flow
z	normal cartesian coordinate (into the paper being positive)
z	complex variable $z = x\hat{i} + y\hat{j}$

Greek letter symbols

γ	positive constant scale for surface tension
δ, $\delta(x)$	thickness of free surface viscous boundary layer
δ_1	displacement thickness of a boundary layer
δ_2	momentum thickness of a boundary layer
Δ	thickness of rigid cold wall viscous boundary layer
ε	constant used in determination of surface boundary layer thickness
η	similarity parameter used in approximate method
κ	thermal diffusivity
λ	shape factor of velocity profile in boundary layer
Λ	shape factor of velocity profile in boundary layer
μ	dynamic or absolute viscosity
ν	kinematic viscosity
ξ	downstream coordinate
ρ	fluid density (mass per unit volume)
σ	mean surface tension
σ_c	mean surface tension at the cold wall
τ	shear stress (force per unit area)
τ_0	skin friction, or shear stress evaluated at the free surface
ϕ	velocity potential
ψ	stream function
ω	vorticity

ACKNOWLEDGMENTS

ALL IN GOOD TIME THERE WILL COME A CLIMAX WHICH WILL LIFT ONE TO THE HEIGHTS, BUT FIRST A FOUNDATION MUST BE LAID, BROAD, DEEP AND SOLID... — *Winfred Ernest Garrison*

First of all, I owe many thanks to my advisor, Professor David Canright, for offering the reading courses, for keeping my focus in the right direction, and for the constant encouragement, mentoring, and even the *GO* lessons. I value his judgment and advice tremendously.

Next, I thank my doctoral committee, Professors Chris Frenzen (chairman), Indranath Dutta, Alan Fox, Wei Kang, and Guillermo Owen. Their advice and coursework helped me to complete this program. I also appreciate the help of the other professors and staff of the Mathematics Department, who were never too busy to answer a question or offer pertinent advice, especially Professors Craig Rasmussen, Clyde Scandrett, Carlos Borges, and Beny Neta.

Thanks to Professor Stephen Morris, University of California, Berkeley, for helpful discussions concerning the research.

Thanks to Irma Fink and Susan Miller at the Dudley Knox Library Inter-Library Loan section for their exceptional efforts in obtaining the rare references that I requested.

I thank my colleague LTC Phil Beaver for his sponsorship and words of encouragement. I also wish to thank COL Chris Arney and COL Gary Krahn of the United States Military Academy for giving me the opportunity to attend the Naval Postgraduate School and study for this degree.

I dedicate this dissertation to my wife, Teresa, and to my children, Nick, Kirstin, and Steffi. Their patience, sacrifices, support, and understanding were genuine and fully appreciated.

Any errors contained in this dissertation are solely my responsibility.

THIS PAGE INTENTIONALLY LEFT BLANK

I. INTRODUCTION

ONE MUST LEARN BY DOING THE THING; FOR THOUGH YOU THINK YOU KNOW IT, YOU HAVE NO CERTAINTY UNTIL YOU TRY. — *Sophocles*

The purpose of this research is to examine the velocity and temperature fields in a two-dimensional fluid flow problem embodying a thermocapillary feedback mechanism. The structure of the velocity and thermal fields will change, based upon whether the heat transfer is conductive or convective in nature, as well as whether inertia plays a dominant role or not. One of the governing parameters, the Marangoni number M, measures the importance of thermal convection relative to thermal diffusion. A second governing parameter, the Prandtl number P, gives the ratio of viscous to thermal diffusion for the material. In this research, we study the effects of a high Marangoni number, indicative of convective heat transfer, combined with a low Prandtl number, indicative of inertial flow. The most important regime for materials processing is that regime where thermal convection is dominant and the flow is inertial, with viscous boundary layers forming. This dissertation outlines a model for this important regime, with the goal of predicting the velocity and thermal fields which will occur.

Chapter II gives a background on the importance of this research and possible physical applications, followed by a survey of related work in thermocapillary flows by previous researchers. In our literature search, we did not find any other researchers who had studied the cold corner region with large Marangoni numbers and small Prandtl numbers. A representative velocity vector field (using Canright's numerical data [Ref. 1]), which serves as a guiding principle for our assumptions, is shown at the chapter's end.

Chapter III formulates the problem mathematically and gives all assumptions and a thorough scaling analysis. It is important to obtain a summary of theoretical

scales of the thermal length, viscous thickness and length, and surface velocity. Although the scalings derived are different than those previously published, they agree better with the published numerical data.

Chapter IV contains the conservation equations and how they affect each of four regions within the cold corner. Using the appropriate scaling factors, once the velocity is determined in one region, it is matched to that in all neighboring regions.

Chapter V discusses the approximation methods employed to describe the velocity profiles in the viscous boundary layers and core flow region. Two methods from the literature were modified to predict velocity behavior along the free surface and the rigid wall. The modification along the free surface introduces a new technique to predict the velocity from a free surface with a thermal gradient boundary condition and no non-slip condition through a viscous boundary layer into the core flow region. The flow from the corner down the rigid wall is treated as a plane wall jet. An expression for the temperature solution in the domain is then determined.

Chapter VI shows the numerical results obtained from various techniques. The alternating direction implicit (ADI) method is the basis for solving the two-dimensional unsteady heat equation. Various tests against problems with known solutions are performed to validate the code, followed by the solution of the present problem. The scheme is also modified to update the velocity profile during the time-step iterations to model the physical feedback. A modification to a wall jet profile is incorporated into the scheme. The results are presented as a uniform velocity field, combining the boundary layers and core flow, for comparison with previous numerical results.

Chapter VII gives the conclusions and a few discussions associated with them. Chapter VIII lists selected areas of possible future research.

Appendices A, C, and D show work which attempted to improve the model in the surface and wall boundary layers. We ultimately did not use these methods (for reasons given in each appendix), but we felt we should include them. Appendix B

gives a derivation of an important and often-used constant. The numerical codes are listed in Appendix E.

THIS PAGE INTENTIONALLY LEFT BLANK

II. BACKGROUND

WE DO NOT SET OUT ON THIS PATH OF ENQUIRY JUST AS ADVENTURERS. WE FOLLOW THE FOOTSTEPS OF SUCH GIANTS AS EULER AND LAGRANGE, WHO ALSO WONDERED WHERE IT LED, AND PRANDTL, WHO WALKED IT AND FOUND THE ANSWER. — *David Pnueli and Chaim Gutfinger*

A. MOTIVATION

Materials processing often involves the melting and solidification of the material. Several practical processes, such as welding, containerless processing of materials, float-zone purification, and Czochralski crystal growth, involve a pool of molten metal with a free surface [Ref. 1]. The purest large-volume silicon single crystals are being commercially grown by floating-zone melting [Ref. 2, 3]. Inevitably, there exists a fluid flow within this molten region.

When heavier fluid is on top of lighter fluid, the weight of the heavier, denser fluid makes it tend to sink, while the lighter, less dense fluid tends to rise. This sets up motion within the fluid known as *buoyancy-driven convection* or *natural convection*, also known as *Rayleigh convection.* One of the most commercially important materials processes that are subject to buoyancy-driven convection is that of crystal growth. A major advantage of performing experiments in a space laboratory is being able to minimize gravitational effects and therefore reduce buoyancy-driven convection [Ref. 4]. There are important reasons to avoid having buoyancy-driven convection during crystal growth. Convection can alter trace element distribution in the resulting crystal and may degrade its quality. Many other physical processes can greatly affect crystal growth, such as radiation heat transfer and surface tension driven flow. Typically, all of these processes happen at the same time on Earth. Buoyancy-driven convection is the predominant fluid flow on Earth, since the gravitational forces are stronger than surface tension forces [Ref. 5]. In microgravity, however, buoyancy-driven convection

is reduced by a factor of 10^{-6}, allowing thermocapillary flow to predominate [Ref. 6]. The near elimination of buoyancy-driven convection has promise for materials processing in space, a low-gravity environment. For such applications, it is essential that thermocapillary flow be studied in detail, without the influence of buoyancy-driven convection.

Convection in the molten metal is typically vigorous and can greatly affect the results of the materials process, including the size and shape of the melt pool, the heat transfer, the mixing of solutes, and the final microstructure of the product [Ref. 7]. The buoyancy force can also play a role in establishing the fluid flow. When the dimension of the molten region is small, as in the case of welding and laser materials processing, the buoyancy force becomes unimportant. Beyond the molten region, the absorbed heat is conducted into the substrate and transported away by the motion of the substrate. Surface tension gradient driven flow has been identified to be responsible for ripple formation in the weld [Ref. 7]. When buoyancy, electromagnetic, and surface tension forces were considered in a numerical solution for the convective heat transfer within the molten pool during arc welding, it was found that the surface tension gradient is the dominant factor in many cases [Ref. 8]. Other authors have verified the dominance of thermocapillary flows in materials processing [Ref. 9, 10, 11].

In addition to the heat transport due to the motion of the substrate, there is also the convection due to the fluid flow within the molten pool. Depending on the type of heat source, the fluid flow may be caused by the surface tension gradient [Ref. 7]. When a free surface is heated by a concentrated heat source, the resulting temperature distribution causes a nonuniform surface tension distribution [Ref. 12]. Typically, surface tension is a decreasing function of temperature. Thus, the fluid layer on the surface experiences a shear force pulling the fluid from the warmer central area of the molten pool to the cooler outer region. Since the bulk fluids are viscous, they are dragged along; bulk fluid motion then results from the temperature gradients

along the interface. This phenomenon is known as *thermocapillary* or *Marangoni convection.* The Marangoni effect is associated with movement in a fluid interface, caused by local variations in interfacial tension that are caused in turn by differences in composition or temperature. A drying coat of paint is a simple example where local variations of surface tension set into intricate motion an entire liquid film [Ref. 13]. In the case of the float-zone crystal growth process, a melt zone is moved slowly through a cylindrical, vertically-oriented crystal. The liquid zone between the polycrystalline incoming material and the single crystal that is grown is stabilized by surface tension [Ref. 3]. The temperature distribution varies along the interface of the liquid and gas, which leads to surface-tension gradients, creating a considerable thermal Marangoni flow driving force, or thermocapillary convection.

B. PREVIOUS RESEARCH

There have been many theoretical studies of thermocapillary flows, both numerical and analytical. Ostrach [Ref. 5] reviewed of some of the analytical studies relevant to low-gravity conditions. Some fluid flows, such as buoyancy-driven and g-jitter convection, are acceleration dependent, while others, such as surface-gradient, thermoacoustic, and phase-change convection are independent of the acceleration field. There are forces in a space laboratory which act on experiments in a gravity-like manner. G-jitter (or residual acceleration [Ref. 4]) is the term used when combining these gravity-like forces together. Thermoacoustic convection refers to the pressure-driven convection that results when a confined compressible fluid is heated rapidly; the name describes the sonic character of induced pressure waves. When a fluid solidifies or vaporizes, a change in density associated with the phase transition may also cause a change in volume. A shrinkage occurring during solidification may result in a volume reduction, further resulting in the flow of a liquid toward the solidifying surface. This is known as phase-change convection. Davis [Ref. 9] reviewed thermocapillary instabilities in planar layers. He gave details about studies concerning Marangoni and

hydrothermal instabilities involving the one-layer system geometry. Kuhlmann [Ref. 3] gave a thorough reference list of many processes subject to Marangoni effects, such as the motion of droplets and bubbles, the stabilization of thin films, evaporation and boiling, welding, electrokinetic effects, and crystal growth techniques, to name just a few. Hondros [Ref. 14] offered several examples of phenomena attributed to Marangoni convection relevant to modern technology, such as in hot salt corrosion in turbine blades, the drying of silicon wafers in the electronics industry, and micro-pools produced by plasma disruptions in a prospective thermonuclear fusion reactor.

Cowley and Davis [Ref. 15] analyzed the two-dimensional thermocapillary flow near a hot wall for vigorous, viscous flow (large Marangoni and Prandtl numbers). The fluid flows up a wall, which is kept at a constant high temperature within a finite distance from the free surface, and then turns and flows along the free surface. This is called the hot corner problem. The finite distance determines the length scale. The parameter regimes studied either have no viscous boundary layers or have viscous boundary layers that are much thicker than the thermal layers. The solution they find is the thermocapillary analog of buoyancy-driven convection in a quarter plane described by Roberts [Ref. 16].

Sen and Davis [Ref. 11] studied steady flow in two-dimensional slots, which are differentially heated, inducing the surface-tension gradient along the interface. They studied the case with the aspect ratio A (ratio of the depth to the width) approaching zero. The ends of the slots are maintained at a fixed temperature difference. Flows on the interfaces are directed from the hot towards the cold end and return along a region removed from the interfaces. The pressure is higher at the cold end and the interface thus bulges near the cold end and is constricted near the hot end. The leading-order outer solutions having parallel flow and flat interfaces continue to be the leading order outer approximations even when conditions on the Reynolds number and Marangoni number are relaxed from $O(A)$.

Zebib, Homsy, and Meiburg [Ref. 17] conducted numerical studies of flow in

a two-dimensional square cavity with one hot wall and one cold wall. They showed that for moderate to small Prandtl numbers, the cold corner has the stronger effect on both the flow and the heat transfer of the cavity. Their results at finite Marangoni number in a finite pool suggest that experimentally observed instabilities may be associated with the rapid turning flows and high vorticity in the cold wall region. Another important finding in this paper was the determination of the scalings for the thermocapillary boundary-layer thickness on the free surface and on the rigid wall. Their results confirmed those of Ostrach [Ref. 5, 24].

Ohring and Lugt [Ref. 10] studied the onset of Marangoni convection in a float zone of liquid silicon from a state at rest in the absence of gravity, with high Marangoni numbers. They found the existence of a critical Marangoni number at which the steady flow field becomes unstable and changes to an axisymmetric oscillatory field. Also, they concluded that a deformable free surface, even a very small one on the order of 10^{-4} cm, is necessary for the onset of instability. The velocity at the free surface is extremely high. The temperature field oscillates and causes uneven heat transfer at the walls, which is not desirable for silicon crystal growth.

Chan, Mazumder, and Chen [Ref. 18] developed a three-dimensional model of the fluid flow and heat transfer of a laser melted pool. Using a perturbation solution, they found that the presence of the thermocapillary convection causes the physics of the problem to change from conduction to convection dominated. The pool geometry then changes dramatically, resulting in up to a 150 percent increase in the aspect ratio as compared to the pure conduction case. In another paper [Ref. 12], they presented solutions of thermocapillary convection in the central region of a nonuniformly heated surface for the asymptotic limits of very high and very small Prandtl numbers. The model is valid when the viscous and thermal boundary layers are small compared to the depth and width of the melt pool. In addition, the intensity of the thermocapillary convection and the boundary-layer thicknesses in the stagnation region depend primarily on the curvature of the heat flux distribution. In a comprehensive report,

Mazumder, Chen, Chan, and Zehr [Ref. 7] developed a three-dimensional perturbation model for surface tension driven flow with a flat surface which predicted velocity field, temperature field, effect of trace elements and a self-consistent prediction of the pool shape and cooling rate. The three-dimensional problem is represented by two sets of two-dimensional governing equations. It is found that a particle recirculates many, many times in the molten pool before it resolidifies, showing that the solute can be well mixed. Regarding free surface deformation, thermocapillarity drives the surface fluid radially outward at extremely high velocities. These high velocities displace more mass from the surface region than can be replaced by the recirculating flow, which thus causes a depression. The displaced mass builds up at a solid/liquid interface, which causes the surface to bulge upward where the liquid turns downward into the molten pool. Experiments were performed to examine the validity of the theoretical models, and both theoretical models and experiments predict the same trend in aspect ratio: the aspect ratio increases with laser power.

Masud, Kamotani, and Ostrach [Ref. 19] experimentally investigated high Prandtl number flow in a half-zone configuration. Specifically, they studied the effects of buoyancy and column shape on the onset conditions of oscillations. There is a minimum critical Marangoni number, below which no oscillations appear. They speculated that both convection and a dimensionless surface deformation parameter must be taken into account together to explain the oscillation mechanism. Kamotani and Ostrach [Ref. 20] then conducted a theoretical analysis of the half-zone configuration. They concluded that free surface deformation plays an important role in oscillatory thermocapillary flow in high Prandtl number fluids. The deformation induces a change in the surface flow and alters the driving force in the hot corner. This then triggers oscillation cycles in which the flow at the surface alternates between fast and slow. Finally, they derive a surface deformation parameter by scaling analysis, alluded to in their earlier paper [Ref. 19]. The scaling for the core velocity found by Cowley and Davis was confirmed for several high Prandtl number flows in

the Kamotani and Ostrach paper. Kuhlmann [Ref. 3] points out that this behavior suggests that for high Prandtl numbers and Reynolds numbers that are not too large, the hot corner can determine the scalings of the surface temperature and the core velocity.

As stated earlier, the Marangoni effect is caused by a jump in shear stress across the interface which balances the surface-tension gradient along the interface. Scriven and Sternling [Ref. 13] give a short but interesting historical review of this phenomenon, including causes and resistance to surface movements. Batischev, Kuznetsov, and Pukhnachov [Ref. 21] investigated the Marangoni effect, dividing the cases involving the thermocapillary effect into classes for which the motion shows similarity, but they mainly considered the case where the Reynolds number is high and the Prandtl number is of order unity. They define the Marangoni boundary layer as a surface layer where intensive convection quickly decays in depth. The fluid in the Marangoni boundary layer differs in a qualitative sense from that in the Prandtl classic boundary layer, which is initiated by an external fluid flow due to the no-slip condition at a rigid wall. The Marangoni boundary layer is initiated by forces acting on a free surface and subsequently initiates the fluid flow inside the entire volume [Ref. 21]. Pukhnachov [Ref. 22] systemized the similarity solutions of the Navier-Stokes equations in another paper, distinguishing and justifying boundary-layer asymptotics when the viscosity goes to zero, describing the construction of nonstationary boundary layers on a liquid free surface and providing descriptions of asymptotic solutions in several cases.

Napolitano [Ref. 23] also studied Marangoni boundary layers between two immiscible fluids in the plane, restricting analysis to the case with a Prandtl number of order unity. Three necessary conditions for the existence of a Marangoni boundary layer were given. First, the region must be sufficiently far away from solid boundaries; second, surface driving forces must be of the same order of magnitude as viscous forces; and third, the thickness of the region must be much smaller than the thickness of the

interface between the two immiscible fluids. The influence of the flow field on the dynamic interface's shape was also calculated in terms of characteristic length ratios. Napolitano [Ref. 23] and Ostrach [Ref. 24] separately derived the scaling law of low Prandtl number inertial flow in a free surface layer.

Strani, Piva, and Graziani [Ref. 25] also studied thermocapillary convection in a rectangular cavity. They found an asymptotic solution in the limiting case where the aspect ratio goes to zero. For increasing values of the aspect ratio, the motion is confined in a region near the free surface. As with other investigators, Strani, Piva, and Graziani concluded that any surface deformation seems to have a negligible influence on the qualitative aspects of the flow field. The solution method employed, although independently derived, turns out to be a special case of the method proposed by Sen and Davis [Ref. 11]. Regarding the cold corner, they concluded that the larger surface temperature gradient near the cold wall develops a local increase in the driving force. This leads to a complex stagnation flow field, with significant acceleration near the wall, positive until the maximum velocity is reached, then negative to meet the boundary condition of zero velocity. A boundary-layer-type flow grows downward along the cold wall, starting from the stagnation point at the surface.

Canright [Ref. 1] introduced study of the dynamics restricted solely to the cold corner region, where the flow along the free surface toward the cold wall compresses the thermal gradient, thereby enhancing the flow in a sort of positive feedback. This is known as the cold corner problem. This feedback results in small local length scales and high velocities near the corner. Numerical results are consistent with scaling analysis. In particular, for fully convective flow, the corner behavior is locally determined. Scaling limits for the Reynolds and Marangoni numbers are given for four different regimes: conductive-viscous, convective-viscous, conductive-inertial, and convective-inertial. Canright concluded that increasing the global Marangoni number decreases the local length scale to give an effective local Marangoni number of unity [Ref. 1]. In contrast to the hot corner problem posed by Cowley and Davis,

Canright found that no thermal boundary layer forms when the Prandtl number is large. This is due to the surface forcing being limited to a relatively concentrated region in the cold corner, while for the hot corner, the forcing is distributed over a broad region, since the thermal variations in the horizontal direction are extended by convection. Canright also validated his scales by comparing his results with those of Zebib, Homsy, and Meiburg [Ref. 17], who showed that the temperature gradient on the free surface can vary considerably within a small distance from either of the hot and cold walls. Canright's scaling of the boundary layers were also published in a treatment of the cold corner by Kuhlmann [Ref. 3].

Huber [Ref. 26] extended the study of the cold corner problem, examining the problem numerically for different low Marangoni numbers using a Green's function flow representation for the viscous case, in the limit as the Reynolds number approaches zero. One advantage of the Green's function is that the flow can still be represented over the entire quarter plane, so that there is no artificial recirculation due to imposed artificial boundaries. The Green's function approach does not require flow boundary conditions at the computational domain's boundaries. The flow is assumed isothermal across the boundary and is recirculating, decaying with distance.

Canright's work in 1994 concentrated on the Marangoni number dependence of the cold corner problem. A representative velocity vector field (using Canright's numerical data) is shown in Figure 1. This work reconsiders the problem, refining the Prandtl number dependence of the variables. All the graphs shown in [Ref. 1] are correct, but we will now show that the theoretical scales in the cold corner for the convective inertial case are different than those previously published, in terms of the Prandtl number dependence. Canright's numerical results reflect a boundary-layer structure that we assume throughout this work and use as a guiding principle. The task is to solve for the flow and/or heat in each region and match it to that in neighboring regions in order to predict future flow conditions. The scalings derived herein are different than those published by Canright; nonetheless, they agree better

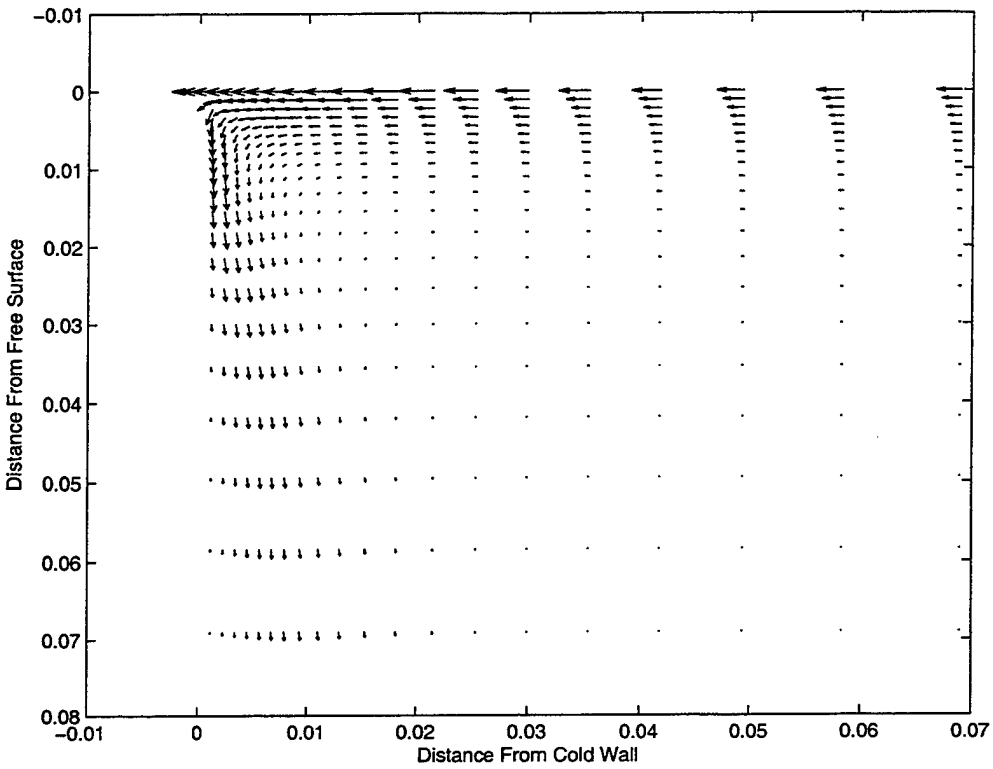

Figure 1. Velocity Vector Field

with his numerical data.

III. PROBLEM STATEMENT

MOST OF THE FUNDAMENTAL IDEAS OF SCIENCE ARE ESSENTIALLY SIMPLE, AND MAY, AS A RULE, BE EXPRESSED IN LANGUAGE COMPREHENSIBLE TO EVERYONE. —*Albert Einstein*

A. MATHEMATICAL FORMULATION OF THE PROBLEM

A pool of incompressible Newtonian fluid is bounded on the left by a vertical solid wall, maintained at a cold temperature T_c, while the undisturbed fluid far from the cold corner is at the hot ambient temperature T_h of the core flow (see Figure 2 below).

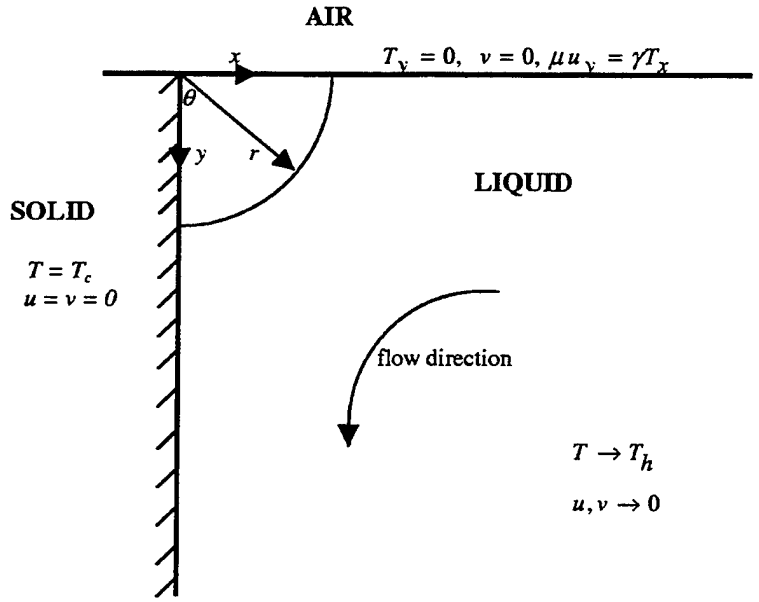

Figure 2. Problem Formulation

Above the horizontal free surface of the liquid is an inviscid, nonconducting gas. Surface tension is assumed strong enough to keep the free surface flat (small

Capillary number), but with surface tension variations due to a linear dependence on temperature. The resulting flow is assumed to be two-dimensional and steady.

The equations governing the thermocapillary convection in the cold corner are the conservation of mass, the conservation of momentum, and the conservation of energy equations:

$$\nabla \cdot \vec{u} = 0 \tag{III.1}$$

$$\rho \vec{u} \cdot \nabla \vec{u} = -\nabla p + \mu \nabla^2 \vec{u} \tag{III.2}$$

$$\rho c_p \vec{u} \cdot \nabla T = k \nabla^2 T \tag{III.3}$$

with the boundary conditions that at $y = 0$, $T_y = 0$, $v = 0$, and $\mu u_y = \gamma T_x$. At $x = 0$, $T = T_c$, and $u = v = 0$. As $(x, y) \to \infty$, $T \to T_h$, and $u, v \to 0$.

In these equations, $\vec{u}$ is the velocity vector with components u and v in the x (horizontally rightward) and y (vertically downward) directions, p is the pressure, T is the temperature, ρ is the density, μ is the viscosity, c_p is the specific heat, k is the thermal conductivity, and the surface tension is assumed to be of the form $\sigma = \sigma_c - \gamma (T - T_c)$, with γ a positive constant. The boundary conditions specify that the cold wall is isothermal with fluid obeying the no-slip condition, and the flat free surface is thermally insulated, with thermocapillary forcing.

To nondimensionalize the equations, a heat flux scale of Q and a temperature scale (relative to the cold temperature) of $\Delta T \equiv T_h - T_c$ are introduced. Thermal conduction gives the length scale of $d \equiv Q / k \Delta T$, the thermocapillary coupling gives the velocity scale $u \equiv \gamma \Delta T / \mu$, and the viscous pressure scale is $p \equiv \mu u / d = k \gamma (\Delta T)^2 / Q$. In summary, the nondimensional scales are:

$$x \equiv (Q / k \Delta T) x' \tag{III.4}$$

$$u \equiv (\gamma \Delta T / \mu) u' \tag{III.5}$$

$$p \equiv (k \gamma (\Delta T)^2 / Q) p' \tag{III.6}$$

$$T' \equiv (T - T_h) / (T_c - T_h) \tag{III.7}$$

which implies $T \equiv T_h - (\Delta T)\, T'$, where the variables with primes are dimensionless. Begin with the conservation of energy equation, which can be rewritten as

$$\vec{u} \cdot \nabla T = \kappa \nabla^2 T \tag{III.8}$$

where κ is the thermal diffusivity. Substituting the dimensionless scales into this form of the energy equation yields

$$\frac{\gamma Q}{\mu \kappa k}[\vec{u'} \cdot \nabla T'] = \nabla^2 T' \tag{III.9}$$

Dropping the primes and defining a dimensionless parameter M, the Marangoni number, as $M \equiv \frac{\gamma Q}{\mu \kappa k}$, the nondimensional conservation of energy equation becomes

$$M\ (\vec{u} \cdot \nabla T) = \nabla^2 T. \tag{III.10}$$

Next, the conservation of momentum equation may be rewritten as:

$$\vec{u} \cdot \nabla \vec{u} = -\frac{1}{\rho} \nabla p + \nu \nabla^2 \vec{u} \tag{III.11}$$

where ν is the kinematic viscosity. Substituting the dimensionless scales into the momentum equation yields

$$\frac{\gamma Q}{\mu \nu k} \left[\vec{u'} \cdot \nabla \vec{u'}\right] = -\nabla p' + \nabla^2 \vec{u'}. \tag{III.12}$$

Dropping the primes and defining a dimensionless parameter R, the Reynolds number, as $R \equiv \frac{\gamma Q}{\mu \nu k}$, the nondimensional conservation of momentum equation becomes

$$R\ (\vec{u} \cdot \nabla \vec{u}) = -\nabla p + \nabla^2 \vec{u}. \tag{III.13}$$

Situations in which the Reynolds number is small are called slow viscous flows, because the viscous forces arising from shearing motions of the fluid predominate over inertial forces associated with the acceleration or deceleration of the fluid particles. The thermocapillary boundary condition is also nondimensionalized by substituting (III.4) and (III.5) into $\mu\, u_y = \gamma\, T_x$, obtaining (dimensionless) $u_y = T_x$. In addition, the mass conservation equation, $\nabla \cdot \vec{u} = 0$, remains unchanged after nondimensionalization.

The ratio of the Marangoni number and the Reynolds number gives the nondimensional Prandtl number

$$P \equiv \nu/\kappa = M/R. \tag{III.14}$$

We want to analyze the system for large values of the Marangoni number, M, which measures the importance of thermal convection relative to thermal diffusion. For large enough M, convection becomes important and the strong surface flow towards the cold wall compresses the thermal gradient along the surface, which in turn strengthens the local driving force for the flow. Also, since $R = M/P$, the effect of making $R \gg 1$ is to make the inertia force much greater than the viscous force, so that inertia and pressure forces are dominant, except along the rigid wall and free surface, where viscous boundary layers are formed.

Near the surface, vorticity must be taken into account. Vorticity is the curl of the velocity, $\vec{\omega} \equiv \nabla \times \vec{u}$, which (in two-dimensional flow) reduces to the one component along the axis normal to the x-y plane, yielding $\omega = v_x - u_y$. Thus, eliminating pressure by taking the curl of the momentum equation, the following equation is obtained:

$$\vec{u} \cdot \nabla\vec{\omega} = \nu \nabla^2\vec{\omega} \tag{III.15}$$

This equation is referred to as the *vorticity transport,* or *vorticity transfer, equation.* It states that the substantive variation of vorticity, which consists of the local and convective terms, is equal to the rate of diffusion of vorticity through friction. In our non-dimensionalized form, the vorticity equation becomes $R\,(\vec{u} \cdot \nabla\vec{\omega}) = \nabla^2\vec{\omega}$. At the surface, the thermocapillary condition gives $\omega = T_x$, which comes from $\omega = v_x - u_y$, and the fact that $v_x = 0$ at the surface.

B. ASSUMPTIONS AND SCALING ANALYSIS

A few assumptions concerning the scaling analysis are made. First, a high Reynolds number, R, implies that inertial forces are dominant, outside the viscous boundary layers. Second, a high Marangoni Number, M, implies that thermal con-

vection is important. Third, a low Prandtl Number, P, implies that there exists a low ratio of viscous to thermal diffusion and the region is inertial.

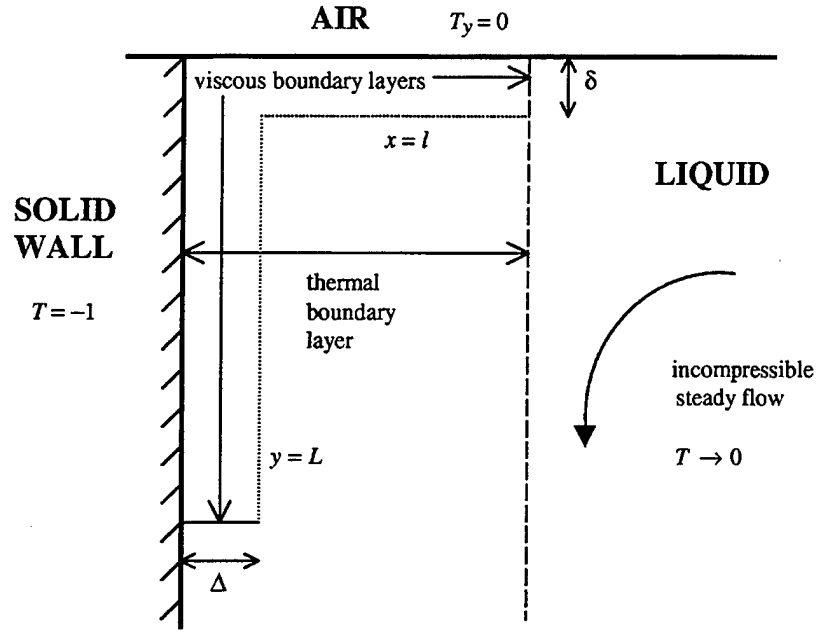

Figure 3. Scaling of the Domain

Recall that we are assuming the structure based on Canright's numerical data. Figure 3 shows a schematic of the corner with viscous boundary layers along the free surface and rigid wall. The depth and width of the pool are large compared to all local length scales, so the pool appears semi-infinite both horizontally and vertically.

To distinguish the various notations, a hat ($\hat{}$) will denote the original nondimensionalized variables. Capital letters will denote the core scaling, and lowercase letters will denote boundary-layer variables that do not have the same scaling as the core variables.

Let the core velocity scale be denoted by U. Let the characteristic velocity scale along the free surface be u. We assume that surface thermal variations will be confined to a region with a horizontal characteristic length scale of l. We also assume that vorticity will be confined to thin viscous boundary layers. The flow in the core region is dominated by inertia. (This "defines" the core region as the area

with negligible vorticity). The solid boundary acts as a source of vorticity, which is then diffused away by viscosity and convected downstream with the fluid.

Along the surface, the boundary layer results from thermocapillary stresses and will have thickness δ. Along the wall, the boundary layer results from the no-slip condition and will have thickness Δ. Thus, δ is the vertical length scale of velocity shear along the free surface, and Δ is the horizontal length scale of velocity shear along the rigid wall.

In case of large M, convection is important and the rapid surface flow into the cold corner compresses the thermal gradient along the surface, reducing l. The length l will be reduced to the point that thermal diffusion away from the rigid wall will balance the strong convection toward the wall.

In case of large R, inertia is dominant and there will be two viscous boundary layers of thickness δ and Δ ($\sim \delta$) along the surface and rigid wall, respectively. The effect of increasing the Reynolds number to values large compared with unity is to confine the vorticity diffused from the rigid wall to a layer of relatively small thickness. As R increases, δ, the thickness of the boundary layer, decreases. Convection contains the vorticity inside the boundary layer.

Surface tension variations are due to an assumed linear dependence on the temperature. For the boundary layer along the free surface, the thermocapillary stress condition at the surface gives $u_y \sim T_x$. This provides the relation $\frac{u}{\delta} \sim \frac{1}{l}$, or, solving for the surface velocity in the horizontal direction, $u \sim \frac{\delta}{l}$. The continuity condition $\nabla \cdot \vec{u} = 0$ gives the relation $u_x \sim v_y$. Therefore, $\frac{u}{l} \sim \frac{v}{\delta}$, or $v \sim \frac{u\delta}{l}$, which gives $v \sim \left(\frac{\delta}{l}\right)^2$ as the vertical component of the velocity near the surface.

At the boundary-layer edge/core region interface, normal velocities must match, so $v \sim V$, and continuity requires that $V_y \sim U_x$. Thus $V_y \sim \frac{u\delta}{l^2} \sim U_x \sim \frac{U}{l}$, which gives the relation $\frac{U}{u} \sim \frac{\delta}{l}$.

Next, a check of the dominant balance of terms is required. In the vorticity equation, $R\left(\frac{u}{l^2} + \frac{u}{l^2}\right) \sim \frac{1}{l^3} + \frac{1}{l\delta^2}$. Ignore $\frac{1}{l^3}$ as too small, since $l \gg \delta$. This implies

that $R\frac{u}{l^2} \sim \frac{1}{l\delta^2}$, or that $R\frac{u\delta^2}{l} \sim 1$. Therefore, this gives an expression for u in terms of the Reynolds number, $u \sim \frac{l}{\delta^2}\frac{1}{R}$, or $u \sim \frac{l}{\delta^2}\frac{P}{M}$.

Similarly, in the energy equation applied to the core region, $MUT_x \sim T_{xx}$ (this dominant balance will be described in detail later; for now, assume T_y and T_{yy} scale comparably to T_x and T_{xx} in the core flow region). Thus, $MUT_x \sim M\frac{U}{l} \sim T_{xx} \sim \frac{1}{l^2}$, so that $M\frac{u\delta}{l^2} \sim \frac{1}{l^2}$, which yields another relationship for the surface velocity, $u \sim \frac{1}{\delta M}$.

We assume that the wall boundary layer is passive, fed by the mass flux from the surface layer (due to conservation of mass). We can derive its scales by using the mass flux, continuity and vorticity equations. Conservation of mass implies that the velocity out of the corner is the same as that into the corner ($v \sim u$). The momentum equation gives $R\left(Uv_x + vv_Y\right) = v_{xx} + v_{YY}$, and continuity gives $U_x \sim v_Y$. This means $\frac{U}{\Delta} \sim \frac{v}{L}$, or $v \sim \frac{UL}{\Delta}$. Substituting, $\frac{M}{P}\left(U\frac{UL}{\Delta^2} + \frac{UL}{\Delta}\frac{UL}{\Delta L}\right) \sim \frac{UL}{\Delta^3} + \frac{UL}{\Delta L^2}$. $\frac{UL}{\Delta^3} \gg \frac{UL}{\Delta L^2}$, leaving $\Delta \sim M^{-1}PU^{-1}$ and $L \sim v\Delta U^{-1}$.

To obtain scales for the lengths and velocity, use the three relationships for the free surface horizontal velocity scaling: $u \sim \frac{1}{\delta M} \sim \frac{\delta}{l} \sim \frac{l}{\delta^2}\frac{P}{M}$. Solving for the horizontal boundary layer length l, $l \sim \delta^2 M \sim \frac{\delta}{P}$, which implies that $\delta \sim \frac{1}{MP}$. Thus, $l \sim \frac{1}{MP^2}$, $u \sim P$, and $U \sim P^2$. Further, $\Delta \sim \frac{1}{MP} \sim \delta$ and $L \sim \frac{1}{MP^2} \sim l$.

To summarize, using the boundary condition at the free surface gives a starting point for the scalings and dominant balance. It is important to obtain relations for the thermal length scale l, the viscous thickness δ, the surface velocity u, and the core velocity U scales in the cold corner, in terms of the dimensionless parameters M and P. These scalings are

$$\begin{aligned} \delta &\sim M^{-1}P^{-1}, \\ l &\sim M^{-1}P^{-2}, \\ u &\sim P, \\ U &\sim P^2. \end{aligned}$$

These scalings are consistent with the numerical results obtained by Canright in his 1994 work [Ref. 1].

IV. THE COLD CORNER REGIONS

IT IS NOT KNOWLEDGE, BUT THE ACT OF LEARNING, NOT POSSESSION, BUT THE ACT OF GETTING THERE, WHICH GRANTS THE GREATEST ENJOYMENT. —*Carl Friedrich Gauss*

A. OVERVIEW

The flow into the corner is assumed to be convective and inertial, due to the large Marangoni number and small Prandtl number ($M \gg 1, P \ll 1$), governed by the system of equations

$$R\left(\vec{\hat{u}} \cdot \nabla \vec{\hat{u}}\right) = \nabla^2 \vec{\hat{u}} \tag{IV.1}$$

$$\nabla \cdot \vec{\hat{u}} = 0 \tag{IV.2}$$

$$M\left(\vec{\hat{u}} \cdot \nabla \hat{T}\right) = \nabla^2 \hat{T} \tag{IV.3}$$

The cold corner is divided into four regions: an outer core region away from the surface and cold wall where the flow is inviscid and relatively simple; an inner viscous boundary layer along the liquid free surface; an inner viscous boundary layer along the wall/liquid interface; and a thermal layer overlapping the viscous layers and the core flow. A representative velocity vector field (using Canright's numerical data) was shown in Figure 1 in Chapter II. The task is to solve for the flow and/or heat in each region and match it to that in neighboring regions in order to predict future flow conditions. The scaling factors are $\delta \sim \Delta \sim M^{-1}P^{-1}$, $l \sim L \sim M^{-1}P^{-2}$, $u \sim P$, and $U \sim P^2$. In the core flow region, let the horizontal and vertical components of the velocity be designated by capital letters. The governing equations in each region will be examined, using the appropriate nondimensionalized scalings.

B. VISCOUS SURFACE BOUNDARY LAYER

A viscous boundary layer forms along the surface, with thickness δ and length l. The scalings used in this region are $\hat{u} = P\,u$, $\hat{v} = P^2 V$, $\hat{x} = M^{-1}P^{-2}\,X$, $\hat{y} = M^{-1}P^{-1}\,y$, $\hat{T} = T + \cdots$, and $\hat{p} = M\,P^3 p$. The pressure scales with the dominant term in the core flow. The momentum equation in the x-direction can be written as

$$u\,u_X + V\,u_y = -P^2\,p_X + P^2\,u_{XX} + u_{yy}, \tag{IV.4}$$

where to leading order we can neglect the terms of order P^2. The boundary conditions at $y = 0$ give $u_y = T_X$ and $V = 0$. The continuity equation becomes

$$u_X + V_y = 0. \tag{IV.5}$$

From the momentum equation in the y-direction, the pressure change in the y-direction is negligible through the boundary layer, indicating that the pressure is effectively constant throughout the layer for each X value. Mathematically, $p_X \gg p_y$. It is assumed then that the pressure distribution in the boundary layer is imposed by the core flow pressure gradient just outside the boundary layer. In Ludwig Prandtl's words, "the pressure distribution will be impressed on the transition layer by the free fluid" [Ref. 27]. Also, the velocity in the free surface boundary layer is continuous with the core velocity U.

The energy equation in the surface viscous boundary layer is derived using a boundary-layer expansion for $\hat{T}$ and will be given later.

C. VISCOUS WALL BOUNDARY LAYER

A viscous boundary layer forms along the wall, with thickness Δ and length L. This viscous boundary layer is different from the surface viscous boundary layer in that there is a no-slip condition at the wall. The scalings used in this region are $\hat{u} = P^2\,U$, $\hat{v} = P\,v$, $\hat{x} = M^{-1}P^{-1}\,x$, $\hat{y} = M^{-1}P^{-2}\,Y$, $\hat{T} = T + \cdots$, and $\hat{p} = M\,P^3\,p$. The momentum equation in the y-direction can be written as

$$U\,v_x + v\,v_Y = -P^2\,p_Y + v_{xx} + P^2\,v_{YY}. \tag{IV.6}$$

where again terms of order P^2 can be neglected to leading order. The no-slip condition at the rigid wall gives $u = v = 0$ at $x = 0$. Similarly, the continuity equation becomes

$$U_x + v_Y = 0. \tag{IV.7}$$

The energy equation for the viscous boundary layer on the wall is

$$U T_x + v T_Y = P^{-1} T_{xx} + P T_{YY} \tag{IV.8}$$

with the boundary condition at $x = 0$ of

$$T = -1 \tag{IV.9}$$

The $P T_{YY}$ term is neglected as small. The T_{xx} term must therefore be small enough to balance the equation. Thus, there is no need to solve the energy equation in this region, as the temperature is basically constant across the wall's viscous layer. Also, due to the conditions of high Marangoni number coupled with low Prandtl number, the larger thermal layer encompasses the viscous boundary layer at the wall.

D. CORE FLOW REGION

1. Flow Equations

The core flow is assumed to be irrotational, which means that there is no vorticity, and also is incompressible, which means that density is not affected by changes in the pressure. When the velocity $\vec{U}$ is solenoidal, we may introduce a stream function ψ which allows us to replace the horizontal and vertical components of velocity by a single function. Define ψ by $u = \frac{\partial \psi}{\partial y}$ and $v = -\frac{\partial \psi}{\partial x}$. These definitions satisfy the continuity equation. When the flow is also irrotational, then the expression of zero vorticity gives Laplace's equation, $\nabla^2 \psi = 0$. Although the equation of motion is nonlinear in $\vec{U}$, the velocity distribution is completely determined by a linear equation derived from the restrictive condition of irrotationality and the mass-conservation equation. The nonlinear equation of motion is needed only for the calculation of the pressure after the velocity distribution has been determined. The

boundary conditions for the core flow must match the normal velocities in each of the boundary layers. Scale the velocity in this region by P^2. Scale the horizontal and vertical lengths by $M^{-1}P^{-2}$. Scale the pressure by MP^3. The momentum equation in the x-direction is

$$U\,U_X + V\,U_Y = -p_X + P\,(U_{XX} + U_{YY}). \tag{IV.10}$$

The momentum equation in the y-direction is

$$U\,V_X + V\,V_Y = -p_Y + P(V_{XX} + V_{YY}). \tag{IV.11}$$

With $M \gg 1$, and $P \ll 1$, these momentum equations reduce to $U\,U_X + V\,U_Y = -p_X$ in the x-direction and $U\,V_X + V\,V_Y = -p_Y$ in the y-direction. The momentum equations could also be written in terms of the stream function, ψ. For example, the momentum equation in the x-direction becomes

$$\psi_Y\,\psi_{XY} - \psi_X\,\psi_{YY} = -p_X + P(\psi_{XXY} + \psi_{YYY}) \tag{IV.12}$$

Laplace's equation can be written as

$$\nabla^2\psi = \frac{\partial^2\psi}{\partial X^2} + \frac{\partial^2\psi}{\partial Y^2} = 0 \tag{IV.13}$$

In a two-dimensional flow, the lines of constant ψ are known as the streamlines, and the difference between the numerical values of two streamlines is equal to the flow rate between the streamlines. An equivalent description of two-dimensional incompressible irrotational flow is in terms of a velocity potential ϕ, such that $\vec{u} = \nabla\phi$. The stream function ψ is harmonic, as is ϕ, and together they satisfy the Cauchy-Riemann equations as conjugate harmonic functions, which means that lines of constant ψ and ϕ are orthogonal. The fact that ψ and ϕ are harmonic and satisfy the Cauchy-Riemann equations is necessary and sufficient for the definition of a complex potential F, defined by $F = \phi + i\psi$, where $z = x + iy$ and the stream function and velocity potential are both functions of x and y. F is analytic, and note that $F'(z) = \phi_x(x,y) + i\psi_x(x,y)$,

or $F'(z) = \phi_x(x,y) - i\phi_y(x,y)$. The velocity thus becomes $\vec{u} = \overline{F'(z)}$, and the speed, or magnitude of the velocity, is found by $|\vec{u}| = |F'(z)|$.

Since the equation $\nabla^2\psi = 0$ is linear, we may superpose solutions for different flows and add directly the values of ψ at every point in the plane to obtain the new values of ψ, which represent physically the direct superposition of the various flows.

2. Dominant Balance

NAIVE APPLICATION OF THE METHOD OF DOMINANT BALANCE IS BOOTLESS. — *Carl M. Bender and Steven A. Orszag*

How does the temperature T change across the boundary layer? Let U be the core velocity and T be the core temperature, and u and t are the additional values of the velocity and temperature inside the surface viscous boundary layer, so u and t are significant only inside the layer. The horizontal derivative of the temperature, T_X, in the core flow region is similar to T_X at the surface.

Let $\hat{T} = T(X,Y) + \tau t(X,y)$, where τ is an unknown scale. Further, let $\hat{u} = P^2 U(X,Y) + P\,u(X,y)$, using the known scales: $\hat{x} = \frac{X}{MP^2}$, $\hat{y} = \frac{Y}{MP^2} = \frac{y}{MP}$. To determine the size of τ, substitute the expressions for $\hat{T}$ and $\hat{u}$ into the energy equation. This yields

$$M\left[(P^2U + Pu)(T+\tau t)_{\hat{x}} + P^2V(T+\tau t)_{\hat{y}}\right] = (T+\tau t)_{\hat{x}\hat{x}} + (T+\tau t)_{\hat{y}\hat{y}} \qquad \text{(IV.14)}$$

or, in expanded form,

$$M^2P^4UT_X + M^2P^3uT_X + M^2P^4U\tau t_X + M^2P^3u\tau t_X + M^2P^4VT_Y + M^2P^3V\tau t_y$$

$$= M^2P^4T_{XX} + M^2P^4\tau t_{XX} + M^2P^4T_{YY} + M^2P^3\tau t_{yy}$$

Divide this equation by M^2P^4 and subtract the core flow region equation, $UT_X + VT_Y = T_{XX} + T_{YY}$, which leaves

$$\frac{1}{P}uT_X + \tau Ut_X + \frac{1}{P}\tau ut_X + \frac{1}{P}\tau Vt_y = \tau t_{XX} + \frac{1}{P^2}\tau t_{yy}. \qquad \text{(IV.15)}$$

What is the dominant balance? That is, how must the scale τ be chosen to balance the additional heat convection of the first term in (IV.15)?

Suppose $\frac{1}{P}uT_X \sim \tau U t_X$. Then $\tau \sim \frac{1}{P}$, which implies the next term $\frac{1}{P}\tau u t_X$ is $O(\frac{1}{P^2})$. Since that is much larger, the assumed balance cannot be dominant. Thus, the assumption is not consistent.

Suppose $\frac{1}{P}uT_X \sim \frac{1}{P}\tau u t_X$. Then τ is $O(1)$, and the term $\frac{1}{P^2}\tau t_{yy}$ is larger, which means the assumed balance is not dominant and the assumption is not consistent.

Suppose $\frac{1}{P}uT_X \sim \frac{1}{P}\tau V t_y$. This is equivalent to the previous case, so it is not consistent.

Suppose $\frac{1}{P}uT_X \sim \tau t_{XX}$. Again, this would mean that $\tau \sim \frac{1}{P}$, as in the first case, which is not consistent.

Suppose $\frac{1}{P}uT_X \sim \frac{1}{P^2}\tau t_{yy}$. Then $\tau \sim P$ and all the other terms are small in comparison to the dominant terms. This is the only consistent case. Hence $\tau = P$.

Thus, the *change* in temperature $\hat{T}$ across the boundary layer is Pt, i.e. $O(P)$, so it is negligible. This implies that the temperature gradient T_X at the top of the core is equivalent to that right on the surface, which drives the boundary-layer flow. But the vertical temperature gradient $\hat{T}_{\hat{y}} = MP^2\,[T_Y + t_y]$, so the surface boundary condition $\hat{T}_{\hat{y}} = 0$ implies $T_Y = -t_y$ at $y = 0$. The heat equation for the surface boundary layer is

$$uT_X = t_{yy}. \tag{IV.16}$$

In order to determine how surface layer convection modifies heat flux into the core, use the boundary condition $\hat{T}_{\hat{y}} = 0$ and integrate the left-hand-side of the surface heat equation across the surface boundary layer. As $y \to \infty$, $t_y \to 0$ and the heat flux condition in the core becomes

$$T_Y(X,0) = \int_0^\infty u\,T_X\,dy. \tag{IV.17}$$

Since $\int_0^\infty u\,dy$ is just the mass flux into the corner (or the expression for the stream function, ψ), the heat flux condition becomes

$$T_Y(X,0) = T_X\,\psi(X, y \to \infty). \tag{IV.18}$$

THIS PAGE INTENTIONALLY LEFT BLANK

V. APPROXIMATE METHODS

AN IDEA WHICH CAN BE USED ONCE IS A TRICK. IF IT CAN BE USED MORE THAN ONCE IT BECOMES A METHOD. —*George Polya and Gabor Szego*

The goal of this chapter is to match the velocity in the surface viscous boundary layer to that in the wall viscous boundary layer and to that in the core flow region. The temperature can then be found using the core velocity. For the viscous boundary layers, several approximate methods exist based on integrated forms of the boundary-layer equations. These are integral methods which do not attempt to satisfy the governing equations of the boundary layer for each streamline. Instead, the equations are satisfied on average over the thickness of the boundary layer. First, start with the viscous boundary layer along the free surface, since the surface thermal gradient drives the flow into the corner.

A. VISCOUS SURFACE BOUNDARY LAYER

1. Background

The first approximate method considered is that developed by Pohlhausen in 1921 [Ref. 28]. It is based on integrating the momentum equation across a boundary layer. The integrated momentum equation gives an ordinary differential equation for the thickness of the boundary layer, $\delta(x)$, provided that a suitable form for the velocity profile is assumed. Rosenhead [Ref. 29] and Schlichting [Ref. 30] offer two excellent overviews of this method, as well as descriptions of updated methods in more modern forms. The key to the approximate methods is that they allow calculation of the momentum thickness, the displacement thickness, and the shearing stress at a wall. These will all be defined later. Most of the approximate methods for two-dimensional flows in the literature deal with flow past a rigid wall. No such method

for flow along a free surface (where the no-slip condition of the rigid wall does not apply) has yet been discovered in the literature.

What is the critical boundary-layer thickness, $\delta(x)$? Pohlhausen's method determines the boundary-layer thickness by first writing the momentum equation in terms of the shear stress, the displacement thickness, and the momentum thickness of the boundary layer. The displacement thickness δ_1 has a simple physical interpretation. $U\delta_1$ is the decrease of the mass flux across a normal to the surface, due to the boundary layer. The streamlines of the outer flow are thus displaced away from the surface through a distance δ_1 [Ref. 29]. It is the distance that a wall would have to be displaced outward into the free stream in order not to change the flow field if the fluid were completely inviscid and there were no boundary layer. The fluid becomes slowed down by viscosity near the surface and is thus forced outward, so that the effective surface presented to the oncoming stream is increased (or thickened) by the boundary layer's displacement thickness [Ref. 32]. The momentum thickness has the same physical significance except that it is based on momentum flux instead of mass flux.

Pohlhausen's approach introduces a dimensionless quantity Λ, a shape factor, which can be interpreted physically as the ratio of pressure forces to viscous forces. According to Schlichting [Ref. 30], in order to obtain a quantity with real physical significance, the thickness δ must be replaced by a length which itself has physical significance, such as the momentum thickness. The fundamental idea of approximate methods based on the momentum thickness is to assume that the dependence of the solution, $u(x, y)$, on y can be expressed by some known expression of y, in which coefficients appear, which are unknown functions of x. As the value of y gets large (the distance from the free surface increases), the boundary-layer velocity u approaches the core velocity U outside the boundary layer, and its derivatives tend to vanish. Generally, only as many boundary conditions for $y = 0$ are taken into account as is necessary to determine the unknown coefficients in the velocity profile. This will be

done later in this section.

In view of this, a more accurate method for the present situation is that of Timman [Ref. 31], whose method is a variant of Pohlhausen's. In 1949, Timman developed a family of profiles to model the velocity near a no-slip surface more adequately than Pohlhausen. Timman's method seeks to find an exponential form for the velocity profile $u(x, y)$ which satisfies the momentum equation and some of the boundary conditions, in a case where the velocity profile exponentially decays through the boundary layer. As Rosenhead states, "It is hoped that this form will approximate to the exact profile, which satisfies all of the conditions" [Ref. 29]. The complimentary error function which is introduced by Timman produces the desired asymptotic behavior; namely, the velocity exponentially decays as the distance from the surface increases. We will attempt to use a modification of Timman's method in the case of the velocity flow along the free surface.

2. Timman's Method

The velocity profile form assumed is

$$\frac{u}{U} = f(\eta), \quad \eta = \frac{y}{\delta(X)} \tag{V.1}$$

where $\delta(X)$ is the effective total thickness of the boundary layer and $U(X)$ is the velocity of the external flow. The function f may also depend on X through some of the coefficients which are chosen to be part of the profile in order to satisfy surface boundary conditions. Timman's profile is of the form

$$\frac{u}{U} = f(\eta) = 1 - \int_{\eta}^{\infty} e^{-\eta^2}(a + c\eta^2 + \cdots)\, d\eta - e^{-\eta^2}(b + d\eta^2 + \cdots), \tag{V.2}$$

where a, b, c, and d, etc., are coefficients which will turn out to be functions of X. As $y \to \infty$, it follows that $f \to 1$ to match the external flow. Therefore, only the boundary conditions at the no-slip surface $\eta = 0$ are considered. Only the same number of boundary conditions as unknown coefficients are used.

In Timman's profiles, the velocity difference $f(\eta) - 1 = \frac{u}{U} - 1$ exponentially decays through the boundary layer and satisfies $u = 0$ at the surface. In the core

region, $\eta \to \infty$, $f(\eta) \to 1$, and $u \to U$, or the velocity in the boundary layer matches the core velocity.

In our problem, the surface is a free surface, and the no-slip condition of Timman's method does not apply, since $u \neq 0$ at the surface. The velocity in our modification must be adjusted accordingly to match the free surface boundary conditions. The velocity u stills decays exponentially through the boundary layer, but where Timman's approach assumes $\frac{u}{U} = 0$ at the surface and $\frac{u}{U} = 1$ at the core/boundary-layer edge (where the boundary layer meets the core flow), our problem must be modeled to have u as a maximum at the surface and $u = U \to 0$ at the core/boundary-layer edge, since from Canright's numerical data [Ref. 1] and the scaling analysis, the core velocity is negligible.

Consider again the momentum equation in the free surface boundary layer:

$$uu_X + Vu_y = u_{yy} \tag{V.3}$$

with boundary conditions of $V = 0$ and $u_y = T_X$ when $y = 0$. Combine u times the continuity equation with this momentum equation:

$$u\left(u_X + V_y = 0\right) \oplus \left(uu_X + Vu_y = u_{yy}\right)$$

which gives

$$uu_X + uV_y + uu_X + Vu_y = u_{yy}$$

This can be rewritten as

$$(uu)_X + (uV)_y = (u_y)_y. \tag{V.4}$$

Integrate this expression with respect to y and simplify:

$$\int_0^\infty (uu)_X \, dy + \int_0^\infty (uV)_y \, dy = \int_0^\infty (u_y)_y \, dy \tag{V.5}$$

$$2\int_0^\infty uu_X \, dy + uV\Big|_0^\infty = u_y\Big|_0^\infty = -\left(u_y\right)_{y=0} \tag{V.6}$$

Since $u = V = 0$ as $y \to \infty$ and $V = 0$ at $y = 0$, the expression for u_y along the surface becomes

$$\left(u_y\right)_{y=0} = -2\int_0^\infty uu_X \, dy. \tag{V.7}$$

To begin the approximation, use a value for $T_X = u_y$, the free surface boundary condition. Along the surface, T_X decreases sharply in magnitude as the distance from the wall increases, decaying along the length of the boundary layer. This can be seen in Figure 4, which shows the gradient of the surface temperature in the x-direction, using Canright's numerical temperature data. It also shows the temperature profile (dotted line) along the surface.

Can the revised momentum equation be put into a form that has a displacement and momentum thickness? Expand the upper limit of integration in the momentum equation to infinity, to make it consistent with the range of $u(X, y)$. Define δ_2 as the momentum thickness of the boundary layer. Let

$$\delta_2 = \int_0^\infty u^2 \, dy \tag{V.8}$$

Since $\eta = \frac{y}{\delta}$, where $\delta(X)$ is the surface boundary-layer thickness, $y = \delta\eta$, and $dy = \delta \, d\eta$.

If $f(\eta)$ is defined by $f(\eta) = u$, then

$$\delta_2 = \delta \int_0^\infty f^2(\eta) \, d\eta. \tag{V.9}$$

Thus, the skin friction, or shear stress, can be written in terms of the momentum thickness, yielding a first-order differential equation $\tau_0 = -\frac{d}{dX}(\delta_2)$, or

$$\frac{d}{dX}(\delta_2) + \tau_0 = 0 \tag{V.10}$$

3. Modification to Timman's Method

Consider a family of velocity profiles where all of the coefficients are functions of X, as shown in (V.2). If no terms of higher order than the $c(X)$ and $d(X)$ terms are included, then the modification to Timman's profile yields

$$u(X, y) = f(\eta) = \int_\eta^\infty e^{-t^2} \left(a(X) + c(X)t^2\right) dt - e^{-\eta^2} \left(b(X) + d(X)\eta^2\right), \tag{V.11}$$

where $\eta = \frac{y}{\delta(X)}$. When $y = 0$, the surface velocity becomes

$$u(X, 0) = \frac{\sqrt{\pi}}{2} a(X) + \frac{\sqrt{\pi}}{4} c(X) - b(X). \tag{V.12}$$

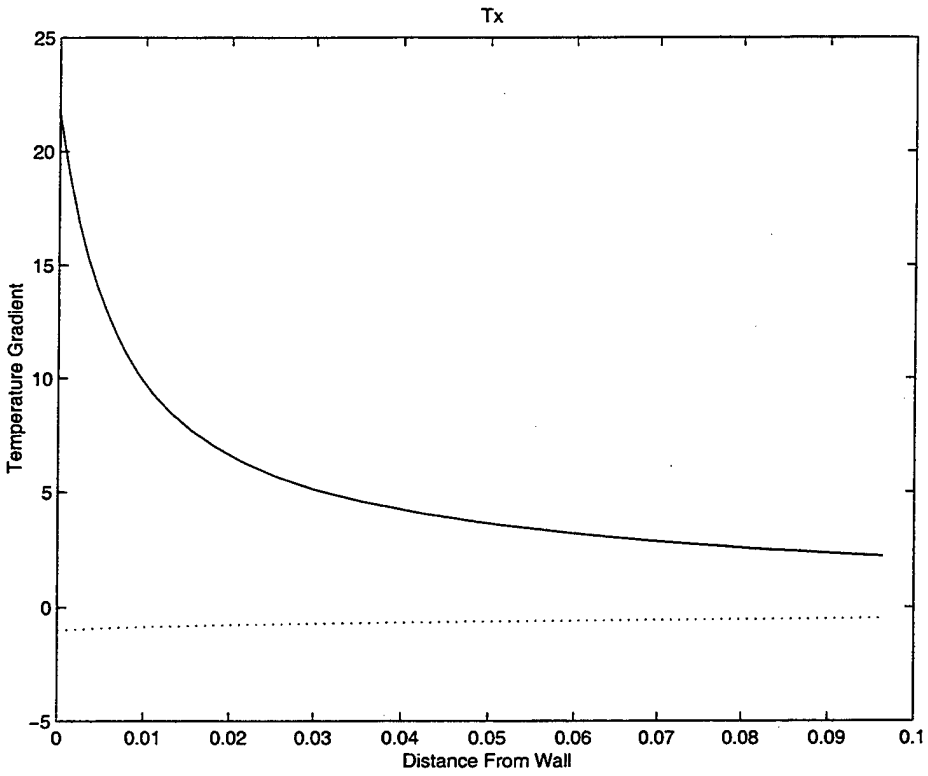

Figure 4. Temperature Gradient along the Free Surface

Due to the complications of this model, we simplify it even further (see Appendix A for our attempt at deriving a full Timman-type model): let $b(X) = c(X) = d(X) = 0$. Then

$$u = f(\eta) = \int_{\eta}^{\infty} a(X) e^{-t^2} dt, \tag{V.13}$$

or

$$f(\eta) = \frac{a(X)\sqrt{\pi}}{2} [1 - \text{erf}(\eta)] = \frac{a(X)\sqrt{\pi}}{2} \text{erfc}(\eta), \tag{V.14}$$

where $\text{erfc}(\eta)$ is the complementary error function of η. A typical characteristic of the complementary error function of η is that as η increases, $\text{erfc}(\eta)$ quickly decays to 0.

Solving the ordinary differential equation (V.10), $\frac{d}{dX}(\delta_2) + \tau_0 = 0$, for the momentum thickness yields

$$\delta_2 = -\int_0^X \tau_0 \, dX' + c_1 \tag{V.15}$$

However, the shear stress $\tau_0 = u_y = T_X$ from the given surface boundary condition, so

$$\delta_2 = -\int_0^X T_{X'}\, dX' + c_1,$$

or $\delta_2 = -T + k_1$. The boundary condition that must be satisfied is that as $X \to \infty$, $\delta_2(X) \to 0$, $u \to 0$, $T \to 0$, and $\tau_0 \to 0$. This implies that $k_1 = 0$. Thus,

$$\delta_2 = -T. \tag{V.16}$$

(Since the temperature is less than zero, δ_2 is a positive quantity). The momentum thickness has a value equal to the magnitude of the temperature. This implies two things. First, the choice for the velocity profile does not explicitly affect the solution of the momentum thickness integral. Second, since the temperature is of order 1, the momentum thickness is of order 1. The question that remains is: what is the boundary-layer thickness δ?

Since $f(\eta) = \frac{1}{2}a(X)\sqrt{\pi}\,\mathrm{erfc}(\eta)$, substitute this expression into the equation for the momentum thickness (V.9) and obtain

$$\delta_2 = -T \tag{V.17}$$

$$= \frac{a^2(X)\pi}{4}\,\delta(X)\int_0^\infty [\mathrm{erfc}(\eta)]^2\, d\eta \tag{V.18}$$

Now determine $\delta(X)$ in terms of the temperature. First, the coefficient $a(x)$ needs to be determined. Recall that $f(\eta) = u$, so that

$$u_y = \frac{\partial f}{\partial y} = \frac{1}{\delta(X)} f'(\eta),$$

where the prime denotes differentiation with respect to η. Thus, $f'(\eta) = \delta(X)\, u_y = \delta(X)\, T_X$ along the surface.

Differentiating the velocity profile yields

$$f'(\eta) = -a(X)\, e^{-\eta^2}. \tag{V.19}$$

Along the surface, $y = \eta = 0$, so that $f'(0) = -a(X)$, which implies $a(X) = -\delta(X)\, u_y = -\delta(X)\, T_X$. Thus

$$\delta_2 = \frac{T_X^2 \pi}{4}\, \delta^3(X) \int_0^\infty [\mathrm{erfc}(\eta)]^2\, d\eta = -T \tag{V.20}$$

This allows the determination of the boundary-layer thickness $\delta(X)$ to be

$$\delta(X) = \left[-\frac{T}{T_X^2\, \varepsilon} \right]^{1/3}. \tag{V.21}$$

where

$$\varepsilon = \frac{\pi}{4} \int_0^\infty [\mathrm{erfc}(\eta)]^2\, d\eta = \frac{\sqrt{\pi}}{2} \left(1 - \frac{\sqrt{2}}{2} \right). \tag{V.22}$$

Numerically, $\varepsilon \approx 0.2596$ (see Appendix B for derivation). So, $\delta(X)$ is positive and of order 1, which is not unreasonable.

Assembling the components of the profile, the velocity can be modeled as

$$u = -\frac{\sqrt{\pi}}{2}\, \varepsilon^{-1/3}\, (-T)^{1/3}\, (T_X)^{1/3}\, \mathrm{erfc}(\eta). \tag{V.23}$$

Examining each term, $(-T)^{1/3}$ decays to 0 as the distance from the wall, X, gets large. $(T_X)^{1/3}$ also decays to 0 as X increases. In addition, $\mathrm{erfc}(\eta)$ decays rapidly to 0 as the distance from the surface, y, increases, which shows that u goes to 0 at the edge of the surface boundary layer. As seen in Figure 5, there is excellent agreement between the predicted velocity profile along the surface (discrete points) and the velocity profile generated from Canright's numerical data (solid curve). In order to evaluate the velocity u, Canright's surface temperature data was used. Also, taking a vertical slice of u through the boundary layer also gives reasonably good agreement between the predicted profile and the numerical profile. Typical profiles for a y-direction slice of the horizontal component of the velocity, u, are shown in Figure 6. As can be seen, the value of u increases exponentially as the depth below the surface decreases. In this figure, u increases by more than an order of magnitude as it passes through the boundary layer. The predicted velocity is given at distances of $X = 0.0299$ and $X = 0.0494$ (dotted lines) from the wall, and are compared to

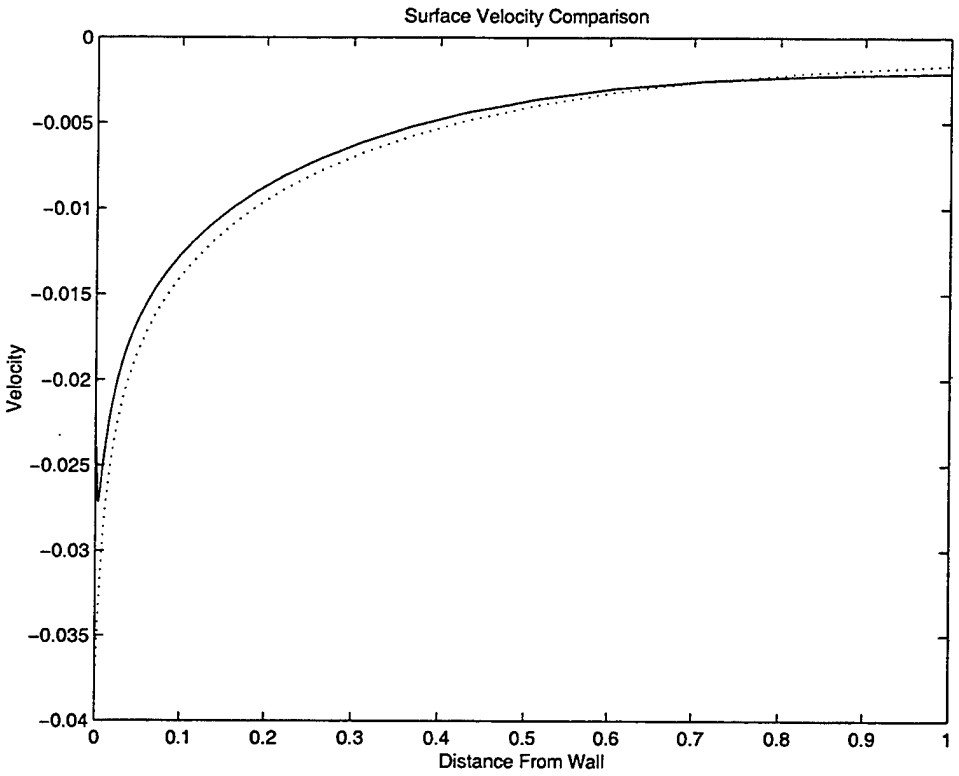

Figure 5. Comparison of Surface Velocity Profiles using Timman's Method Prediction and Canright's Numerical Data

velocity profiles taken at the same x-distances using Canright's data (solid lines). The profiles using Timman's model decay much faster than the profiles of the numerical data as the distance from the surface increases. This might be due to the lack of a second parameter in the model. Also, note that the surface boundary condition ($u_y \sim T_X$) matches for each corresponding plot.

B. VISCOUS WALL BOUNDARY LAYER

1. Background

The behavior of the velocity along the vertical rigid wall is similar to that outlined in Timman's paper. The no-slip condition exists at the wall, so the vertical component of velocity is zero at the wall, increases to a peak position (where the vorticity is zero), and then decreases to match the value of the core velocity at the

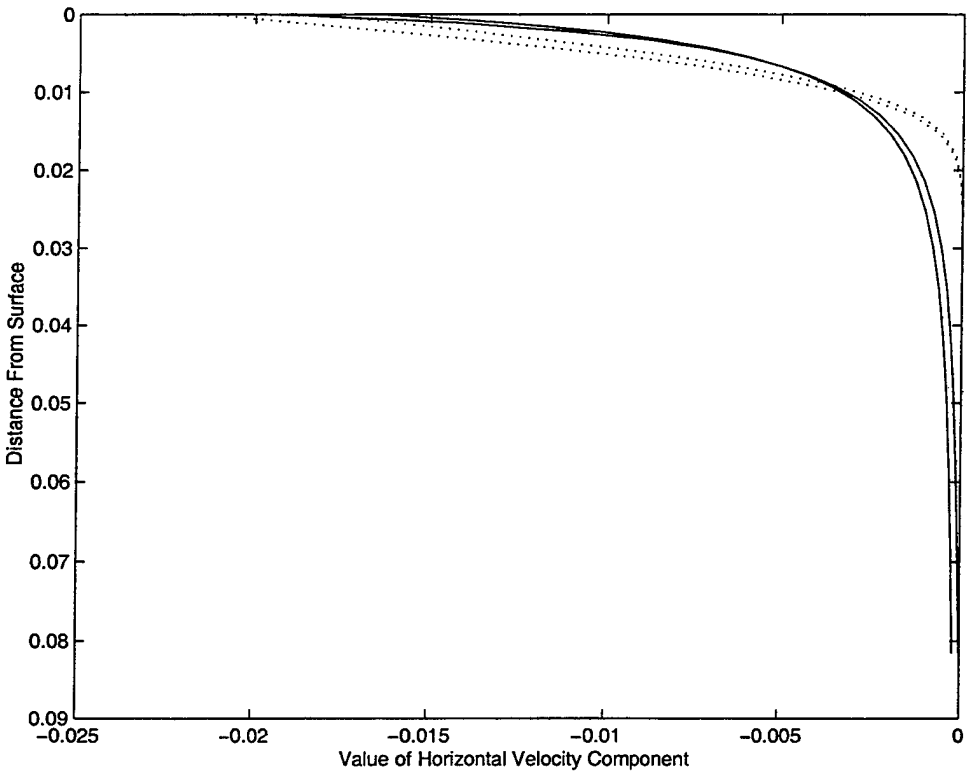

Figure 6. Typical Profiles of Velocity (u) through the Surface Boundary Layer

edge of the viscous boundary layer. Two approaches are studied. The first is a method by Glauert, which considers the velocity profile through the wall boundary layer as similar to that near a plane wall jet. The Glauert approximation matches numerical work done by Canright [Ref. 1] in 1994 quite well. A discussion of the vorticity flux is also included as an appendix, as the vorticity ω can be represented by the gradient of the vertical component of the velocity, v_x. An interesting conclusion is reached. The second method is a Timman-type approximation, but since four parameters are needed for accuracy, this method involves solving coupled nonlinear differential equations. Since the Timman method worked with the surface boundary layer, its use with the wall boundary layer was investigated and is given as an appendix. The Glauert approach is more desirable due to its simplicity.

2. Glauert's Method

Suppose the fluid flow from the free surface into the cold corner turns down the wall and acts in the manner of a plane wall jet. There is a similarity solution for the velocity profile through the wall boundary layer. Following Glauert [Ref. 36], start with the dimensionless momentum equation, assuming the pressure is everywhere uniform,

$$U v_x + v v_Y = v_{xx}. \tag{V.24}$$

Combine the continuity equation with a definition of a stream function ψ, defined by $U = \frac{\partial \psi}{\partial Y}$ and $v = -\frac{\partial \psi}{\partial x}$. Consider the possibility that there shall be a similarity solution of these equations, with the velocity proportional to Y^a and the jet thickness proportional to Y^b. The two sides of the momentum equation (V.24) will vary with Y in the same manner if $a + 2b = 1$. For a wall jet, fluid momentum is not conserved, due to shear stress from the wall.

Write the stream function as

$$\psi = -Y^{1-b} f(\eta)$$

where

$$\eta = (1-b) x Y^{-b}.$$

Then

$$v = (1-b) Y^{1-2b} f'(\eta)$$

and (V.24) becomes

$$f''' + f f'' + \alpha f'^2 = 0 \tag{V.25}$$

where $\alpha = (2b-1)/(1-b)$. The boundary conditions require that $f(0) = f'(0) = 0$ and $f'(\infty) = 0$. Integrating (V.25) between the limits η and ∞ yields

$$f'' + f f' - (\alpha - 1) \int_\eta^\infty f'^2 d\eta = 0. \tag{V.26}$$

Let $g(\eta) = \int_\eta^\infty f'^2 d\eta$, such that

$$f'' + f f' - (\alpha - 1) g = 0. \tag{V.27}$$

Notice that $g > 0$. Multiply both sides of the above expression by f', yielding

$$f'f'' + ff'^2 - (\alpha - 1)gf' = 0. \tag{V.28}$$

Integrate again, using integration by parts on the last two terms and thus

$$\frac{1}{2}f'^2 - fg + (\alpha - 2)\int_\eta^\infty f'g\,d\eta = 0. \tag{V.29}$$

If $f = 0$ when $f' = 0$, then $\alpha = 2$, since $\int_\eta^\infty f'g\,d\eta > 0$. This gives $a = -\frac{1}{2}$ and $b = \frac{3}{4}$.

Regarding what Glauert terms the external momentum flux, start again with the momentum equation (V.24). Integrate this with respect to x between the limits x and ∞, using the conditions that $v \to 0$ as $x \to \infty$.

$$\int_x^\infty U\,v_x\,dx + \int_x^\infty v\,v_Y\,dx = \int_x^\infty v_{xx}\,dx \tag{V.30}$$

By continuity, $U_x = -v_Y$, and from integration by parts, the first term above becomes

$$\int_x^\infty U\,v_x\,dx = -Uv + \int_x^\infty v\,v_Y\,dx \tag{V.31}$$

Substituting,

$$\frac{\partial}{\partial Y}\int_x^\infty v^2 dx - Uv + v_x = 0 \tag{V.32}$$

Multiply this equation by v and integrate with respect to x between 0 and ∞.

$$\frac{\partial}{\partial Y}\int_0^\infty v\left(\int_x^\infty v^2 dx'\right)dx - \int_0^\infty v_Y\left(\int_x^\infty v^2 dx'\right)dx - \int_0^\infty v^2 U\,dx + \frac{1}{2}v^2\Big|_0^\infty = 0 \tag{V.33}$$

The last term on the left is zero, and from continuity,

$$\begin{aligned} -\int_0^\infty v_Y\left(\int_x^\infty v^2 dx'\right)dx &= U\int_x^\infty v^2 dx\Big|_0^\infty + \int_0^\infty v^2 U\,dx \\ &= \int_0^\infty v^2 U\,dx \end{aligned}$$

Thus,

$$\frac{\partial}{\partial Y}\int_0^\infty v\left(\int_x^\infty v^2\,dx'\right)dx = 0, \tag{V.34}$$

since $U(0) = v(0) = 0$.

Let

$$F = \int_0^\infty v \left(\int_x^\infty v^2 \, dx' \right) dx \tag{V.35}$$

Then $\frac{\partial F}{\partial Y} = 0$, and $F =$ constant, independent of the distance Y from the free surface. However, realistically, there may be some interference from the velocity leaving the surface and coming from the corner. Glauert states that physically, the "flux of the exterior momentum flux is constant, but this is hardly a familiar concept." [Ref. 36].

It is worth pausing here to find a rough estimate of the magnitude of the flux of the exterior momentum flux, F. With a knowledge of the conditions in the impinging free jet, based on the entry conditions from the corner, start with

$$F = \int_0^\infty v \left(\int_x^\infty v^2 \, dx' \right) dx \approx v^* \int_0^\infty v \left(\int_x^\infty v \, dx' \right) dx, \tag{V.36}$$

where v^* is a typical jet velocity. Write

$$\frac{\partial}{\partial x} \left(\int_x^\infty v \, dx \right)^2 = -2v \left(\int_x^\infty v \, dx \right) \tag{V.37}$$

So,

$$F \approx \frac{1}{2} v^* \int_0^\infty -\frac{\partial}{\partial x} \left(\int_x^\infty v \, dx' \right)^2 dx \tag{V.38}$$

However,

$$\int_0^\infty -\frac{\partial}{\partial x} \left(\int_x^\infty v \, dx' \right)^2 dx = \left(\int_0^\infty v \, dx \right)^2$$

which concludes that

$$F \approx \frac{1}{2} v^* \left(\int_0^\infty v \, dx \right)^2 \tag{V.39}$$

This means that

$$F = \frac{1}{2} (\text{typical velocity}) \times (\text{mass flux})^2 \tag{V.40}$$

in the plane jet case. Neither the mass flux nor the magnitude of the fluid velocity will vary much when a plane jet is deflected off of the vertical wall, so (V.40) is a good estimate of the constant flux of exterior momentum flux, F. A more accurate

calculation of F will be given later. Keep in mind that this approximation for F has a singularity at the origin, where $Y = 0$.

The similarity form of the velocity distribution depends only on F and is given Glauert's paper [Ref. 36] as

$$f''' + ff'' + 2f'^2 = 0 \tag{V.41}$$

with boundary conditions $f(0) = f'(0) = 0$ and $f(\infty) = 0$. (As an aside, Batchelor refers to a steady narrow two-dimensional jet of fluid adjoining a plane rigid wall and offers $4f''' + ff'' + 2f'^2 = 0$ as the differential equation [Ref. 37].)

Start with Glauert's equation, (V.41). Multiply the equation by f. Integrate the first term by parts:

$$\int ff''' = ff'' - \int f'f'' = ff'' - \frac{1}{2}f'^2$$

The second and third terms in the velocity distribution form a perfect differential,

$$\int \left(f^2 f'' + 2ff'^2\right) = f^2 f'$$

Thus,

$$ff'' - \frac{1}{2}f'^2 + f^2 f' = \text{const} = 0, \tag{V.42}$$

since $f'(\infty) = 0$.

Multiply now by $f^{-3/2}$:

$$f^{-1/2}f'' - \frac{1}{2}f^{-3/2}f'^2 + f^{1/2}f' = 0. \tag{V.43}$$

Integrate again to obtain (this time, the first two terms form a perfect differential)

$$f^{-1/2}f' + \frac{2}{3}f^{3/2} = \text{constant} \tag{V.44}$$

If $f_0(\eta)$ is a solution of the original third-order differential equation, then so is $f_1(\eta) = Af_0(A\eta)$ for any constant A, and f_1 satisfies the boundary conditions if f_0 does. According to Glauert [Ref. 36], without loss of generality, select the solution with $f(\infty) = 1$ and take the above constant to have the value of $\frac{2}{3}$.

Now, write $f = g^2$. Then $f' = 2gg'$ and the differential equation in f becomes

$$g' = \frac{1}{3}(1 - g^3) \tag{V.45}$$

which gives as a solution

$$\eta = \ln\left(\frac{\sqrt{g^2+g+1}}{(1-g)}\right) + \sqrt{3}\arctan\left(\frac{\sqrt{3}g}{2+g}\right). \tag{V.46}$$

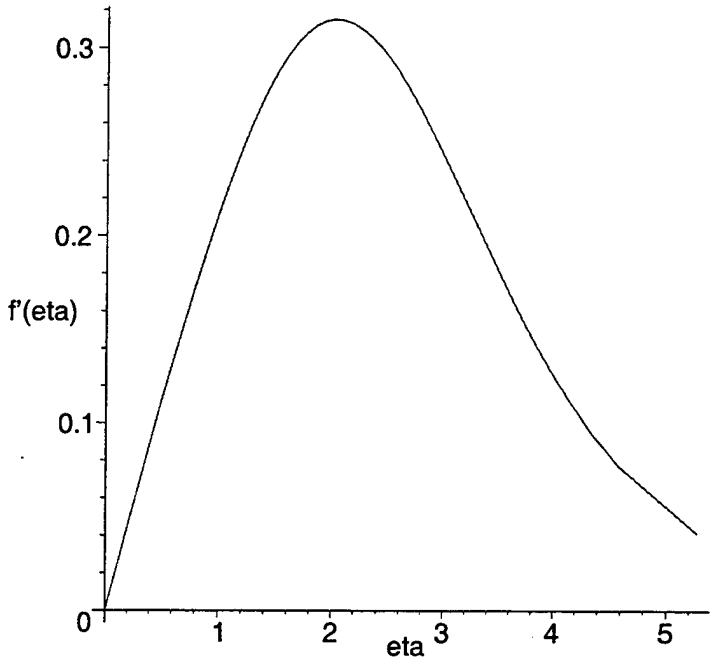

Figure 7. Velocity Profile from Glauert's Method

A plot of the variation of Glauert's velocity profile ($f'(\eta)$ vs η) is given in Figure 7. This profile is similar to the profile determined using Timman's approach and to the profile obtained using the numerical data from Canright [Ref. 1].

The velocity and position equations may be written as

$$v = \left(\frac{5F}{2Y}\right)^{1/2} f'(\eta) \tag{V.47}$$

and

$$\eta = \left(\frac{5F}{32\,Y^3}\right)^{1/4} x. \tag{V.48}$$

Recalling that $\eta = \frac{x}{\Delta}$, the above equation can be used to give an expression for the boundary-layer thickness, Δ:

$$\Delta = \left(\frac{5F}{32\,Y^3}\right)^{-1/4}. \tag{V.49}$$

There is a drawback to Glauert's method. The momentum flux has a singularity when $Y = 0$, which will not allow the velocity into the corner (along the surface at $X = 0$) to match the velocity out of the corner (along the wall at $Y = 0$). This means that the surface velocity is based on one ratio of the temperature gradient ($u \propto T_X^{1/3}$), while Glauert's suggested matching (V.40) bases the wall velocity on the inverse ratio ($v \propto T_X^{-1/3}$). Thus, along the surface, as the temperature profile is compressed, the velocity into the corner increases. However, along the wall, as the isotherms are compressed, the velocity decreases, which is not reasonable.

As an alternative matching condition, to eliminate the singularity of the similarity solution at the origin, calculate F when Y is a distance equal to the boundary-layer thickness, Δ. This will give a strength value for F which is relatively equal to the value at the corner, but the singularity is now avoided. Let

$$Y = \Delta = \left(\frac{5F}{32\,Y^3}\right)^{-1/4}. \tag{V.50}$$

Solving for Y yields

$$Y = \frac{32}{5F}. \tag{V.51}$$

Now, matching the magnitude of the surface velocity expression into the corner to the maximum wall velocity expression out of the corner, we find

$$\frac{\sqrt{\pi}}{2}\left(\frac{T_X}{\varepsilon}\right)^{1/3} = 2^{-5/3}\left(\frac{5F}{2Y}\right)^{1/2} \tag{V.52}$$

which reduces to

$$F = \frac{16\sqrt{\pi}}{5}\left(\frac{T_X}{2\varepsilon}\right)^{1/3}. \tag{V.53}$$

This matching condition for F embodies the positive feedback mechanism of the cold corner.

C. CORE FLOW REGION

I NEVER COME ACROSS ONE OF LAPLACE'S "*THUS IT PLAINLY APPEARS*" WITHOUT FEELING SURE THAT I HAVE HOURS OF HARD WORK BEFORE ME TO FILL UP THE CHASM AND FIND OUT AND SHOW *HOW* IT PLAINLY APPEARS. —*N. Bowditch*

1. The Green's Function

Recall that the core velocity U is treated as incompressible irrotational flow. As explained earlier, a stream function ψ is introduced such that $\nabla^2\psi = 0$. Define a Green's function $G(\vec{x}, \vec{x_0})$ for Laplace's equation. Thus, $\nabla^2 G(\vec{x}, \vec{x_0}) = \delta(\vec{x} - \vec{x_0})$, where $\vec{x_0}$ is an arbitrary point in the domain. The solution can then be represented in integral form. First, however, the boundary conditions in the core flow region must be prescribed in terms of ψ. The core flow must match the entrainment into the boundary layers, that is, the normal velocities. Along the wall boundary layer, $U(x \to \infty, Y) = \psi_Y(X \to 0, Y)$. Along the surface boundary layer, $V(X, y \to \infty) = -\psi_X(X, Y \to 0)$. These conditions can be simplified to Dirichlet conditions, matching the stream function ψ at the outer edges of the boundary layers.

The Green's function is determined using the method of images. Start with the solution in a quarter plane and use symmetry in the other quadrants to match the boundary conditions. There are four quadrants with logarithmic singularities. The defining problem for the Green's function, $\nabla^2 G(\vec{x}, \vec{x_0}) = \delta(\vec{x} - \vec{x_0})$, satisfies the corresponding homogeneous boundary conditions, $G(x, 0; x_0, y_0) = G(0, y; x_0, y_0) = 0$. Here, the notation that $G(\vec{x}, \vec{x_0}) = G(x, y; x_0, y_0)$ is used. The quarter-infinite space $(x > 0, y > 0)$ has no sources except at a concentrated source at $\vec{x} = \vec{x_0}$.

Using the method of images in the core flow region, the Green's function for Laplace's Equation on a quarter-plane $(X > 0, Y > 0)$ is

$$\begin{aligned} G(\vec{X}, \vec{X_0}) &= \frac{1}{4\pi}\Big\{\ln\left[(X - X_0)^2 + (Y - Y_0)^2\right] - \ln\left[(X - X_0)^2 + (Y + Y_0)^2\right] \\ &\quad -\ln\left[(X + X_0)^2 + (Y - Y_0)^2\right] + \ln\left[(X + X_0)^2 + (Y + Y_0)^2\right]\Big\} \end{aligned}$$

$$= \frac{1}{4\pi}\ln\left\{\frac{[(X-X_0)^2+(Y-Y_0)^2]\,[(X+X_0)^2+(Y+Y_0)^2]}{[(X-X_0)^2+(Y+Y_0)^2]\,[(X+X_0)^2+(Y-Y_0)^2]}\right\}, \quad \text{(V.54)}$$

To check the boundary conditions, start with the Green's function and set X or Y, respectively, equal to zero. Thus it plainly appears that $G\Big|_{X=0} = G\Big|_{Y=0} = 0$. Since the boundary condition for the Green's function is the Dirichlet kind at $Y = 0$, and at $X = 0$, then a positive image source must be used for $Y < 0$ and $X < 0$, and negative sources must be used for $X > 0, Y < 0$ and for $X < 0, Y > 0$. In this way, equal but opposite sources are located at the symmetry locations of $\vec{X_0}$ in the four quadrants of the plane, and there is no flow along $Y = 0$ and $X = 0$, as desired.

To solve Laplace's equation, multiply the Green's function identity by ψ, giving

$$\psi\left[\nabla^2 G(\vec{X}, \vec{X_0}) = \delta(\vec{X} - \vec{X_0})\right].$$

Multiply Laplace's equation by G, yielding

$$G\left[\nabla^2\psi = 0\right].$$

Subtracting and integrating over the domain A gives

$$\int\int_A \left(\psi\,\nabla^2 G - G\,\nabla^2\psi\right) dA = \psi\left(\vec{X_0}\right) \quad \text{(V.55)}$$

Using Green's second identity, Laplace's equation in two dimensions becomes:

$$\int\int_A \left(\psi\,\nabla^2 G - G\,\nabla^2\psi\right) dA = \oint_s (G\,\nabla\psi - \psi\,\nabla G)\cdot\hat{n}\,ds = \psi\left(\vec{X_0}\right), \quad \text{(V.56)}$$

where $\hat{n}$ is the normal to the boundary (inward normal) and s is the arc length along the boundary. Consider a large quarter-circle (in the limit as the radius tends to infinity). The inward normal for the top (boundary layer along the free surface) is $\hat{j}$ and the inward normal for the side (boundary layer along the wall) is $\hat{i}$. It will be shown that the contribution at ∞ tends to vanish if $\psi \to 0$ sufficiently fast.

$$\oint_s (G\,\nabla\psi - \psi\,\nabla G)\cdot\hat{n}\,ds = \int_0^\infty \left(G\frac{\partial\psi}{\partial X} - \psi\frac{\partial G}{\partial X}\right)\Big|_{X=0} dY + \int_0^\infty \left(G\frac{\partial\psi}{\partial Y} - \psi\frac{\partial G}{\partial Y}\right)\Big|_{Y=0} dX$$

$$+ \lim_{|\vec{X}|\to\infty} \oint_s (G\,\nabla\psi - \psi\,\nabla G)\cdot\hat{n}\,ds \tag{V.57}$$

The last term on the right is the contribution as the radius of the quarter circle (or $|\vec{X}|$) tends to infinity. It will vanish if $\psi \to 0$ sufficiently fast, or if $\psi \sim \frac{1}{|\vec{X}|}$. To show this, integrate in polar coordinates, for which $ds = r\,d\theta$ ($r = |\vec{X}|$):

$$\lim_{r\to\infty} \oint (G\,\nabla\psi - \psi\,\nabla G)\; r\,d\theta = 0. \tag{V.58}$$

Substituting G and evaluating $\oint d\theta = 2\pi$ yields the necessary condition

$$\lim_{r\to\infty} \left(r\,\ln r\,\frac{\partial\psi}{\partial r} - \psi \right) = 0. \tag{V.59}$$

If $\psi \to 0$ sufficiently fast, or if $\psi \sim \frac{1}{|\vec{X}|}$, then the contributions of this "boundary" term will vanish.

Hence,

$$\psi\left(\vec{X}_0\right) = \int_0^\infty \left(G\,\frac{\partial\psi}{\partial X} - \psi\,\frac{\partial G}{\partial X} \right)\Big|_{X=0} dY + \int_0^\infty \left(G\,\frac{\partial\psi}{\partial Y} - \psi\,\frac{\partial G}{\partial Y} \right)\Big|_{Y=0} dX \tag{V.60}$$

Since $G\big|_{X=0} = G\big|_{Y=0} = 0$,

$$\psi\left(\vec{X}_0\right) = \int_0^\infty \left(-\psi\,\frac{\partial G}{\partial X} \right)\Big|_{X=0} dY + \int_0^\infty \left(-\psi\,\frac{\partial G}{\partial Y} \right)\Big|_{Y=0} dX \tag{V.61}$$

Recall that $U = \frac{\partial\psi}{\partial Y}\big|_{X=0}$ and $V = -\frac{\partial\psi}{\partial X}\big|_{Y=0}$. Since the boundary conditions give $G = 0$ at $X = Y = 0$, and $-\frac{\partial\psi}{\partial X}\big|_{X=0} = 0$, we only need to find $\frac{\partial G(\vec{X},\vec{X}_0)}{\partial Y}\big|_{Y=0}$, which is

$$\frac{\partial G(\vec{X},\vec{X}_0)}{\partial Y}\Big|_{Y=0} = \frac{1}{\pi}\left[\frac{Y_0}{(X+X_0)^2 + Y_0^2} - \frac{Y_0}{(X-X_0)^2 + Y_0^2} \right] \tag{V.62}$$

Thus, for the core flow due to the surface boundary layer, insert the mass flux into the corner for $\psi\big|_{Y=0}$, yielding

$$\psi = -\int_0^\infty \psi_{\text{surface}}(X,0)\,\frac{\partial G(\vec{X},\vec{X}_0)}{\partial Y}\Big|_{Y=0} dX, \tag{V.63}$$

As stated previously, one advantage of the Green's function is that the flow can still be represented over the entire quarter plane, so that there is no artificial

recirculation due to imposed artificial boundaries. Thus, only the boundary conditions at the boundary layer/core region interfaces are required. The Green's function approach does not require flow boundary conditions at the computational domain's boundaries.

2. Mass Flux Calculations

In order to obtain a solution to Laplace's Equation in the core flow region, the boundary conditions from the surface and wall boundary layers must be addressed. Recall that along the surface boundary layer, the velocity is modeled as

$$u = \frac{\sqrt{\pi}}{2}\,\varepsilon^{-1/3}\,(-T)^{1/3}\,(T_X)^{1/3}\,\mathrm{erfc}(\eta). \tag{V.64}$$

As explained previously, the horizontal velocity component u decays to zero as X and η increase.

To determine the mass flux along the surface layer into the cold corner, sum the velocity component as (the correct scalings for the velocity and the boundary-layer thickness are inserted as appropriate)

$$\begin{aligned}
\psi_{\text{surface}} &= \int_0^\infty u\,dy \\
&= \int_0^\infty \left[-\frac{\sqrt{\pi}}{2}\,\varepsilon^{-1/3}\,(-T)^{1/3}\,(T_X)^{1/3}\,\mathrm{erfc}(\eta)\right] dy \\
&= -\int_0^\infty \frac{\sqrt{\pi}}{2}\left[\varepsilon^{-1/3}\,(-T)^{1/3}\,(T_X)^{1/3}\,\mathrm{erfc}(\eta)\right]\delta\,d\eta \\
&= -\int_0^\infty \frac{\sqrt{\pi}}{2}\left[\varepsilon^{-1/3}\,(-T)^{1/3}\,(T_X)^{1/3}\,\mathrm{erfc}(\eta)\right]\left[\varepsilon^{-1/3}\,(-T)^{1/3}\,(T_X)^{-2/3}\right] d\eta \\
&= -\frac{\sqrt{\pi}}{2}\,\varepsilon^{-2/3}\,(-T)^{2/3}\,(T_X)^{-1/3}\int_0^\infty \mathrm{erfc}(\eta)\,d\eta \\
&= -\frac{1}{2}\,\varepsilon^{-2/3}\,(-T)^{2/3}\,(T_X)^{-1/3}
\end{aligned} \tag{V.65}$$

When $X = 0$, the stream function (mass flux) into the corner can be calculated as $\frac{1}{2}\,\varepsilon^{-2/3}\,(-T_0)^{2/3}\,(T_{X_0})^{-1/3}$. This value will be compared to the mass flux out of the corner shortly.

To determine the mass flux down the wall, sum the vertical velocity component, v. Recall that

$$v = \left(\frac{5F}{2Y}\right)^{1/2} f'(\eta),$$

where

$$\eta = \frac{x}{\Delta} = \left(\frac{5F}{32\,Y^3}\right)^{1/4} x.$$

Thus, the stream function (mass flux with appropriate scalings for the velocity and boundary-layer thickness) is

$$\begin{aligned}
\psi_{\text{wall}} &= -\int_0^\infty v\,dx \\
&= -\int_0^\infty v\,\Delta\,d\eta \\
&= -\left(\frac{5F}{2Y}\right)^{1/2}\left(\frac{5F}{32\,Y^3}\right)^{-1/4}\int_0^\infty f'(\eta)\,d\eta \\
&= -(5F)^{1/4}\,(2)^{3/4}\,Y^{1/4}\,f(\eta)\Big|_0^\infty \qquad \text{(V.66)}
\end{aligned}$$

We have shown that $f(0) = 0$ and $\lim_{\eta\to\infty} f(\eta) = 1$, so that the mass flux down the wall is

$$\psi_{\text{wall}} = -\,(40\,F\,Y)^{1/4} \qquad \text{(V.67)}$$

D. POTENTIAL FLOW DUE TO A WALL JET

The next test for our problem is to check the potential flow due to a wall jet in the quarter-plane. A jet is a flow in which the width, or cross-stream scale, is considerably smaller than the downstream scale. For a wall jet, this type of flow occurs along a solid boundary. In Glauert's discussion of the wall jet, he postulated that the

entire flow of the wall jet cannot conform to one similarity solution over the entire domain [Ref. 36]. Glauert divided the flow region into inner and outer portions, treating the two portions separately. The dividing line for the two portions was the point of maximum velocity. Additionally, as we have demonstrated previously, Glauert also showed that the "flux of exterior momentum flux" across the viscous boundary layer is constant [Ref. 36]. The plane wall jet is created when a jet flow is discharged in a tangential direction along the plane surface; in this case, the wall. Plotkin [Ref. 40] studied a higher-order correction to Glauert's solution, providing a second-order solution including displacement. The first-order inner viscous solution induces a correction in the outer inviscid core flow solution. Plotkin matched the inner and outer solutions and developed a solution which satifies the boundary conditions in a semi-infinite plane, where $\psi(x,0) = 4x^{1/4}$ for $x > 0$, and $\psi = 0$ for $x < 0$. His solution satisfies Laplace's equation and is

$$\psi(x,y) = 4\left[\mathcal{R}(x+iy)^{1/4} - \Im(x+iy)^{1/4}\right] \tag{V.68}$$

where $\mathcal{R}$ and $\Im$ denote the real and imaginary parts, respectively, for $0 \leq \arg(x+iy) \leq 2\pi$.

In the present problem, Plotkin's solution must be modified to match the boundary conditions in the quarter-plane, namely, that $\psi(0,Y) = -(40FY)^{1/4}$ and when $Y = 0$ and $X > 0$, $\psi = 0$. The angle is $\frac{\pi}{2}$, and after taking the fourth-root, the argument for the complex variable becomes $\frac{\pi}{8}$. Taking into account that the jet flows down the wall (in the y-direction), the potential solution becomes

$$\psi(X,Y) = -(40F)^{1/4}\left[\mathcal{R}(Y+iX)^{1/4} - \frac{\sqrt{2+\sqrt{2}}}{\sqrt{2-\sqrt{2}}}\Im(Y+iX)^{1/4}\right]. \tag{V.69}$$

which simplifies to

$$\psi(X,Y) = -(40F)^{1/4}\left[\mathcal{R}(Y+iX)^{1/4} - \left(1+\sqrt{2}\right)\Im(Y+iX)^{1/4}\right]. \tag{V.70}$$

This also satisfies Laplace's equation in the quarter-plane. This expression for $\psi(X,Y)$ is used to determine the core velocity field due to the wall boundary layer.

VI. NUMERICAL RESULTS

REFINEMENT OF THE METHOD ALSO REQUIRES A MORE REFINED USER. — *Federico Paris and Josè Cañas*

THE PURPOSE OF COMPUTATION IS INSIGHT, NOT NUMBERS. — *Richard W. Hamming*

A. SOLVING LAPLACE'S EQUATION

Before solving Laplace's equation in the core-flow region, the numerical code to solve Laplace's Equation was tested on a simple problem with a known solution, the point vortex. The two-dimensional solenoidal flow in the core flow region associated with a straight line vortex may be described in terms of a stream function as

$$\psi = -\frac{\kappa}{2\pi}\log\sigma, \tag{VI.1}$$

where κ is the strength of circulation and $\sigma = \sqrt{(x-x_0)^2+(y-y_0)^2}$. In a flow field which is entirely two-dimensional, the appropriate term for the singularity is *point vortex.* The line vortex, a line in space that has a given circulation, or vorticity, becomes a point vortex when a single plane cuts through it. For simplicity, set $\kappa = 1$ and find ϕ, the harmonic conjugate of ψ. Since the two scalar functions $\phi(x,y)$ and $\psi(x,y)$ both satisfy Laplace's equation, they also provide alternative specifications of a core flow vector $\vec{U}$ which is both irrotational and solenoidal [Ref. 37]. Thus, given ψ above, and the fact that

$$\frac{\partial\psi}{\partial y} = U = \frac{\partial\phi}{\partial x} \text{ and } -\frac{\partial\psi}{\partial x} = V = \frac{\partial\phi}{\partial y}, \tag{VI.2}$$

ϕ is found to be

$$\phi = \frac{\kappa}{2\pi}\tan^{-1}\left(\frac{x}{y}\right). \tag{VI.3}$$

To find the velocity anywhere in the fluid, find the distance and direction to the point vortex. The direction of the fluid is always a circle surrounding the point. The magnitude of the velocity is given by

$$|\vec{U}| = \frac{\kappa}{2\pi\sigma}. \tag{VI.4}$$

The horizontal and vertical components of velocity, evaluated at $x = 0$ and $y = 0$, respectively, are

$$U = \frac{\partial\phi}{\partial x}\Big|_{x=0} = -\frac{1}{y}, \quad V = \frac{\partial\phi}{\partial y}\Big|_{y=0} = \frac{1}{x} \tag{VI.5}$$

The Laplace's equation solver was run on this point vortex problem, treating the point vortex at the origin and evaluating the ϕ distribution in a quarter-plane with a uniform grid. A trapezoidal scheme for integration is used. The output matched the behavior of the known solution, as seen in Figure 8. The plot of the $\tan^{-1}(y/x)$ gives straight lines through the origin. The numerical code integrates to regions beyond the area of interest (due to the Green's function), and then the area of interest – the corner region – can be analyzed in detail. This was useful to test the code, although the stream function ψ will be used instead of the velocity potential ϕ.

B. SOLVING THE HEAT EQUATION

The full two-dimensional time-dependent problem can be expanded as

$$\left(\frac{\partial T}{\partial t} + U\frac{\partial T}{\partial X} + V\frac{\partial T}{\partial Y}\right) = \frac{\partial^2 T}{\partial X^2} + \frac{\partial^2 T}{\partial Y^2}. \tag{VI.6}$$

The boundary conditions for the quarter-plane are that when $y = 0$, $T_y = 0$, and when $x = 0$, $T = -1$. Artificial boundaries were introduced to modify the quarter-plane problem into a rectangle problem. Since we are concerned with the activity in the corner, the domain was chosen large enough that the temperature gradients and velocity values decayed to zero far from the corner (as $X, Y \to 0$, $\nabla T, U, V \to 0$). Specifically, on the right boundary, $T = 0$ for the hot incoming fluid, and on the bottom boundary, $T_Y = 0$ to minimize downstream influence. Along the surface layer,

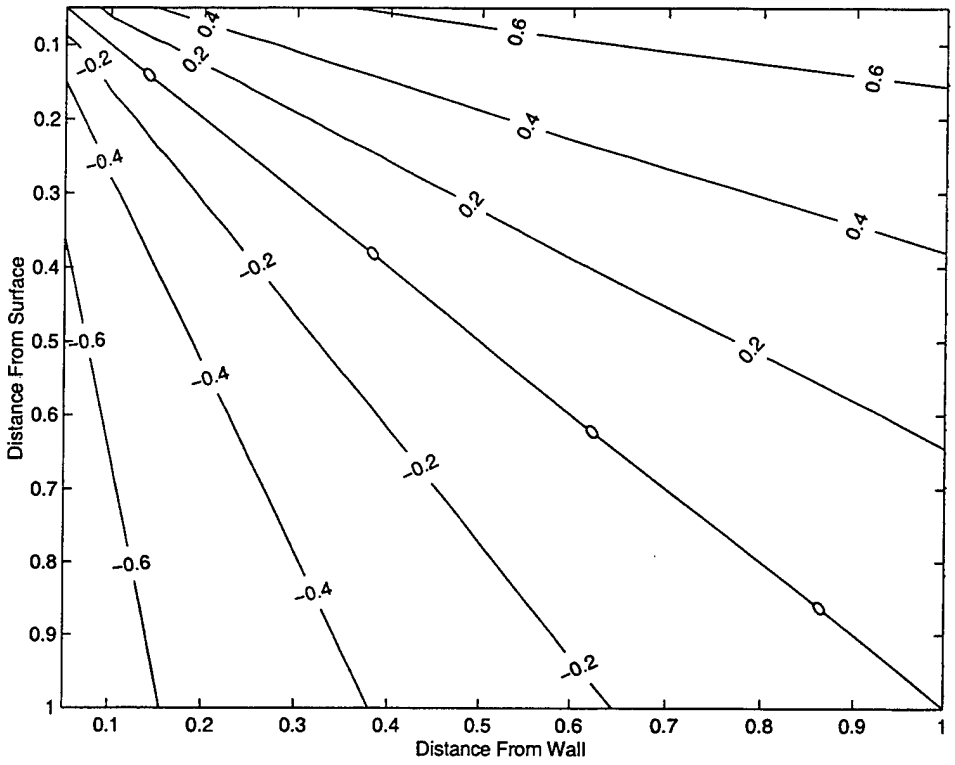

Figure 8. Contour Plot of Numerically-Solved Phi for Point Vortex

the heat flux T_Y condition (IV.17) is incorporated into the scheme. It is assumed that the time-dependent solution will converge to a steady-state solution. Hence, the initial conditions can be chosen arbitrarily.

Equation (VI.6) was solved using an alternating direction implicit (ADI) method as developed by Polezhaev in 1967 [Ref. 39]. This method treats each time step as two half steps. The above equation can be substituted into the scheme as:

STEP 1:

$$\left[1+\frac{\Delta t}{2}\left(U_{i,j}\frac{\bar{\delta}_X}{2\Delta X}-\hat{\delta}_X^2\right)\right]T_{i,j}^{*}=\left[1-\frac{\Delta t}{2}\left(V_{i,j}\frac{\bar{\delta}_Y}{2\Delta Y}-\hat{\delta}_Y^2\right)\right]T_{i,j}^{n} \qquad \text{(VI.7)}$$

STEP 2:

$$\left[1+\frac{\Delta t}{2}\left(V_{i,j}\frac{\bar{\delta}_Y}{2\Delta Y}-\hat{\delta}_Y^2\right)\right]T_{i,j}^{n+1}=\left[1-\frac{\Delta t}{2}\left(U_{i,j}\frac{\bar{\delta}_X}{2\Delta X}-\hat{\delta}_X^2\right)\right]T_{i,j}^{*} \qquad \text{(VI.8)}$$

where the central-difference operators $\bar{\delta}$ and $\hat{\delta}^2$ are defined as:

$$\begin{aligned} \bar{\delta}_X T_{i,j} &= T_{i+1,j} - T_{i-1,j} \\ \bar{\delta}_Y T_{i,j} &= T_{i,j+1} - T_{i,j-1} \end{aligned} \tag{VI.9}$$

and

$$\begin{aligned} \hat{\delta}_X^2 T_{i,j}^n &= \frac{T_{i+1,j}^n - 2T_{i,j}^n + T_{i-1,j}^n}{(\Delta X)^2} \\ \hat{\delta}_Y^2 T_{i,j}^n &= \frac{T_{i,j+1}^n - 2T_{i,j}^n + T_{i,j-1}^n}{(\Delta Y)^2} \end{aligned} \tag{VI.10}$$

As a result of splitting the time step in this algorithm, only tridiagonal systems of linear algebraic equations must be solved (at each half-step). This method is first-order accurate in time but second-order in space, with a truncation error of $O[\Delta t, (\Delta x)^2, (\Delta y)^2]$ and is unconditionally stable for the linear (no convection) case.

The scheme was coded using the C programming language with a uniform ($\Delta x = \Delta y$) rectangular grid. The problem's boundary conditions as stated earlier were incorporated into the scheme. A copy of this code is attached in Appendix E. To set the boundary conditions at each of the four sides of the rectangle, some of the coefficients for $T_{i,j}^n, T_{i,j}^*$, and $T_{i,j}^{n+1}$ had to be manipulated. These manipulations ensured adherence to the boundary conditions without altering the solution method inside the boundaries. For example, second-order difference equations for the first and second spatial derivatives were modified at the surface and at the bottom of the grid.

A subroutine *tridiag.c* is called in the execution, which solves the tridiagonal set of equations $A\vec{x} = \vec{b}$ for the unknown left-hand-side of each equation in STEP 1 and STEP 2 of the ADI method. In this case, the matrix A is the coefficient matrix involving velocity and time-derivative terms, $\vec{b}$ is the vector consisting of the right-hand-side of each equation in STEP 1 and STEP 2 (the known temperature), and $\vec{x}$ is the vector of the unknown temperature.

The method was tested against known problems involving mixed boundary conditions and various scenarios of velocity, with and without convective terms, and

after iteration, a steady-state was reached, i.e., the solution converged. The ADI method is unconditionally stable but may converge slowly. An alternate technique is to update each row or column in the step temperature as it is solved. This leads to a faster convergence; however, it is not clear if this modified technique is unconditionally stable.

The first sample problems that the ADI method were tested against involved zero velocity ($\frac{\partial T}{\partial t} = \nabla^2 T$ – pure diffusion, no convection). The solutions were linear in x: $T(x,y) = \frac{x-L}{L}$, where L is the distance to the boundary in the x-direction. Other sample problems involved a non-zero velocity in one direction ($\frac{\partial T}{\partial t} + \vec{u} \cdot \nabla T = \nabla^2 T$ – diffusion and convection). In the latter case, one example used involved a unit square domain, with Dirichlet conditions ($T = 0$) on the left and right boundaries and Neumann conditions on the bottom ($T_y = 0$) and surface:

$$T_y = f(x) = e^{1/2} \sin(\pi x) \sinh\left(\frac{\sqrt{1+4\pi^2}}{2}\right).$$

The velocity field was $(U, V) = (0, -1)$ in this example. The solution to the problem is

$$T(x,y) = \sin(\pi x)\left[\frac{e^{\frac{(\sqrt{1+4\pi^2}-1)(y-1)}{2}}}{\sqrt{1+4\pi^2}-1} + \frac{e^{-\frac{(\sqrt{1+4\pi^2}+1)(y-1)}{2}}}{\sqrt{1+4\pi^2}+1}\right]$$

The ADI algorithm converged to four-decimal accuracy in 49 iterations, yielding the solution shown in Figure 9. The grid had a uniform spacing of 0.05. The time step per iteration was 0.002.

C. THE ADI METHOD

The ADI method was used to solve the two-dimensional unsteady heat equation, beginning with an initial temperature field which was exponentially decaying on the surface and zero elsewhere. This temperature field was then iterated in two loops: the inner loop had a fixed number of iterations which was simply the ADI algorithm marching in time; the outer loop updated the velocity profile with another fixed number of iterations. Since the velocity field is based upon the temperature

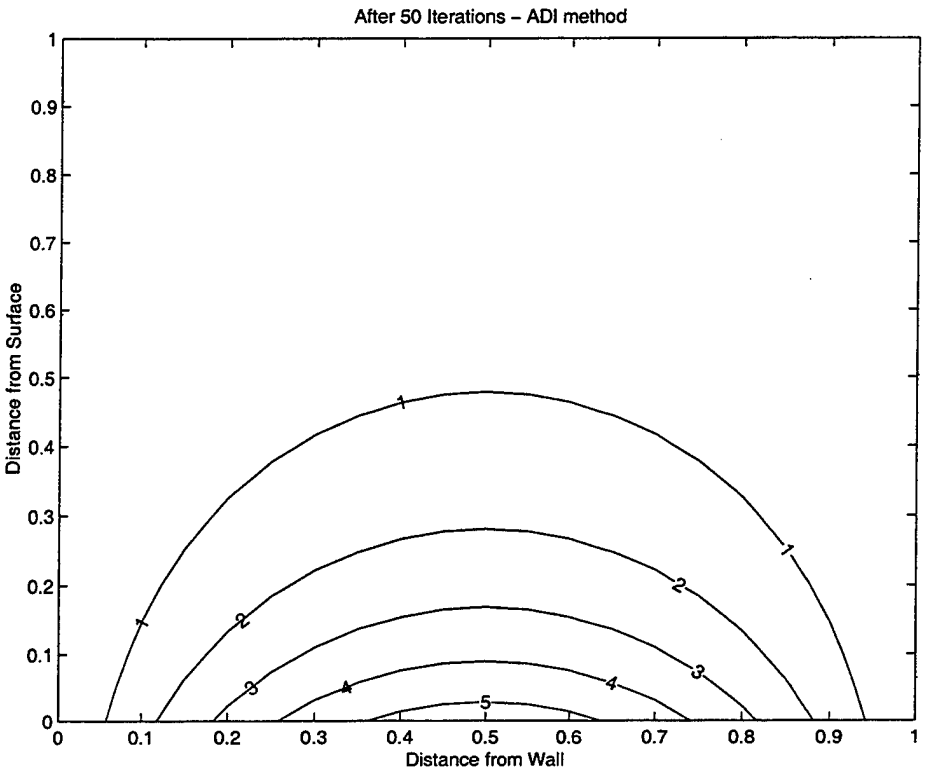

Figure 9. Contour Plot of Numerically-Solved Temperature for Test Case

and its derivatives, the interim temperature solution (after each set of inner loop iterations) was used to calculate the velocity, which was then fed into the ADI solver for another series of inner loop iterations, yielding another, more accurate, temperature solution. This process was repeated a number of times equal to number of the outer loop iterations. Once the difference between successive temperature solutions fell below a certain tolerance (in this case, 0.00001), steady-state was reached. Figure 10 shows a typical steady-state temperature solution. The spatial step size is 0.01 in both directions.

The thermal field is compressed against the wall by the velocity into the corner. The problem used 20 iterations in each inner loop, and it converged in only 12 outer loop iterations. A closer view of the corner is shown in Figure 11, which also compares our approach (on the left) with Canright's numerical data (on the right). The comparison is encouraging, particularly since the model has no adjustable parameters.

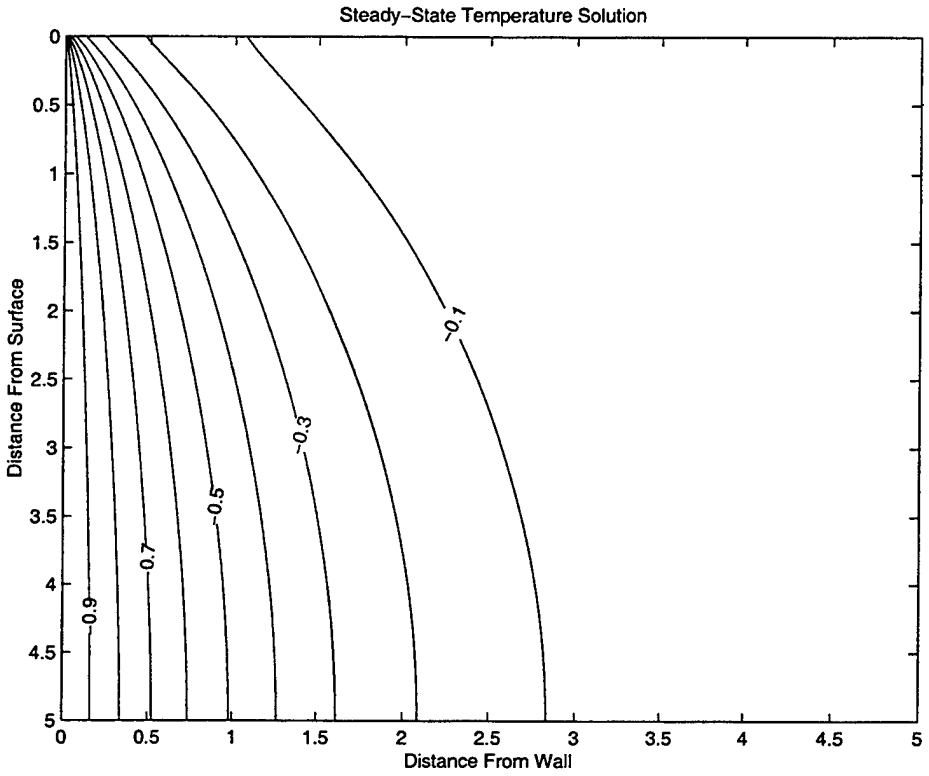

Figure 10. Steady State Temperature Contour Plot

To get a better indication of our method, surface temperatures are plotted, in Figure 12. There is excellent agreement of the temperature gradient from the corner into the core flow region, well beyond the boundary-layer thickness.

D. UNIFORM VELOCITY

Following the boundary-layer matching theory outlined in Bender & Orszag, [Ref. 41], the uniform velocity for the entire domain can be written as

$$\vec{U}_{\text{uniform}} = \vec{U}_{\text{inner}} + \vec{U}_{\text{outer}} - \vec{U}_{\text{match}} \tag{VI.11}$$

The inner solution is composed of the velocity components in the two boundary layers,

$$\vec{U}_{\text{inner}} = \vec{U}_{\text{surface}} + \vec{U}_{\text{wall}}, \tag{VI.12}$$

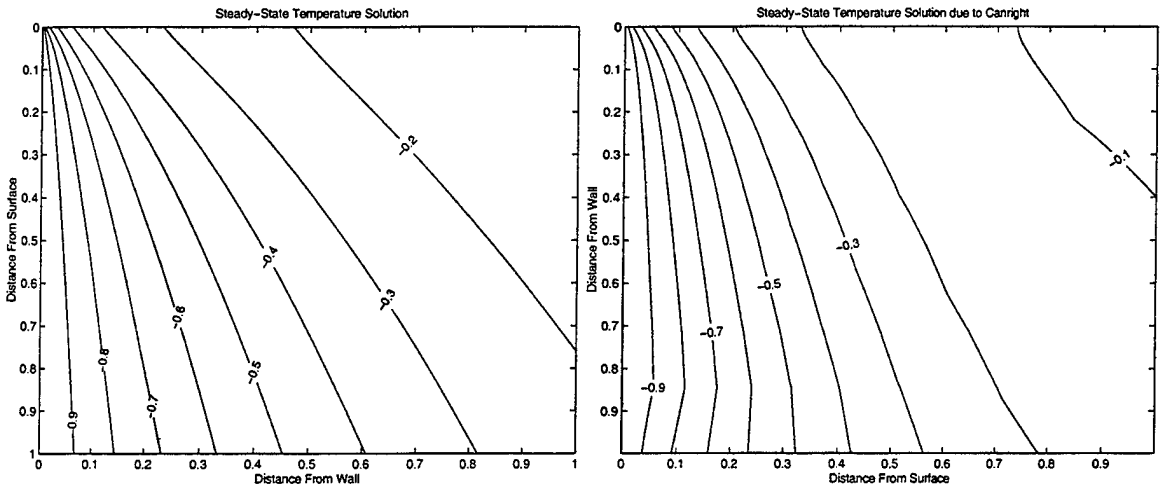

Figure 11. Steady State Temperature Contour Plot – Comparison with Canright's Data

while the outer solution is made up of the two components of the core velocity, due to the similarity solution and the Green's function:

$$\vec{U}_{\text{outer}} = \vec{U}_{\text{green}} + \vec{U}_{\text{sim}} = \vec{U}_{\text{core}}. \tag{VI.13}$$

In the above expressions, $\vec{U}_{\text{surface}}$ refers to the surface boundary layer velocity component obtained using the modified Timman approach, due to the thermal gradient along the surface, T_x. $\vec{U}_{\text{wall}}$ refers to the wall boundary layer velocity component obtained using Glauert's method, fed from the surface mass flux. The core velocity component $\vec{U}_{\text{green}}$ is a velocity field obtained using the Green's function (from solving Laplace's equation in the core region) and due to the entrainment into the surface layer, and the core component $\vec{U}_{\text{sim}}$ is the velocity field due to the similarity solution of the potential from the wall jet (due to the Plotkin modification). Determine the uniform flow in terms of the stream function, ψ.

Consider first the surface velocity vector. As shown earlier,

$$u_{\text{surface}} = -\frac{\sqrt{\pi}}{2}\,\varepsilon^{-1/3}\,(-T)^{1/3}\,(T_X)^{1/3}\,\text{erfc}(\eta). \tag{VI.14}$$

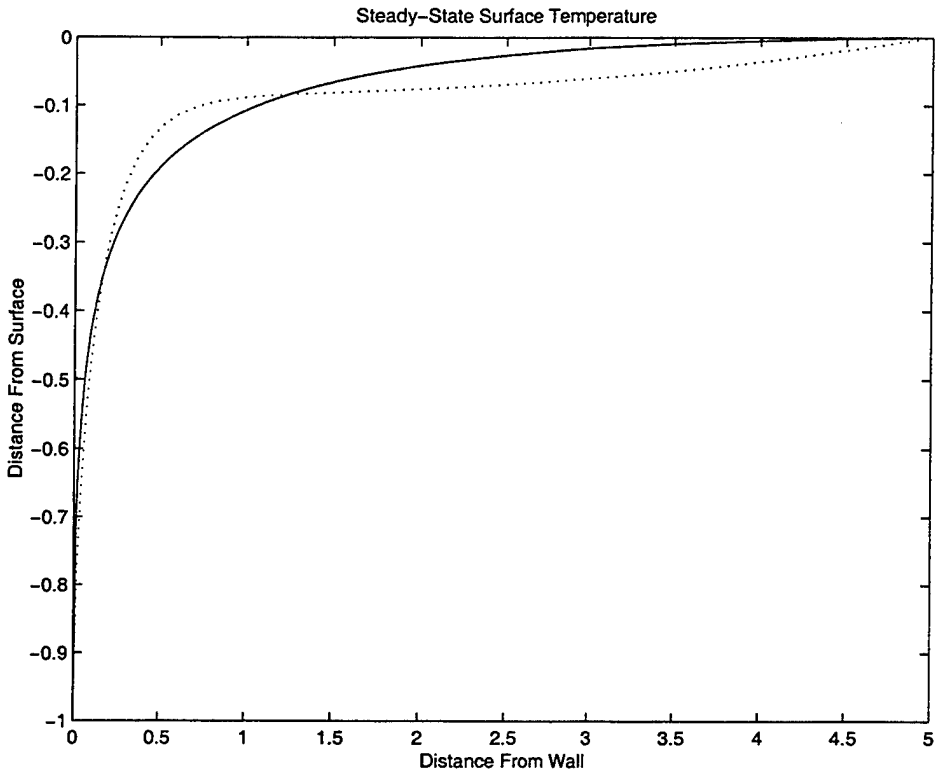

Figure 12. Steady State Surface Temperature Plot

Let $g(\eta) = \int_\eta^\infty e^{-s^2}\, ds = \frac{\sqrt{\pi}}{2}\,\mathrm{erfc}(\eta)$, where $\eta = y/\left[\frac{-T}{\varepsilon T_X^2}\right]^{1/3}$. Define $\mathrm{G}(\eta) = \int_0^\eta g(s)\, ds = \frac{1}{2}(1 - e^{-\eta^2}) + \eta\, g(\eta)$. Now, the stream function may be written as

$$\psi_{\text{surface}} = \int_0^y u\, dy' = -\left[\frac{(-T)^2}{\varepsilon^2 T_X}\right]^{1/3} \mathrm{G}(\eta) = \int_0^Y U\, dY' \qquad \text{(VI.15)}$$

The scalings are $V = -\psi_X$, $U = u/P$, and $Y = Py$.

Next, consider the wall velocity component. The stream function may be written as

$$\psi_{\text{wall}} = -\int_0^x v\, dx' = -\int_0^X V\, dX' = -(40FY)^{1/4}\, f(\eta), \qquad \text{(VI.16)}$$

where

$$\begin{aligned} v &= \left[\frac{5F}{2Y}\right]^{1/2} f'(\eta) \\ \eta &= \left[\frac{5F}{32Y^3}\right]^{1/4} x \end{aligned}$$

The scalings are $U = \psi_Y$, $V = v/P$, and $X = Px$. Here F is found from (V.53) to match the surface flow to the wall jet.

For the similarity component to the core velocity, U_{sim}, which is due to the wall jet, the stream function may be written as

$$\psi_{\text{sim}} = -\left[40F\right]^{1/4}\left[\mathcal{R}(Y+iX)^{1/4} - \left(1+\sqrt{2}\right)\,\Im(Y+iX)^{1/4}\right], \tag{VI.17}$$

with the two boundary conditions that $\psi(0,Y) = -\left[40F\right]^{1/4} Y^{1/4}$ and $\psi(X,0) = 0$.

For the potential component to the core velocity using the Green's function, U_{green}, the stream function may be written as

$$\psi_{\text{green}} = -\int_0^\infty \frac{1}{2}\left[\frac{(-T)^2}{\varepsilon^2 T_X}\right]^{1/3} \frac{\partial G(\vec{X},\vec{X}_0)}{\partial y}\Big|_{y=0} dX, \tag{VI.18}$$

where the Green's function is

$$\begin{aligned} G(\vec{X},\vec{X}_0) &= \frac{1}{4\pi}\Big\{\ln\left[(x-x_0)^2+(y-y_0)^2\right] - \ln\left[(x-x_0)^2+(y+y_0)^2\right] \\ &\quad -\ln\left[(x+x_0)^2+(y-y_0)^2\right] + \ln\left[(x+x_0)^2+(y+y_0)^2\right]\Big\} \\ &= \frac{1}{4\pi}\ln\left\{\frac{\left[(x-x_0)^2+(y-y_0)^2\right]\left[(x+x_0)^2+(y+y_0)^2\right]}{\left[(x-x_0)^2+(y+y_0)^2\right]\left[(x+x_0)^2+(y-y_0)^2\right]}\right\}, \end{aligned} \tag{VI.19}$$

and

$$\frac{\partial G(\vec{X},\vec{X}_0)}{\partial y}\Big|_{y=0} = \frac{1}{\pi}\left[\frac{y_0}{(x+x_0)^2+y_0^2} - \frac{y_0}{(x-x_0)^2+y_0^2}\right] \tag{VI.20}$$

Finally, summing all of the components yields the uniform velocity, which can be written as

$$\begin{aligned} \psi_{\text{uniform}}(X,Y) &= \psi_{\text{sim}}(X,Y) + \psi_{\text{green}}(X,Y) + \psi_{\text{surface}}(X,Y/P) + \psi_{\text{wall}}(X/P,Y) \\ &\quad -\psi_{\text{surface}}(X,\infty) - \psi_{\text{wall}}(\infty,Y) \end{aligned} \tag{VI.21}$$

The Prandtl number P is simply a parameter in the model that represents how thin the boundary layers are. The boundary-layer model should be independent of P. Using the uniform stream function, a streamline field can be plotted. This is shown

in Figure 13. The horizontal velocity component increases as the distance to the wall decreases, and the vertical wall jet can clearly be seen. The flow into the corner along the surface turns down the wall, due to the jet. The upper left figure shows the complete contour plot of the stream function in the domain. The upper right figure shows the core stream function, $\psi_{\text{core}}(X,Y)$. The middle set of figures represent that portion of the stream function which is due to the wall components, $\psi_{\text{wall}}(X,Y) + \psi_{\text{sim}}(X,Y) - \psi_{\text{wall}}(\infty,Y)$ on the left and the similarity solution $\psi_{\text{sim}}(X,Y)$ on the right. The bottom row of figures shows those portions of the uniform stream function which are due to the surface components $(\psi_{\text{green}}(X,Y) + \psi_{\text{surface}}(X,Y/P) - \psi_{\text{surface}}(X,\infty))$ on the left and that due to the Green's function $(\psi_{\text{green}}(X,Y)$ on the right. A closer detail of the corner stream function dynamics is shown in Figure 14.

As can be seen, the velocity field appears to be strong enough to compress the thermal field into the cold corner. The wall jet similarity solution dominates the Green's function solution in the core flow region and overall in the steady-state solution. The few streamlines near the corner in the Green's function contour plot suggest that $h(x) = \left[\frac{(-T)^2}{\epsilon^2 T_X}\right]^{1/3}$ reaches a local maximum along the surface, not far from the corner, and the impact of $h(x)$ is strong enough to alter the velocity field in this view. However, overall, $h(x)$ does not appear to change the expected behavior of the velocity field.

E. UNIFORM TEMPERATURE

In a similar fashion to finding the uniform velocity approximation, the uniform temperature for the entire domain can be written as

$$\hat{T}_{\text{uniform}} = \hat{T}_{\text{inner}} + \hat{T}_{\text{outer}} - \hat{T}_{\text{match}}, \tag{VI.22}$$

where $\hat{T}_{\text{inner}}$ is the temperature solution pertaining to the surface boundary layer, $\hat{T}_{\text{outer}}$ is the numerically-obtained temperature solution from the ADI method (solving the unsteady two-dimensional heat equation with periodic velocity updates), and $\hat{T}_{\text{match}}$ is the matching condition which satisfies the flux condition at the surface.

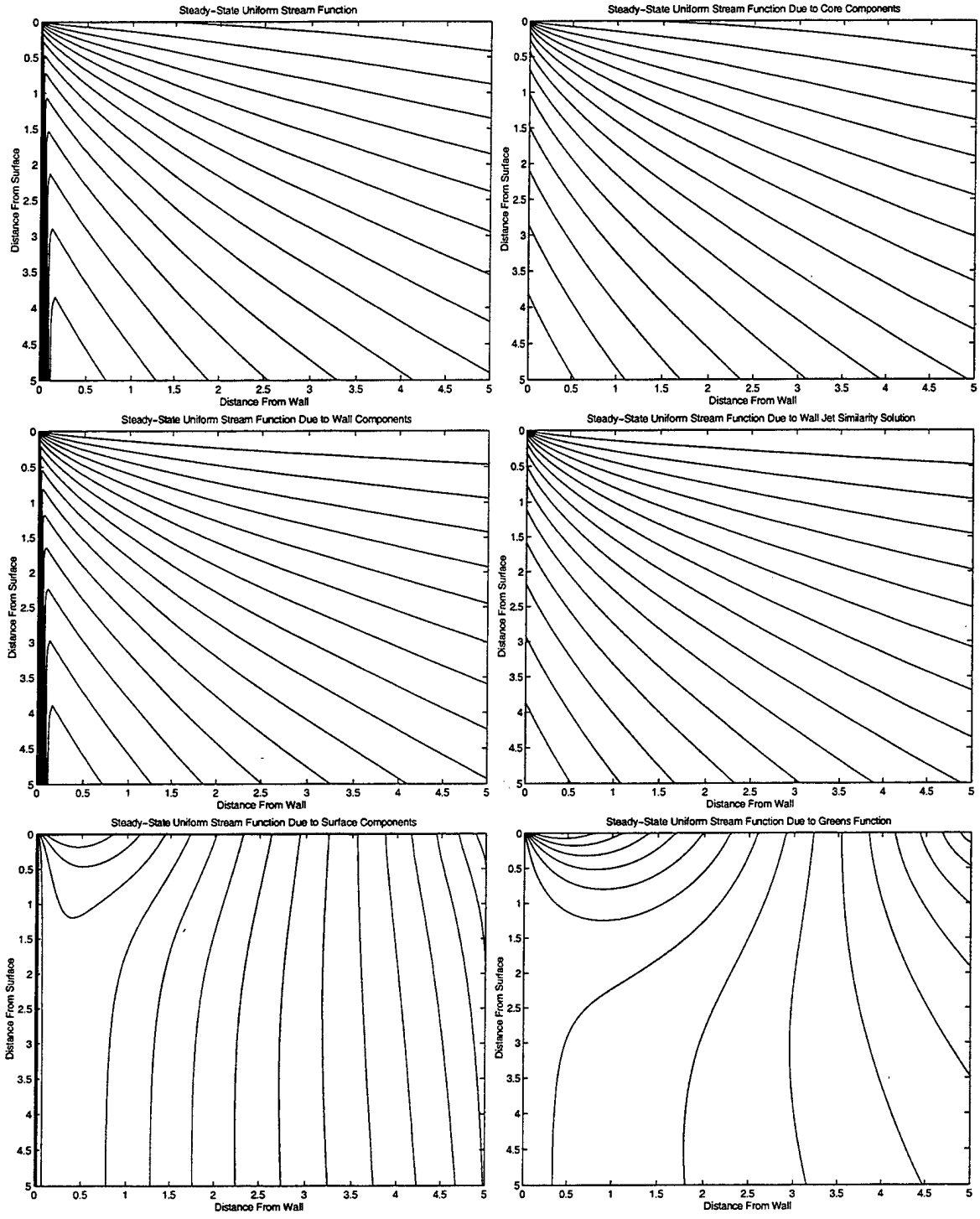

Figure 13. Uniform Stream Function and its Components

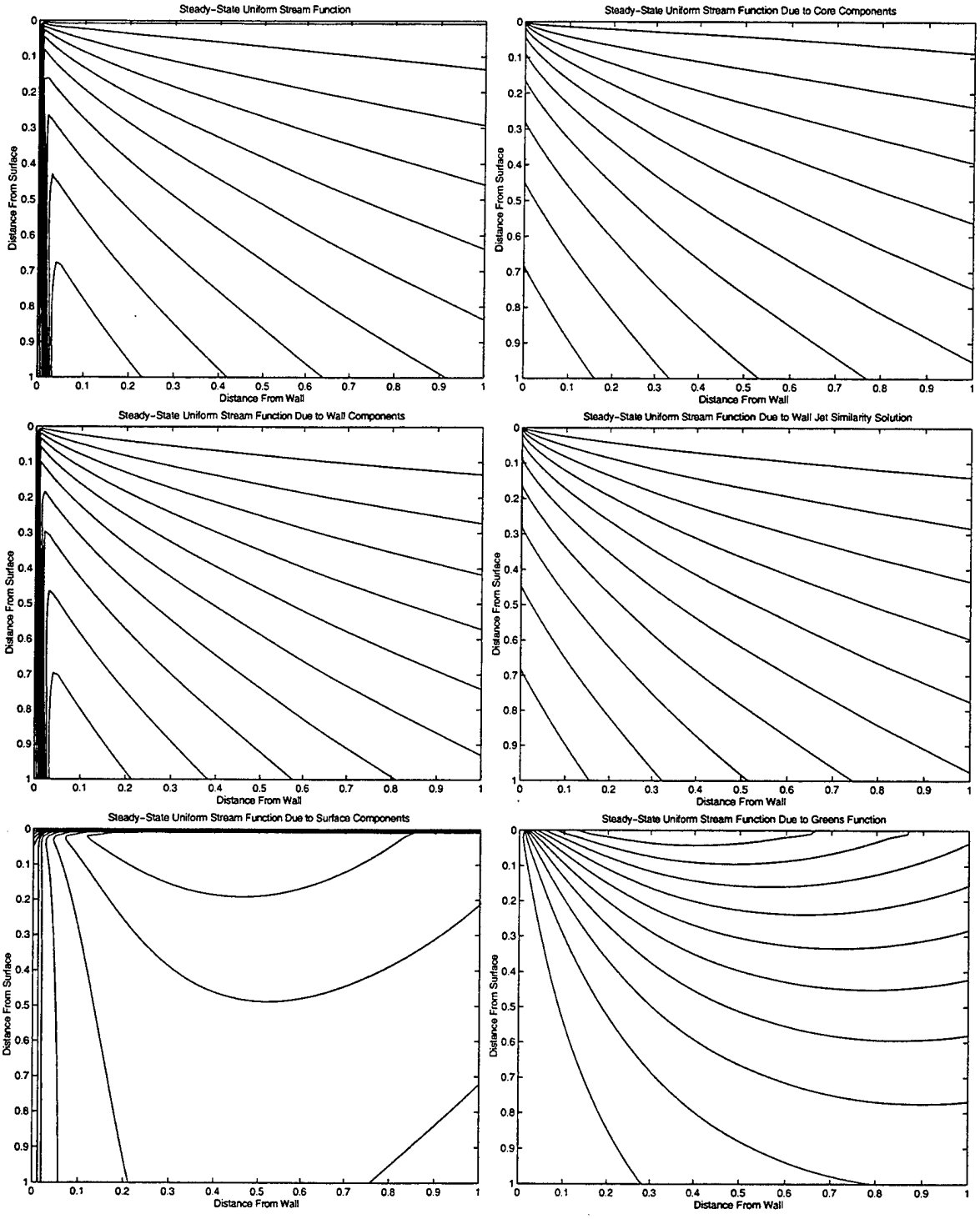

Figure 14. Uniform Stream Function and its Components — Closer Detail

Recall that the dominant balance argument gives $uT_X = t_{yy}$ as the surface heat equation (see Chapter IV).

Integrating the surface heat equation through the boundary layer gives

$$\begin{aligned} t_y(X,y) - t_y(X,0) &= \int_0^y u\,T_X\,dy' \approx T_X(X,0)\int_0^y u\,dy' \\ &= T_X(X,0)\,\psi(X,y) = t_y(X,y) + T_Y(X,0) \end{aligned} \tag{VI.23}$$

As $y \to \infty$, $t_y \to 0$, and the heat flux condition in the core region becomes

$$T_Y(X,0) = T_X(X,0)\,\psi(X,\infty) \tag{VI.24}$$

Solving for t_y yields

$$t_y(X,y) = T_X(X,0)\,[\psi(X,y) - \psi(X,\infty)] = -T_X(X,0)\int_y^\infty u\,dy' \tag{VI.25}$$

Integrating this expression from y to ∞ gives

$$t(X,\infty) - t(X,y) = -T_X(X,0)\int_y^\infty \left(\int_{y'}^\infty u\,dy''\right) dy' \tag{VI.26}$$

or

$$t(X,y) = T_X(X,0)\int_y^\infty \int_{y'}^\infty u\,dy''\,dy' \tag{VI.27}$$

From Timman's method, the horizontal component of velocity is $u = -\left[\frac{(-T)\,T_X}{\varepsilon}\right]^{2/3} g(\eta)$, where $\eta = y/\delta$, $\delta = \left[\frac{-T}{\varepsilon T_X^2}\right]^{1/3}$, $\mathrm{G}(\eta) = \int_0^\eta g(\xi)\,d\xi$, and $g(\eta) = \int_\eta^\infty e^{-s^2}\,ds = \frac{\sqrt{\pi}}{2}\mathrm{erfc}(\eta)$. Thus,

$$\begin{aligned} t_y &= T_X\,(\psi - \psi_\infty) \\ &= \left[\frac{(-T)\,T_X}{\varepsilon}\right]^{2/3}\left[-\frac{\sqrt{\pi}}{2}\int_\eta^\infty \mathrm{erfc}(\eta')\,d\eta'\right] \\ &= -\left[\frac{(-T)\,T_X}{\varepsilon}\right]^{2/3}[\mathrm{G}(\eta) - \mathrm{G}(\infty)] \\ &= \left[\frac{(-T)\,T_X}{\varepsilon}\right]^{2/3}\left[\frac{1}{2}e^{-\eta^2} - \eta\,g(\eta)\right] \end{aligned} \tag{VI.28}$$

and the temperature t may be written as

$$\begin{aligned} t &= T_X \int_y^\infty (\psi - \psi_\infty)\, dy' \\ &= -\left(\frac{-T}{\varepsilon}\right)\left[\frac{\sqrt{\pi}}{2}\int_\eta^\infty \int_{\eta'}^\infty \operatorname{erfc}(\eta'')\, d\eta''\, d\eta'\right] \\ &= \left(\frac{-T}{4\varepsilon}\right)\left[\left(1+2\eta^2\right) g(\eta) - \eta\, e^{-\eta^2}\right] \end{aligned} \tag{VI.29}$$

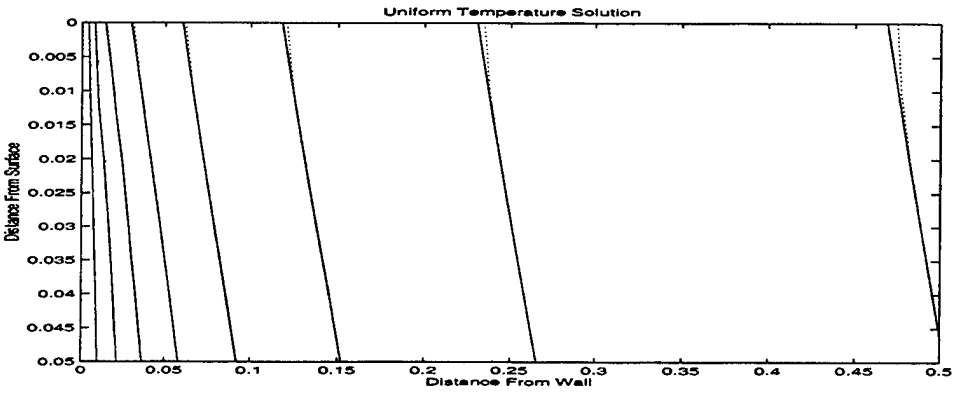

Figure 15. Uniform Temperature Solution

As can be seen in Figure 15, the uniform temperature solution (dotted contour lines) matches the steady-state solution (solid contour lines) far from the surface (as η gets large), but there is a slight difference when η is small (close to the surface), due to the G(0) term. The uniform temperature prediction *bends* toward the surface to intersect it perpendicularly, satisfying the $T_y = 0$ boundary condition.

F. VORTICITY

The vorticity plays a major role in the cold corner, turning the flow from the surface down the wall. Our model has no vorticity in the core flow region; however, the numerical data shows some vorticity there, so the flow fields look different. This is due to the hypothesis that the vorticity that is created far upstream from the corner (along the surface) diffuses into the slow flow and gets transported to the region *near* the cold corner and not into the boundary layer regions. Figure 16 shows a contour plot of the stream function (dotted contour lines) and vorticity (solid contour lines) in

the cold corner, due to Canright's numerical data. Most of the vorticity is confined to thin regions along the surface and wall (the boundary layers), but some vorticity is in the core flow region (where the streamlines are sufficiently far apart to designate slow flow). The main result is that core vorticity is not essential to the feedback process, based on the comparison of the thermal fields of the model and numerical results.

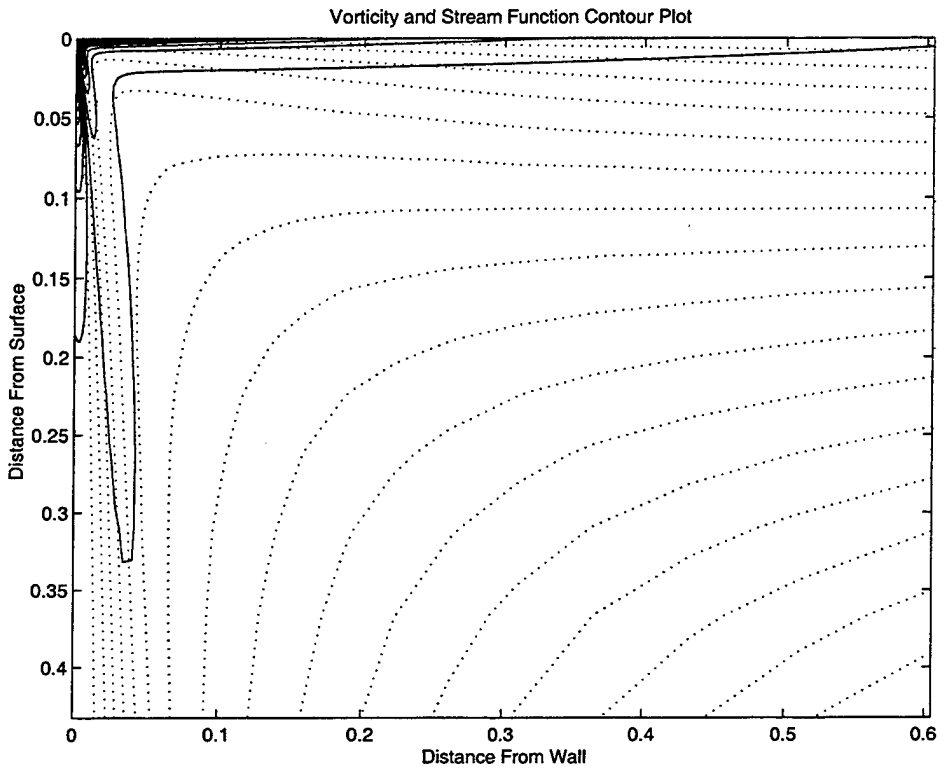

Figure 16. Vorticity and Stream Function Contour Plot (due to Canright)

To quantify Figure 16, far from the corner ($x \approx 3$), the surface value of vorticity is $O(10^3)$ smaller than than surface vorticity value at the corner ($x \to 0$). Recall that $\omega = 0$ at $x = y = 0$. Even at a distance of δ from the corner (from both the surface and the wall), the vorticity value is $O(10^2)$ smaller than the peak value in the corner. Thus, the vorticity outside the boundary layers is non-zero but insignificant compared to the boundary-layer values and is not essential to our model.

VII. CONCLUSIONS AND DISCUSSION

COMPLEX HAPPENS. — *David Canright*

The thermocapillary stress condition at the free surface gives a starting point for the scalings and dominant balance. We have obtained relations for the thermal length scale l, the viscous thickness δ, the surface velocity u, and the core velocity U scales in the cold corner, in terms of the dimensionless parameters M and P. These scalings are

$$\begin{aligned} \delta &\sim M^{-1}P^{-1}, \\ l &\sim M^{-1}P^{-2}, \\ u &\sim P, \\ U &\sim P^2. \end{aligned}$$

These scalings are consistent with the numerical results obtained by Canright in his 1994 work [Ref. 1].

The temperature gradient, T_X, on the surface drives the strong surface flow, similar to a surface jet. In the viscous surface boundary layer, a modification to Timman's method was employed which allowed the surface velocity to be modeled as

$$u = -\frac{\sqrt{\pi}}{2}\,\varepsilon^{-1/3}\,(-T)^{1/3}\,(T_X)^{1/3}\,\mathrm{erfc}(\eta), \tag{VII.1}$$

where ε is a constant and $\eta = y/\delta$. The boundary-layer thickness δ in terms of the surface temperature is

$$\delta(X) = \left[-\frac{T}{T_X^2\,\varepsilon}\right]^{1/3}. \tag{VII.2}$$

The surface flow then feeds into the corner and into the wall flow, similar to a wall jet. In the viscous wall boundary layer, a modification to Glauert's method was

employed which allowed the wall velocity to be modeled as

$$v = \left(\frac{5F}{2Y}\right)^{1/2} f'(\eta), \tag{VII.3}$$

where

$$\eta = \left(\frac{5F}{32\,Y^3}\right)^{1/4} x \tag{VII.4}$$

and F, the flux of exterior momentum flux, is found from matching the surface velocity as

$$F = \frac{16\sqrt{\pi}}{5}\left(\frac{T_X}{2\varepsilon}\right)^{1/3}. \tag{VII.5}$$

Using these expressions for the velocity components, the stream functions were calculated. The strong flow in the viscous boundary layers induces a relatively weak irrotational flow in the core region. Two approaches were employed to find the core velocities: a Laplace's equation solver using a Green's function, and a complex-variables solution modeled after a self-similar plane wall jet. These velocities were then substituted into the unsteady heat equation and an alternating-direction implicit (ADI) numerical scheme was employed to solve for the temperature. The weak core flow then contains a thermal gradient which was used to determine the T_X on the surface. Once found, the surface temperature gradient was used to update the surface velocity and the process was iterated until steady state was reached.

When the flow along the wall is modeled as a wall jet, a modification to Plotkin's second-order approach was used to match our boundary conditions in the quarter-plane. Thus, the potential solution becomes

$$\psi(X,Y) = -4\left[\mathcal{R}(Y+iX)^{1/4} - \left(1+\sqrt{2}\right)\,\Im(Y+iX)^{1/4}\right]. \tag{VII.6}$$

The velocity components may be found by $U = \frac{\partial\psi}{\partial Y}$ and $V = -\frac{\partial\psi}{\partial X}$.

It is found that the flow into the cold corner is strong enough to contain the thermal field. The isotherms are compressed along the wall after steady-state is reached. The temperature profile obtained from the ADI method compares favorably

with Canright's numerical data from 1994. Considering the simplicity of our model, the results are very encouraging. The thermal field results are self-consistent.

The prediction model of the uniform velocity vector field is encouraging, in that it matches the inner, boundary-layer flow to the outer, core flow, and subtracts the matching flow elements. The basic model applies for the whole range of Marangoni and Prandtl numbers in the convective-inertial regime. The uniform flow *picture* will change with a changing Prandtl number, reflecting the relative thickness of the viscous boundary layers, but the underlying *model* does not change. In addition, because this model seems to capture the cold corner feedback process, these results could be useful as a local solution in a larger numerical problem, without the need to numerically resolve the viscous boundary layers.

THIS PAGE INTENTIONALLY LEFT BLANK

VIII. FUTURE WORK

WE ASK, WITH THE EXTENSION OF MATHEMATICAL KNOWLEDGE WILL IT NOT FINALLY BECOME IMPOSSIBLE FOR THE SINGLE INVESTIGATOR TO EMBRACE ALL THE DEPARTMENTS OF THIS KNOWLEDGE? — *David Hilbert*

There are a few limitations to this work. The grid used in the numerical approximations is uniform. To get a more accurate description of the velocity and temperature fields, a non-uniform grid should be employed, which is finer near the corner and more coarse away from the corner, as in Canright's 1994 work. Even so, the current data shows good correlation with the previous work. A nonuniform grid would require a more complicated algorithm but may run faster for a given resolution in the corner, especially since running of the current ADI codes with updates required hours for several thousand iterations.

More effort should be placed on the effects of vorticity in the corner. In the numerical data, the vorticity does not appear to be entirely confined to the boundary layers, yet the vorticity in the core flow region seems to have no significant impact on the temperature field solution. It appears that the core flow does not turn down the wall if vorticity is not present. The vorticity in the surface and wall boundary layers must be strong enough to force the nonlinear flow at the free surface down the rigid wall. At this point, we can estimate the magnitude of the vorticity, but more research is needed to determine how to combine the vorticity into the potential flow. A meaningful approach to modeling the vorticity throughout the domain would provide a good understanding of the rotation mechanism in the flow. This was addressed in Chapter VI.

This research simplified the physical problem. The geometry was revised, some material properties were ignored, and the free surface was assumed flat due to the

amount of surface tension. If a geometry change occurs, that should be investigated in future research.

Also, higher-order modifications to Timman's method should be attempted. This would provide more accuracy near the free surface. The current model predicts the decay of the velocity through the boundary layer fairly well, until the interface with the core region is approached, and then the Timman modification decays faster. If a four-parameter model could be developed, it might better depict the velocity profile using the thermocapillary condition at the surface.

As more experiments are conducted in the low-gravity environment, such as those using the NASA space shuttles by Kamotani and Ostrach and others, a validation of the current work using experimental techniques should be attempted.

APPENDIX A. TIMMAN'S METHOD ALONG THE SURFACE

Even though the one-parameter model is very encouraging, the goal is to try to derive a more accurate velocity profile than the simplest approach in Chapter V, since the surface tension and thermocapillary condition at the surface is driving the flow. Now, suppose the velocity profile for $u(y)$ (where the X dependence is implicit) is

$$u(y) = f(\eta) = \int_{\eta}^{\infty} e^{-t^2} \left(a(X) + c(X)t^2\right) dt - b(X)e^{-\eta^2}. \tag{A.1}$$

This introduces a damping term into the velocity profile. Is there a more accurate expression for the boundary-layer thickness? At the surface, $y = \eta = 0$, which implies that

$$\begin{aligned} u(0) = f(0) &= \int_{0}^{\infty} e^{-t^2} \left(a(X) + c(X)t^2\right) dt - b(X) \\ &= \frac{\sqrt{\pi}}{2}a(X) + \frac{\sqrt{\pi}}{4}c(X) - b(X) \end{aligned} \tag{A.2}$$

In the core flow region, as $y \to \infty$, $\eta \to \infty$, and $f(\infty) = 0$.

Differentiating $f(\eta)$, $f'(\eta) = e^{-\eta^2}\left[-a(X) - c(X)\eta^2 + 2b(X)\eta\right]$. Evaluating this at the surface gives $f'(0) = -a$, which yields $a(X) = -\delta(X)T_X$, just as in Chapter V (when $b(X) = c(X) = 0$).

Differentiating further yields $f''(\eta)$, which when evaluated at the surface gives $f''(0) = 2b(X)$. Since $f(\eta) = u$, $f'(\eta) = \delta(X)u_y$, and $f''(\eta) = \delta^2(X)\,u_{yy}$. Thus, $b(X) = \frac{1}{2}\,\delta^2(X)\,u(0)\,u_X(0)$ at the surface.

Taking the third derivative of $f(\eta)$, $f'''(\eta)$ is a very lengthy expression. u_{yyy} can be rewritten as $\frac{d}{dy}\,(u_{yy})$, which after substitution into the momentum equation becomes $\frac{d}{dy}(u\,u_x + V\,u_y)$. This can be simplified using the continuity equation and the fact that $v(0) = 0$. Evaluation at the surface yields $f'''(0) = \delta^3\,u(0)\,T_{XX}$. Since $f'''(0) = 2a(X) - 2c(X)$, we can solve for $c(X)$.

The proposed velocity profile at the surface is therefore

$$u(y) = f(\eta) = -\int_{\eta}^{\infty} \left[\delta(X)T_X + \left\{\delta T_X + \frac{1}{2}\delta^3 u(0)T_{XX}\right\} t^2\right] e^{-t^2} dt - \frac{1}{2}\delta^2(X)u(0)u_X(0)e^{-\eta^2}. \tag{A.3}$$

Hence, a first-order, nonlinear, nonhomogeneous ordinary differential equation for the velocity can be developed in terms of the boundary-layer thickness and the temperature gradient as (let $u(0) = u_0$):

$$u_0 u_0' + u_0\left(\frac{2}{\delta^2} + \frac{\sqrt{\pi}}{4}\delta T_{XX}\right) = -\frac{3\sqrt{\pi}}{2\delta}T_X \tag{A.4}$$

where $u_0' = \frac{d}{dX}u(0)$. This gives one equation with two unknowns, $u_0(X)$ and $\delta(X)$. We also have $\delta_2 = -T = \delta\int_0^{\infty} u^2 d\eta$. This type of ordinary differential equation (A.4) can be known as an Abel Equation of the Second Kind [Ref. 33]. Finding a solution to this type of equation is available only for certain cases, such as if the coefficients of $u_0 u_0'$ and u_0 fall into special categories outlined in [Ref. 34, 35]. Unfortunately, this particular ODE does not fall into one of those special cases.

A second approach to modeling the velocity with a Timman-type method of two parameters is algebraic. Write the velocity profile as

$$u = f(\eta) = \int_{\eta}^{\infty} ae^{-t^2} dt - be^{-\eta^2}.$$

(Remember that the variables a and b are functions of X; however, for simplicity, the $a(X)$ and $b(X)$ will be replaced by a and b). Using three derivatives evaluated at $y = 0$ will enable us to obtain an expression for u in terms of the boundary-layer thickness and then in only temperature terms. Recall that

$$f(0) = \frac{\sqrt{\pi}}{2}a - b$$

Taking derivatives of f with respect to η and using the chain rule since $y = \delta\eta$, we obtain

$$\begin{aligned} f'(\eta) &= e^{-\eta^2}(-a + 2b\eta) = \delta u_y \\ f'(0) &= -a = \delta\left(u_y\right)_{y=0} = \delta T_X \end{aligned} \tag{A.5}$$

Thus, $a = -\delta T_X$. Continuing,

$$\begin{aligned} f''(\eta) &= e^{-\eta^2}(2b + 2a\eta - 4b\eta^2) = \delta^2 u_{yy} \\ f''(0) &= 2b \end{aligned} \tag{A.6}$$

$$\begin{aligned} f'''(\eta) &= e^{-\eta^2}\left[2a - 8b\eta - 2\eta(2b + 2a\eta - 4b\eta^2)\right] = \delta^3 u_{yyy} \\ f'''(0) &= 2a = -2\delta T_X \end{aligned} \tag{A.7}$$

Recall that $u_{yyy} = \frac{d}{dy}(u_{yy}) = \frac{d}{dy}(uu_X + Vu_y) = u\,T_{XX}$. Thus

$$f'''(0) = \delta^3 u(0)\,T_{XX} = \delta^3\left(\frac{\sqrt{\pi}}{2}a - b\right)T_{XX} = \delta^3\left(-\frac{\sqrt{\pi}}{2}\delta T_X - b\right)T_{XX}$$

which, when equating the $f'''(0)$ terms, finally yields

$$2\delta T_X = \delta^3\left(\frac{\sqrt{\pi}}{2}\delta T_X + b\right)T_{XX} \tag{A.8}$$

so that

$$b = \frac{2T_X}{\delta^2 T_{XX}} - \frac{\sqrt{\pi}}{2}\delta T_X \tag{A.9}$$

and the velocity profile can now be modeled as

$$\begin{aligned} u &= -\int_\eta^\infty \delta T_X\, e^{-t^2}\, dt - \left[\frac{2T_X}{\delta^2 T_{XX}} - \frac{\sqrt{\pi}}{2}\delta T_X\right] e^{-\eta^2} \\ &= -\frac{\sqrt{\pi}}{2}\,\delta T_X\,\mathrm{erfc}(\eta) - \left[\frac{2T_X}{\delta^2 T_{XX}} - \frac{\sqrt{\pi}}{2}\delta T_X\right] e^{-\eta^2}. \end{aligned} \tag{A.10}$$

Recalling (V.9), the boundary-layer thickness δ can be solved as

$$\delta(X) = \frac{-T}{\int_0^\infty u^2\, d\eta} \tag{A.11}$$

This yields a quadratic equation in δ^3, which is:

$$\delta^6\left[T_X^2\left\{\varepsilon + \pi^{3/2}\left(\frac{2+\sqrt{2}}{16}\right)\right\}\right] + \delta^3\left[T - \frac{\pi T_X^2}{2T_{XX}^2}\left(\sqrt{2}-1\right)\right] + \frac{\sqrt{2\pi}\,T_X^2}{T_{XX}^2} = 0 \tag{A.12}$$

At the corner, with T, T_X, and T_{XX} values taken from the numerical data at $x = 0$, the boundary-layer thickness $\delta(X)$ is $O(M^{-1}P^{-1})$, as expected. As X

increases from the wall, $\delta(X)$ decreases in value, also as expected. However, after a certain value of X, still within the corner region, the solution to (A.12) results in complex roots. Unfortunately, this means that the algebraic two-parameter approach had to be abandoned.

APPENDIX B. CALCULATION OF ε

In the surface boundary-layer thickness equation, (V.22), the constant

$$\varepsilon = \frac{\pi}{4}\int_0^\infty [\mathrm{erfc}(\eta)]^2\, d\eta$$

is found to be

$$\varepsilon = \frac{\sqrt{\pi}}{2}\left(1 - \frac{\sqrt{2}}{2}\right).$$

Here is the work. Integration by parts is necessary. Define $I = \int_0^\infty [\mathrm{erfc}(\eta)]^2\, d\eta$, such that $\varepsilon = \frac{\pi}{4}I$. Let $u = [\mathrm{erfc}(\eta)]^2$ and $dv = d\eta$. Then $du = \mathrm{erfc}(\eta)\left(-\frac{4}{\sqrt{\pi}}e^{-\eta^2}\right)d\eta$ and $v = \eta$. Thus

$$I = \eta\,[\mathrm{erfc}(\eta)]^2\Big|_0^\infty + \frac{4}{\sqrt{\pi}}\int_0^\infty \eta\, e^{-\eta^2}\,\mathrm{erfc}(\eta)\, d\eta$$

Since $\mathrm{erfc}(\infty) = 0$,

$$I = \frac{4}{\sqrt{\pi}}\int_0^\infty \eta\, e^{-\eta^2}\,\mathrm{erfc}(\eta)\, d\eta$$

$$= \frac{2}{\sqrt{\pi}}\int_0^\infty 2\eta\, e^{-\eta^2}\mathrm{erfc}(\eta) d\eta$$

Integrate by parts again. Let $u = \mathrm{erfc}(\eta)$ and $dv = 2\eta\, e^{-\eta^2} d\eta$. Then $du = -\frac{2}{\sqrt{\pi}}e^{-\eta^2}d\eta$ and $v = -e^{-\eta^2}$. Hence,

$$I = \frac{2}{\sqrt{\pi}}\left[-e^{-\eta^2}\mathrm{erfc}(\eta)\Big|_0^\infty - \frac{2}{\sqrt{\pi}}\int_0^\infty e^{-2\eta^2} d\eta\right]$$

$$= \frac{2}{\sqrt{\pi}}\left[1 - \frac{2}{\sqrt{\pi}}\int_0^\infty e^{-2\eta^2} d\eta\right]$$

Use the transformation $w = \sqrt{2}\eta$. Then $dw = \sqrt{2}d\eta$. Substituting,

$$I = \frac{2}{\sqrt{\pi}}\left[1 - \frac{2}{\sqrt{\pi}}\frac{1}{\sqrt{2}}\int_0^\infty e^{-w^2} dw\right]$$

$$= \frac{2}{\sqrt{\pi}}\left[1 - \frac{\sqrt{2}}{\sqrt{\pi}}\frac{\sqrt{\pi}}{2}\right] = \frac{2}{\sqrt{\pi}}\left(1 - \frac{\sqrt{2}}{2}\right)$$

Therefore,

$$\begin{aligned}\varepsilon &= \frac{\pi}{4} I \\ &= \frac{\pi}{4} \frac{2}{\sqrt{\pi}} \left(1 - \frac{\sqrt{2}}{2}\right) \\ &= \frac{\sqrt{\pi}}{2} \left(1 - \frac{\sqrt{2}}{2}\right).\end{aligned}$$

APPENDIX C. VORTICITY FLUX

The vorticity equation in the wall boundary layer is

$$U\,\omega_x + v\,\omega_Y = \omega_{xx}$$

This can be rewritten as $(U\,\omega)_x + (v\,\omega)_Y = \omega_{xx}$ using continuity. Now, integrate this with respect to x, obtaining

$$U\,\omega\Big|_{x=0}^{\infty} + \frac{d}{dY}\int_0^{\infty} v\,\omega\,dx = \omega_x\Big|_{x=0}^{\infty} \tag{C.1}$$

As $x \to \infty$, $\omega \to 0$ (and $\omega_x \to 0$), and when $x = 0$, $U = 0$, so that

$$\frac{d}{dY}\int_0^{\infty} v\,\omega\,dx = -\omega_x\Big|_{x=0} \tag{C.2}$$

The vorticity can also be written as $\omega = v_x - U_Y$. From the continuity equation,

$$U = -\int_0^x v_Y\,dx$$

which yields

$$\omega = v_x + \frac{d}{dY}\int_0^x v_Y\,dx = v_x + \int_0^x v_{YY}\,dx. \tag{C.3}$$

A scaling analysis is performed on the vorticity terms. In the wall boundary layer, $\hat{x} \sim \Delta \sim M^{-1}P^{-1}\,x$, $\hat{y} \sim L \sim M^{-1}P^{-2}\,Y$, $\hat{u} \sim P^2\,U$, $\hat{v} \sim P\,v$, and $\hat{\omega} \sim MP^2\omega$. Substituting into $\hat{\omega} = \hat{v}_{\hat{x}} - \hat{u}_{\hat{y}}$ yields $MP^2\omega = MP^2\,v_x + MP^4\,U_Y$. The last term on the right is much smaller than the first term on the right (since $P \ll 1$), giving $\omega = v_x$. Thus, the vorticity ω can be characterized by v_x, ignoring the $\int_0^x v_{YY}\,dx$ term as small. This result is consistent with the numerical data of Canright [Ref. 1], as shown in Figure 17 (the vorticity plot is the solid line, the velocity derivative plot is the dotted line). As can be seen, the two plots are virtually identical for given horizontal slices of the vorticity and vertical velocity flux (in this case, at a depth of $U = 0.0584$).

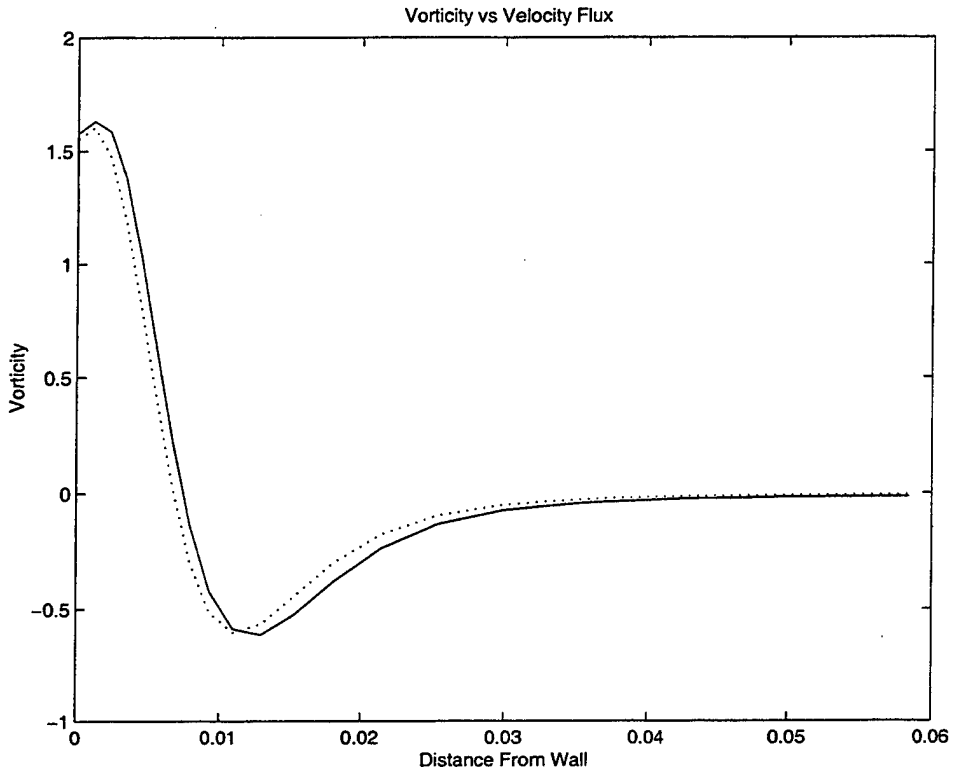

Figure 17. Typical Vorticity and Vertical Velocity Flux Profiles at the same Depth from the Free Surface

Back to the equation for the vorticity flux,

$$\begin{aligned} \omega_x\Big|_{x=0} &= -\frac{d}{dY}\int_0^\infty v\, v_x\, dx \\ &= -\frac{1}{2}\frac{d}{dy}\left(v^2\Big|_0^\infty\right)dx \\ &= 0 \end{aligned} \tag{C.4}$$

This shows that the vorticity flux at the wall is zero! Very unexpected. Substituting in the expression for v and v_x and then evaluating the integral does indeed yield 0. Perhaps a higher order expansion for the velocity is needed, such as $v \approx Pv_1 + P^2v_2 + \cdots$, to resolve the diffusion of vorticity from the wall.

APPENDIX D. TIMMAN'S METHOD ALONG THE WALL

The velocity profile approximation for the wall boundary layer is a little more complicated than the surface profile approximation. The no-slip condition at the wall requires that the velocity is zero when $x = 0$. Also, the core velocity goes to 0, so the boundary condition as $x \to \infty$ requires a zero velocity. Between these two values of x, the velocity increases to the point in the boundary layer where the positive vorticity goes to zero, then the velocity decays through the boundary layer where the vorticity is negative (that vorticity which is convected down from the surface) until the velocity decays to zero.

The following approximate velocity profile is assumed:

$$v(x) = f(\eta) = -\int_{\eta}^{\infty} e^{-t^2}(a + ct^2)\,dt + e^{-\eta^2}(b + d\eta^2), \tag{D.1}$$

where $f(\eta) = v$, the vertical (dominant) component of the wall velocity, and $\eta = \frac{x}{\Delta}$, where Δ is the thickness of the wall boundary layer. The boundary conditions are: at $x = 0$, $\eta = 0$, and $f(\eta) = 0$, due to the no-slip condition. As $x \to \infty$, $\eta \to \infty$, and $f(\eta) \to 0$.

The determination of the coefficients a, b, c, and d must be made. All four coefficients are functions of Y, the vertical direction. Start with the momentum direction in the Y-direction,

$$Uv_x + vv_Y = v_{xx} \tag{D.2}$$

Integrate this equation with respect to x, from $x = 0$ at the wall to $x = \infty$, outside the vertical boundary layer. This yields

$$\int_0^{\infty} (Uv_x + vv_Y)\,dx = v_x\Big|_0^{\infty} \tag{D.3}$$

Substitute the shear stress at the wall, τ_0, as $\tau_0 = \left(\frac{\partial v}{\partial x}\right)_{x=0} = v_x$. Thus,

$$-\tau_0 = \int_0^{\infty} (Uv_x + vv_Y)\,dx \tag{D.4}$$

$$= \int_0^\infty (Uv)_x \, dx + \int_0^\infty (vv)_Y \, dx$$

$$= (Uv)\Big|_0^\infty + \int_0^\infty (vv)_Y \, dx$$

$$= \frac{d}{dY} \int_0^\infty v^2 \, dx \tag{D.5}$$

Define the momentum thickness to be Δ_2, where

$$\Delta_2 = \int_{x=0}^\infty v^2 \, dx.$$

Then

$$\Delta_2 = \int_{x=0}^\infty v^2 \, dx = \int_{x=0}^\infty f^2 \, dx. \tag{D.6}$$

Since $\eta = \frac{x}{\Delta}$, $dx = \Delta \, d\eta$, and

$$\Delta_2 = \Delta \int_{x=0}^\infty v^2 \, d\eta, \tag{D.7}$$

with Δ being the boundary-layer thickness. Therefore,

$$-\tau_0 = \frac{d\Delta_2}{dY}. \tag{D.8}$$

The derivative conditions on the function $f(\eta)$ evaluated at the wall are as follows:

$$\begin{aligned} f(0) &= b - \frac{\sqrt{\pi}}{2}\left(a + \frac{c}{2}\right) \\ f'(0) &= a \\ f''(0) &= 2(d - b) \\ f'''(0) &= 2(c - a) \\ f^{\text{iv}}(0) &= 12(b - 2d) \end{aligned}$$

Since $f = v$, $f(0) = 0$, as the velocity at the wall is zero. Since there is no pressure gradient term in the momentum equation, the pressure is constant, and $f''(0) = 0$.

In addition, $f'''(0) = 0$, from the given boundary conditions [Ref. 31]. These last two conditions yield $a = c$ and $b = d$. The first condition gives $a = \frac{4}{3\sqrt{\pi}}b$. One more condition is needed to solve for the four coefficients. The value of the shear stress at the wall is unknown, so $f'(0)$ is not specified, and the expression for $f^{\text{iv}}(0)$ is needed. Taking the fourth derivative of f with respect to η yields $f^{\text{iv}}(\eta) = \Delta^4 v_x v_{xY}$. Since $f'(\eta) = \Delta v_x$, then $a = \Delta v_x$, evaluated at $x = 0$, and the last condition yields $f^{\text{iv}}(\eta) = \Delta^3 a \frac{d}{dY}\left(\frac{a}{\Delta}\right)$.

Equating the various derivative conditions yields two nonlinear equations involving the boundary-layer thickness Δ and the coefficient a. These are

$$-\tau_0 = \frac{d}{dY}(\Delta_2)$$

and

$$-12b = \Delta^3 a \frac{d}{dY}\left(\frac{a}{\Delta}\right)$$

Evaluating the integral associated with Δ_2 numerically, the first equation can be worked to the form

$$\begin{aligned} -\tau_0 &= \frac{d}{dY}\Delta_2 \\ -v_x\big|_{x=0} &= \frac{d}{dY}\left(\frac{1}{3}a^2\Delta\right) \\ \frac{a}{\Delta} &= \frac{1}{3}\left(a^2\Delta_Y + 2a\Delta a_Y\right) \\ \frac{3}{\Delta} &= a\Delta_Y + 2\Delta a_Y \end{aligned} \tag{D.9}$$

while the second equation can be worked to a similar form

$$\begin{aligned} -12b = -9\sqrt{\pi} &= \Delta^3 a \frac{d}{dY}\left(\frac{a}{\Delta}\right) \\ -9\sqrt{\pi} &= \Delta^3\left(\frac{1}{\Delta}a_Y - \frac{a}{\Delta^2}\Delta_Y\right) \end{aligned}$$

$$\frac{9\sqrt{\pi}}{\Delta} = a\Delta_Y - \Delta a_Y \tag{D.10}$$

These equations may be further reduced to

$$a_Y = \frac{1}{\Delta^2}(1 - 3\sqrt{\pi}) \tag{D.11}$$

and

$$\Delta_Y = \frac{1}{\Delta a}(1 + 6\sqrt{\pi}) \tag{D.12}$$

Initial conditions need to be specified on the displacement thickness (call it the mass flux) and on the flux of vorticity. The mass flux and the vorticity flux must be matched to the free surface boundary layer, so more than one free parameter may be needed.

If $d = 0$, then from the initial conditions, $b = 0$, which further means that $a = -\frac{c}{2}$. The velocity profile is then

$$f(\eta) = v = a\int_{\eta}^{\infty} e^{-t^2}(2t^2 - 1)\,dt. \tag{D.13}$$

This approach proved to be more difficult than expected and was abandoned in favor of the modification to Glauert's method.

APPENDIX E. NUMERICAL CODES

MAY YOU CONVERGE WITHOUT DELAY. – *Dan Zinder*

The computer programs listed here are supplied on an "as is" basis, with no warrantees of any kind. The author bears no responsibility for any consequences of using this program.

```
/* this file: fluid.h - header definitions for cold corner */

#include <stdio.h>
#include <math.h>
#define maxx 3001
#define maxxvec (maxx - 2)
#define Ma 10000
#define Pr 0.01
#define eps (sqrt(3.14159265)*(1.0-sqrt(2.0)/2.0)/2.0)

#ifdef MAIN

int i, j, k, nx, ny;
int size;
double hx, hy, dt;
double x[maxx], y[maxx], b[maxx], xx[maxx], f[maxx];
double xcon1, xcon2, ycon1, ycon2;
double c1[maxx][maxx], c2, c3[maxx][maxx], c4[maxx][maxx], c5,
c6[maxx][maxx];
double d1[maxx][maxx], d2, d3[maxx][maxx], d4[maxx][maxx], d5,
d6[maxx][maxx];
double t[maxx][maxx], temp[maxx][maxx], tstar[maxx][maxx];
double hofx[maxx], integrand[maxx], grnfun[maxx];
double gpsi[maxx][maxx], jpsi[maxx][maxx], psi[maxx][maxx];
double wpsi[maxx][maxx], spsi[maxx][maxx], unifpsi[maxx][maxx];
double u[maxx][maxx], v[maxx][maxx];
double surfu, massflux, F, eta, g;
double delta[maxx], seta[maxx];
double tempa[maxxvec], tempb[maxxvec], tempc[maxxvec];
double tstarn[maxx], Tx[maxx], Txx[maxx];
double A[3][maxx], C[3][maxx];

#undef MAIN
#else
extern int i, j, k, nx, ny;
extern int size;
extern double hx, hy, dt;
extern double x[], y[], b[], xx[], f[];
extern double xcon1, xcon2, ycon1, ycon2;
extern double c1[][maxx], c2, c3[][maxx], c4[][maxx], c5, c6[][maxx];
extern double d1[][maxx], d2, d3[][maxx], d4[][maxx], d5, d6[][maxx];
extern double t[][maxx], temp[][maxx], tstar[][maxx];
```

```
extern double hofx[], integrand[], grnfun[];
extern double gpsi[][maxx], jpsi[][maxx], psi[][maxx];
extern double wpsi[][maxx], spsi[][maxx], unifpsi[][maxx];
extern double u[][maxx], v[][maxx];
extern double surfu, massflux, F, eta, g;
extern double delta[], seta[];
extern double tempa[], tempb[], tempc[];
extern double tstarn[], Tx[], Txx[];
extern double A[][maxx], C[][maxx];

#endif
```

```
/* this file: main.c - main program for cold corner */

#define MAIN
#include "fluid.h"
#define LINESIZE 128
#define eps (sqrt(3.14159265)*(1.0-sqrt(2.0)/2.0)/2.0)

main(argc,argv)
int argc; char *argv[];
{

double adi(),  tol=0.001, norm;
int n, m, ninner=6, nouter=6;
if ( argc > 1 ) sscanf( argv[1], "%d", &ninner );
if ( argc > 2 ) sscanf( argv[2], "%d", &nouter );
if ( argc > 3 ) sscanf( argv[3], "%lf", &tol );

n = 10;
adiinit();
for (m = 1; n > 2 && m <= nouter; m++){
   tx();
   strength();
   jet();
   green();

   for (i = 0; i <= nx; i++){
      for (j = 0; j <= ny; j++){
         psi[i][j] = jpsi[i][j] + gpsi[i][j];
      }
   }

   for (i = 0; i <= nx; i++){
      for (j = 0; j <= ny; j++){
         if (i == 0 & j != 0){
            u[i][j] = (psi[i][j+1] - psi[i][j-1]) / ((2.0)*(y[j+1] - y[j]));
            v[i][j] = - (psi[i+1][j] - psi[i][j]) / (x[i+1] - x[i]);}
      else if (j == 0 & i != 0){
            u[i][j] = (psi[i][j+1] - psi[i][j]) / (y[j+1] - y[j]);
            v[i][j] = - (psi[i+1][j] - psi[i-1][j]) / ((2.0)*(x[i+1] - x[i]));}
      else if (i == nx){
            u[i][j] = (psi[i][j+1] - psi[i][j-1]) / (2.0*(y[j+1] - y[j]));
            v[i][j] = - (psi[i][j] - psi[i-1][j]) / (x[i] - x[i-1]);}
```

```
      else if (j == ny){
            u[i][j] = (psi[i][j] - psi[i][j-1]) / (y[j] - y[j-1]);
            v[i][j] = - (psi[i+1][j] - psi[i-1][j]) / (2.0*(x[i+1] - x[i]));
            u[nx][ny] = v[nx][ny] = 0.0;}
      else{
            u[i][j] = (psi[i][j+1] - psi[i][j-1]) / ((2.0)*(y[j+1] - y[j]));
            v[i][j] = - (psi[i+1][j] - psi[i-1][j]) / ((2.0)*(x[i+1] - x[i]));}
/*    printf("%1.2f %1.2f %1.5f %1.5f\n", x[i], y[j], u[i][j], v[i][j]); */
      }
   }

   norm = 1.0;
   for (n = 1; norm > tol && n < ninner; n++){
      norm = adi();
/*    printf("Iteration number %d, norm: %f\n",n,norm); */
   }
   fprintf(stderr, "Iteration = %d\n", m);
}

for (i = 0; i <= nx; i++){
   for (j = 0; j <= ny; j++){
      printf("%1.3f %1.3f %1.6f\n", x[i], y[j], temp[i][j]);
   }
}

}
```

```
/* this file: adiinit.c - initialization for cold corner */

#include "fluid.h"

adiinit() {

nx = ny = maxx - 1;
hx = hy = 3.0 / nx;
dt = 0.4 * hx;

xcon1 = dt / (hx * hx);
xcon2 = dt / (4.0 * hx);
ycon1 = dt / (hy * hy);
ycon2 = dt / (4.0 * hy);
/* printf("%1.4f %1.4f %1.4 %1.4f\n", xcon1, xcon2, ycon1, ycon2); */

c2 = 1.0 + xcon1;
c5 = 1.0 - ycon1;
d2 = 1.0 + ycon1;
d5 = 1.0 - xcon1;

for (i = 0; i <= nx ; i++){
   x[i] = y[i] = i * hx;
   f[i] = 0.0;
}

/* printf("            initial\n");
printf("x[i]  y[j]  temp[i][j]\n"); */
for (i = 0; i <= nx ; i++){
   for (j = 0; j <= ny ; j++){
      if (i == 0)
         temp[i][j] = tstar[i][j] = -1.0;
      else if (i == nx)
         temp[i][j] = tstar[i][j] = 0.0;
      else if (j == 0)
         temp[i][j] = -exp(-10.0 * x[i]);
      else
         temp[i][j] = tstar[i][j] = 0.0;
/*       printf("%1.3f  %1.3f  %1.4f\n", x[i], y[j], temp[i][j]); */
   }
}
}
```

```
/* this file:adiinit2.c - initialization for adi solver at fine grid. */

#include "fluid.h"
#define LINESIZE 128

adiinit() {

nx = ny = maxx - 1;
hx = hy = 3.0 / nx;
dt = 0.4 * hx;

xcon1 = dt / (hx * hx);
xcon2 = dt / (4.0 * hx);
ycon1 = dt / (hy * hy);
ycon2 = dt / (4.0 * hy);
/* printf("%1.4f %1.4f %1.4 %1.4f\n", xcon1, xcon2, ycon1, ycon2); */

c2 = 1.0 + xcon1;
c5 = 1.0 - ycon1;
d2 = 1.0 + ycon1;
d5 = 1.0 - xcon1;

for (i = 0; i <= nx ; i++){
   x[i] = y[i] = i * hx;
   f[i] = 0.0;
}

for (i = 0; i <= nx; i++){
   for(j = 0; j <= ny; j++){
      scanf("%*lf%*lf%lf", &(temp[i][j]));  /* Read in converged data */
      tstar[i][j] = temp[i][j];
   }
}

   for (j = 0; j <= ny ; j++){
         temp[0][j] = tstar[0][j] = -1.0;
         temp[nx][j] = tstar[nx][j] = 0.0;
   }

}
```

```
/* this file: tx.c   This file calculates the thermal gradients,
Tx and Txx, and the heat flux. */

#include "fluid.h"

tx()
{

for (i = 0; i <= nx; i++){
   if (i == 0)
      Tx[i] = (temp[i+1][0]-temp[i][0]) / (x[i+1]-x[i]);
   else if (i == nx)
      Tx[i] = (temp[i][0]-temp[i-1][0]) / (x[i]-x[i-1]);
   else
      Tx[i] = (temp[i+1][0]-temp[i-1][0]) / (2.0* (x[i+1]-x[i]));
/* printf("%1.2f %1.4f %1.4f\n", x[i], temp[i][0], Tx[i]); */
}

for (i = 0; i <= nx; i++){
   if (i == 0)
      Txx[i] = (Tx[i+1] - Tx[i]) / (x[i+1]-x[i]);
   else if (i == nx)
      Txx[i] = 0;
   else
      Txx[i] = (temp[i+1][0]-2*temp[i][0]+temp[i-1][0]) /
pow((x[i+1]-x[i]),2.0);
/* printf("%1.2f %1.4f %1.4f\n", x[i], temp[i][0], Txx[i]); */
}

for (i = 0; i <= nx; i++){
   f[i] = (-1.0/2.0)* pow((fabs(-temp[i][0]*Tx[i])/eps),(2.0/3.0));
}

}
```

```
/* this file: strength2.c   This is a file to determine the
characteristic velocity from the surface boundary layer into the corner. */

#include "fluid.h"

strength()
{

F = fabs((16.0/5.0)*(sqrt(3.14159265))*(pow(Tx[0]/(eps*2.0),1.0/3.0)));
/* printf("F = %1.6f\n", F); */

}
```

```
/* this file: jet.c   This file determines the velocity from the
potential flow due to a wall jet in the quarter-plane. */

#include "fluid.h"

jet()
{

double theta, con;

con = (5.0/2.0) * F;

/* printf("x[i]  y[j]  jpsi[i][j]\n"); */
for (i = 0; i <= nx; i++){
   for(j = 0; j <= ny; j++){
      theta = atan2(x[i],y[j]);
      if (j == 0)
         jpsi[i][j] = 0.0;
      else if (i == 0)
         jpsi[i][j] = -2.0 * pow(con, 0.25) * pow(y[j],0.25);
      else
         jpsi[i][j] = -2.0 * pow(con, 0.25) * pow((x[i]*x[i]+y[j]*y[j]),
0.125) * (cos(theta/4.0) - (1.0+sqrt(2.0))*sin(theta/4.0));
/*    printf("%1.2f  %1.2f  %1.4f\n", x[i], y[j], jpsi[i][j]); */
   }
}

}
```

```
/* this file: green.c   This file solves Laplace's equation in core. */

#include "fluid.h"

green()
{

double piece;

for (i = 0; i <= nx; i++){
   if (i < nx)
      hofx[i] = ( pow( ((-temp[i][0])*(-temp[i][0])/(eps*eps*Tx[i])),
1.0/3.0) ) / (-2.0);
   else
      hofx[i] = 0.0;
/*    printf("%1.2f %1.12f\n", x[i], hofx[i]);  */
}

for (i = 1; i <= nx; i++){
   for(j = 1; j <= ny; j++){
      piece = 0.0;
      integrand[0] = 0.0;
      for (k = 1; k <= nx; k++){
         grnfun[k] = ( y[j]/((x[k]+x[i])*(x[k]+x[i]) + y[j]*y[j]) -
y[j]/((x[k]-x[i])*(x[k]-x[i]) + y[j]*y[j]) )/(3.14159265);
         integrand[k] = (- grnfun[k] * hofx[k]);
         piece +=  ((x[k]-x[k-1]) / 2.0) * (integrand[k]+integrand[k-1]);

/*       printf("%1.4f\n", integrand[k]); */
      }

      gpsi[i][j] = piece + (hofx[0] * (2.0/3.14159265) * atan2(y[j],x[i]));
   }
}

for (i = 0; i <= nx; i++){
   gpsi[0][i] = hofx[0];
   gpsi[i][0] = hofx[i];
}

}
```

```
/*  this file: adi.c - solve the heat equation for the potential flow
due to a wall jet in the cold corner (quarter plane).

                                                 2         2
         d T       d T       d T       d  T     d  T
      M( ---  +  u ---  +  v --- ) = ----  +  ----
         d t       d x       d y            2         2
                                         d x       d y

with BC:
at y = 0:    Ty = 0,   uy = Tx,   v = 0
at x = 0:    T = -1,   u = v = 0

using the symmetric ADI method, which uses two subprograms for computing
the L U decomposition of a tridiagonal matrix and then for solving
L U x = b.  A system of equations then result of the form (a two-step
process):

                             *           n
        (Step 1)        A * T      = B * T
                             x,y         x,y

                             n+1         *
        (Step 2)        C * T      = D * T
                             x,y         x,y

where A, B, C, and D are all tridiagonal matrices.
*/

#include "fluid.h"

double adi()
{

int i, j, m, n;
double max, diff;

/*  Next, bring in the values of u (psi_y) and v (- psi_x) from the
potential flow due to a wall jet.   Input the velocities from file
main.c.  */

/*  STEP 1:  Solve the tridiagonal system
```

```
    *           *           *           n           n           n
c1 T      + c2 T      + c3 T      = c4 T      + c5 T    + c6 T
    x+1,y       x,y         x-1,y       x,y+1       x,y       x,y-1

where the coefficients c1 through c6 are determined by */

for (i = 0; i <= nx ; i++){
   for (j = 0; j <= ny ; j++){
      c1[i][j] = (xcon2 * u[i][j]) - (xcon1 / 2.0);
      c3[i][j] = (-xcon2 * u[i][j]) - (xcon1 / 2.0);
      c4[i][j] = (-ycon2 * v[i][j]) + (ycon1 / 2.0);
      c6[i][j] = (ycon2 * v[i][j]) + (ycon1 / 2.0);
/* printf("%d %d %1.4f %1.2f %1.4f %1.4f %1.2f %1.4f\n", i, j,
c1[i][j], c2, c3[i][j], c4[i][j], c5, c6[i][j]); */
   }
}
/*  c2 and c5 are defined in initialization file. */
/*  Start with the corner.  */

j = 0;
i = 1;
tempa[i-1] = ycon1 * temp[i][j+1] + c5 * temp[i][j] - (ycon1 *
hy * f[i]) - c3[i][j] * temp[i-1][j];
A[1][i-1] = c2;
A[2][i-1] = c1[i][j];
/* printf("%d %d %1.4f\n", i, j, tempa[i-1]); */

/*  Next, go along the surface to the other corner.  */

for (i = 2; i < nx - 1; i++){
   tempa[i-1] = ycon1 * temp[i][j+1] + c5 * temp[i][j] - (ycon1 *
hy * f[i]);
   A[0][i-1] = c3[i][j];
   A[1][i-1] = c2;
   A[2][i-1] = c1[i][j];
/* printf("%d %d %1.4f\n", i, j, tempa[i-1]); */
}

i = nx - 1;
tempa[i-1] = ycon1 * temp[i][j+1] + c5 * temp[i][j] - (ycon1 *
hy * f[i]) - c1[i][j] * temp[i+1][j];
```

```
A[0][i-1] = c3[i][j];
A[1][i-1] = c2;
/* printf("%d %d %1.4f\n", i, j, tempa[i-1]);  */

/* for (m = 0; m < 3; m++){
   for (n = 0; n < ny - 1; n++){
      printf("%d %d %1.4f\n", m, n, A[m][n]);
   }
} */

size = maxxvec;

/*  Use tridiag.c to solve A T* = Tn, where A = is tridiagonal,
Tn is the known temperature (tempa), and T* is the step temperature. */

tridiag(A, tempa, size);

for (i = 1; i <= size ; i++){
   tstar[i][j] = xx[i-1];
/* printf("%d %d %1.4f\n", i, j, tstar[i][j]); */
}
/*  This is the solution to the surface row.  The tstar matrix is
updated with the new surface temperature.  Now, work on the inside
of the regime.  Continue to update the tstar matrix as each row is
solved. */

for (j = 1; j < ny; j++){
   i = 1;
   tempb[i-1] = c4[i][j] * temp[i][j+1] + c5 * temp[i][j] + c6[i][j]
* temp[i][j-1] - c3[i][j] * temp[i-1][j];
   A[1][i-1] = c2;
   A[2][i-1] = c1[i][j];
/* printf("%d %d %1.4f\n", i, j, tempb[i-1]); */

   for (i = 2; i < nx - 1; i++){
      tempb[i-1] = c4[i][j] * temp[i][j+1] + c5 * temp[i][j] + c6[i][j]
* temp[i][j-1];
      A[0][i-1] = c3[i][j];
      A[1][i-1] = c2;
      A[2][i-1] = c1[i][j];
   }
```

```
   i = nx - 1;
   tempb[i-1] = c4[i][j] * temp[i][j+1] + c5 * temp[i][j] + c6[i][j]
* temp[i][j-1] - c1[i][j] * temp[i+1][j];
   A[0][i-1] = c3[i][j];
   A[1][i-1] = c2;
   /* printf("%d %d %1.4f\n", i, j, tempb[i-1]); */

/*  Use crout(A) and croutslv(L, U, tempb) to solve for row j.  Then
update the temp matrix.  */

   tridiag(A, tempb, size);

   for (i = 1; i <= size ; i++){
      tstar[i][j] = xx[i-1];
/*    printf("%d %d %1.4f\n", i, j, tstar[i][j]); */
   }
}
/*  Finally, solve along the bottom row.  */

j = ny;
i = 1;
tempc[i-1] = c5 * temp[i][j] + ycon1 * temp[i][j-1] - c3[i][j]
* temp[i-1][j];
A[1][i-1] = c2;
A[2][i-1] = c1[i][j];
/* printf("%d %d %1.4f\n", i, j, tempc[i-1]); */

for (i = 2; i < nx - 1; i++){
   tempc[i-1] = c5 * temp[i][j] + ycon1 * temp[i][j-1];
   A[0][i-1] = c3[i][j];
   A[1][i-1] = c2;
   A[2][i-1] = c1[i][j];
/* printf("%d %d %1.4f\n", i, j, tempc[i-1]); */
}

i = nx - 1;
tempc[i-1] = c5 * temp[i][j] + ycon1 * temp[i][j-1] - c1[i][j]
* temp[i+1][j];
A[0][i-1] = c3[i][j];
A[1][i-1] = c2;
/* printf("%d %d %1.4f\n", i, j, tempc[i-1]); */
```

```
for (m = 0; m < 3; m++){
   for (n = 0; n < ny - 1; n++){
/*    printf("%d %d %1.4f\n", m, n, A[m][n]); */
   }
}

for (i = 0; i < nx - 1; i++){
/* printf("%1.4f\n", tempc[i]); */
}

tridiag(A, tempc, size);

for (i = 1; i <= size ; i++){
   tstar[i][j] = xx[i-1];
/* printf("%d %d %1.4f\n", i, j, tstar[i][j]); */
}

/*  Print the results of the first step of tstar. */
/* printf("x[i]  y[j]  tstar[i][j]\n"); */
for (i = 0; i <= nx; i++){
   for (j = 0; j <= ny; j++){
/*    printf("%1.2f  %1.2f  %1.4f\n", x[i], y[j], tstar[i][j]); */
   }
}

/* STEP 2: Repeat in the other direction.  Now solve

    n+1          n+1          n+1          *            *          *
d1 T      + d2 T      + d3 T      = d4 T      + d5 T     + d6 T
    x,y+1        x,y          x,y-1        x+1,y        x,y        x-1,y

where the coefficients d1 through d6 are determined by */

for (i = 0; i <= nx ; i++){
   for (j = 0; j<= ny ; j++){
      d1[i][j] = (ycon2 * v[i][j]) - (ycon1 / 2.0);
      d3[i][j] = (-ycon2 * v[i][j]) - (ycon1 / 2.0);
      d4[i][j] = (-xcon2 * u[i][j]) + (xcon1 / 2.0);
      d6[i][j] = (xcon2 * u[i][j]) + (xcon1 / 2.0);
/*    printf("%d %d %1.4f %1.4f %1.4f %1.4f %1.4f %1.4f\n", i, j,
d1[i][j], d2, d3[i][j], d4[i][j], d5, d6[i][j]); */
   }
```

```
}
/*  d2 and d5 are defined in initialization file. */
/*  Only one loop is needed, as the equations are the same for all
i columns.  */

/* printf("x[i]  y[j]  temp[i][j]\n"); */
size = maxx;
max = 0.;
for (i = 1; i < nx; i++){
   j = 0;
   tstarn[j] = d4[i][j] * tstar[i+1][j] + d5 * tstar[i][j] + d6[i][j]
* tstar[i-1][j] - (ycon1 * hy * f[i]);
   C[1][0] = d2;
   C[2][0] = -ycon1;

   for (j = 1; j < ny; j++){
      tstarn[j] = d4[i][j] * tstar[i+1][j] + d5 * tstar[i][j] + d6[i][j]
* tstar[i-1][j];
      C[0][j] = d3[i][j];
      C[1][j] = d2;
      C[2][j] = d1[i][j];
   }

   j = ny;
   tstarn[j] = d4[i][j] * tstar[i+1][j] + d5 * tstar[i][j] + d6[i][j]
* tstar[i-1][j];
   C[0][ny] = -ycon1;
   C[1][ny] = d2;

   tridiag(C, tstarn, size);

   for (j = 0; j < size ; j++){
      diff = fabs( temp[i][j] - xx[j]);
      if (diff > max) {
         max = diff;
/* printf("new max [%d,%d] = %f\n",i,j,max); */
         }
      temp[i][j] = xx[j];
   }
}

/* Print the results for the second step and begin the next iteration
```

```
with the new temp. */

for (i = 0; i <= nx; i++){
   for (j = 0; j <= ny; j++){
/*    printf("%1.2f  %1.2f  %1.4f\n", x[i], y[j], temp[i][j]); */
   }
}

return(max);

}
```

```
/*  this file: tridiag.c   Solve tridiagonal system A x = b.  */

#include "fluid.h"

tridiag(t, b, size)

double t[3][maxx], b[maxx];
int size;

{

double r;

for (j = 1; j< size; j++){
   r = t[0][j] / t[1][j-1];
   t[1][j] -=  r * t[2][j-1];
   b[j] -= r * b[j-1];
}

b[size-1] /= t[1][size-1];
/* printf("%d %1.4f\n", size-1, b[size-1]); */

for (j = size-2; j >= 0; j--){
   b[j] = (b[j] - (t[2][j] * b[j+1])) / t[1][j];
/* printf("%d %1.4f\n", j, b[j]); */
}

/* Solution is stored in xx[].  */
for (j = 0; j< size; j++){
   xx[j] = b[j];
}

}
```

```
/* this file: surface.c   This is a file to determine the stream
function from the surface boundary layer. */

#include "fluid.h"

surface()
{

for (i = 0; i < nx; i++){
   delta[i] = pow(eps,-1.0/3.0) * pow(-temp[i][0],1.0/3.0) *
pow(Tx[i],1.0/3.0);
   seta[i] = - pow(eps,-2.0/3.0) * pow(-temp[i][0],2.0/3.0) *
pow(Tx[i],-1.0/3.0);
   for (j = 0; j <= ny; j++){
      spsi[i][j] =  seta[i] * ( (1.0/2.0) * (1.0 -
exp(- pow(y[j]/(Pr*delta[i]),2.0))) + ((sqrt(3.14159265)/2.0)
* (y[j]/(Pr*delta[i])) *  erfc(y[j]/(Pr*delta[i]))) );
/*    printf("%1.3f %1.3f %1.6f\n", x[i], y[j], spsi[i][j]); */
   }
}

}
```

```
/* this file: wall.c   This is a file to determine the stream
function in the wall boundary layer. */

#include "fluid.h"

wall()
{

double con1, con2, psicon, Delta, feta;
double getg();

con1 = (5.0/2.0) * F;
con2 = 2.0 / pow(con1,1.0/4.0);

for (j = 1; j <= ny; j++){
   Delta = con2 * pow(y[j],3.0/4.0);
   psicon = - 2.0 * pow((con1*y[j]),1.0/4.0);

   for (i = 0; i <= nx; i++){
      eta = x[i] / (Delta * Pr);
/*    printf("eta = %1.3f\n", eta); */
      g = getg(eta);
      feta = g * g;
/*    printf("feta = %1.6f\n", feta); */
      wpsi[i][j] = psicon * feta;
/*    printf("%1.3f %1.3f %1.6f\n", x[i], y[j], wpsi[i][j]); */
   }
}

}
```

```
/* This file: getg.c - This is a file to determine eta using
Newton's Method, to be used in wall.c  */

#include "fluid.h"

double getg(eta)

double eta;

{

double g0, gprime, eta0, tol;

tol = 0.000001;

if (eta > 7.8) return(1.0);

if (eta < exp(1.0))
   g0 = eta / 3.0;
else
   {g0 = 1.0 - sqrt(3.0 / exp(2.0 * eta - 3.14159265 / sqrt(3.0)));}
/* printf("g0 =  %1.6f\n", g0); */

g = g0;
do{
   g0 = g;
   gprime = (1 - g * g * g)/ 3.0;
   eta0 = log((sqrt(1.0+g0+g0*g0))/(1.0-g0)) + (sqrt(3.0)) *
atan(((sqrt(3.0))/3.0)*(1.0+2.0*g0)) - (sqrt(3.0))*(3.14159265/6.0);
   g = g0 + (eta - eta0) * gprime;
/* printf("g =  %1.6f\n", g); */
   } while (fabs(g - g0) > tol);
   return(g);

}
```

```
/* this file: main.c - main program for uniform stream function. */

#define MAIN
#include "fluid.h"
#define LINESIZE 128
#define eps (sqrt(3.14159265)*(1.0-sqrt(2.0)/2.0)/2.0)

main()
{

psiinit();

tx();
strength();

jet();
green();
wall();
surface();

for (i = 0; i <= nx; i++){
   for (j = 0; j <= ny; j++){
      unifpsi[i][j] = jpsi[i][j] + gpsi[i][j] + wpsi[i][j]
+ spsi[i][j] - jpsi[0][j] - gpsi[i][0];
      printf("%1.3f %1.3f %1.6f %1.6f %1.6f %1.6f %1.6f\n",
x[i], y[j], jpsi[i][j], gpsi[i][j], spsi[i][j], wpsi[i][j],
unifpsi[i][j]);
   }
}

}
```

```
/* this file: psiinit.c - initialization for uniform stream function. */

#include "fluid.h"
#define LINESIZE 128

psiinit() {

FILE *file;
char line[LINESIZE];

nx = ny = maxx - 1;
hx = hy = 3.0 / nx;

for (i = 0; i <= nx ; i++){
   x[i] = y[i] = i * hx;
}

file = fopen("input.txt", "r");

for (i = 0; i <= nx; i++){
   for(j = 0; j <= ny; j++){
      fscanf(file,"%lf%lf%lf\n", &(x[i]), &(y[j]), &(temp[i][j]));
   }
}

/* printf("%1.3f %1.3f %1.6f\n", x[1], y[2], temp[1][2]); */

}
```

```
/* this file:unitemp.c - Calculates the uniform temperature solution
by matching Tinner + Touter - Tmatch. */

#define MAIN
#include "fluid.h"
#define LINESIZE 128
#define eps (sqrt(3.14159265)*(1.0-sqrt(2.0)/2.0)/2.0)

main()
{
double unitemp[maxx][maxx], teta;

nx = ny = maxx - 1;
hx = 5.0 / nx;

for (i = 0; i <= nx ; i++){
   x[i] = y[i] = i * hx;
}

for (i = 0; i <= nx ; i++){
   for(j = 0; j <= ny; j++){
      scanf("%*lf%*lf%lf", &(temp[i][j]));
   }
}

for (i = 0; i <= nx; i++){
   if (i == 0)
      Tx[i] = (4.0*temp[1][0]-3.0*temp[0][0]-temp[2][0])/(2.0*x[i+1]);
   else if (i == nx)
      Tx[i] = (temp[nx][0]-temp[nx-1][0]) / (x[i]-x[i-1]);
   else
      Tx[i] = (temp[i+1][0]-temp[i-1][0]) / (2.0* (x[i+1]-x[i]));
/* printf("%1.2f %1.4f %1.4f\n", x[i], temp[i][0], Tx[i]); */
}

for (i = 0; i <= nx ; i++){
   for(j = 0; j <= ny; j++){
      teta = y[j] / (Pr * pow((-temp[i][0])/(eps * Tx[i] * Tx[i]),
1.0/3.0) );
/*    printf("%1.2f %1.2f %1.15f\n", x[i], y[j], teta); */
      unitemp[i][j] = temp[i][j] + (Pr / (4.0*eps)) * temp[i][0] *
( ((sqrt(3.14159265)) * (erfc(teta))) * (0.5 + teta * teta) -
```

```
(teta * exp(- teta * teta)) );
      printf("%1.2f %1.2f %1.5f\n", x[i], y[j], unitemp[i][j]);
   }
}

}
```

LIST OF REFERENCES

[1] D. Canright. Thermocapillary flow near a cold wall. *Phys. Fluids*, 6 (4): 1415 - 1424, April 1994.

[2] J. Bohm, A. Lüdge, and W. Schröder. Crystal growth by floating zone melting. In *Handbook of crystal growth, Vol 2a, Basic Techniques*, D. T. J. Hurle (ed.), North-Holland, Amsterdam, 1994.

[3] H. C. Kuhlmann. *Thermocapillary convection in models of crystal growth*, Springer-Verlag, New York, 1999.

[4] E. S. Nelson. An examination of anticipated g-jitter on space station and its effects on materials processes, *NASA Technical Memorandum 103775*, May 1991.

[5] S. Ostrach. Low-gravity fluid flows. *Ann. Rev. Fluid Mech.*, 14: 313 - 345, 1982.

[6] Y. Kamotani, S. Ostrach and A. Pline. A thermocapillary convection experiment in microgravity. *ASME Journal of Heat transfer*, 118: 191 - 197, 1995.

[7] J. Mazumder, M. M. Chen, C. L. Chan, and R. Zehr. Effect of convection on weld pool shape and microstructure. *Technical Report to U.S. Navy N00014-84-K-0315*, July 1986.

[8] G. M. Oreper, T. W. Eagar, and J. Szekely. Convection in arc weld pools. *Welding Journal*, 63: 307s - 312s, 1983.

[9] S. H. Davis. Thermocapillary Instabilities. *Ann. Rev. Fluid Mech.*, 19: 403 - 435, 1987.

[10] S. Ohring and H. J. Lugt. *Marangoni convection in a gravity-free silicon float zone.* Technical Report CARDIVNSWC-94/003 to Carderock Division, Naval Surface Warfare Center, April 1994.

[11] A. K. Sen and S. H. Davis. Steady thermocapillary flows in two-dimensional slots. *J. Fluid Mech.*, 121: 163 - 186, 1982.

[12] C. L. Chan, M. M. Chen, and J. Mazumder. Asymptotic solution for thermocapillary flow at high and low Prandtl numbers due to concentrated surface heating. *Transactions of the ASME*, 110: 140-146, February 1988.

[13] L. E. Scriven and C. V. Sternling. The Marangoni effects. *Nature*, 187: 186 - 188, July 16, 1960.

[14] E. D. Hondros. Introduction: significance of capillary driven flows in materials processing. *Philosophical Transactions: Mathematical, Physical, and Engineering Sciences*, 356 (1739): 815 - 818, 15 April 1998.

[15] S. J. Cowley and S. H. Davis. Viscous thermocapillary convection at high Marangoni number. *J. Fluid Mech.*, 135: 175 - 188, 1983.

[16] G. O. Roberts. Fast viscous convection. *Geophys. Astrophys. Fluid Dynamics*, 8: 197 - 233, 1977.

[17] A. Zebib, G. M. Homsy, and E. Meiburg. High Marangoni number convection in a square cavity. *Phys. Fluids*, 28 (12): 3467 - 3476, December 1985.

[18] C. L. Chan, J. Mazumder, and M. M. Chen. Effect of surface tension gradient driven convection in a laser melt pool: Three-dimensional perturbation model. *J. Appl. Phys.*, 64 (11): 6166 - 6174, December 1988.

[19] J. Masud, Y. Kamotani and S. Ostrach. Oscillatory thermocapillary flow in cylindrical columns of high Prandtl number fluids. *Journal of Thermophysics and Heat Transfer*, 11 (1): 105 - 111, January - March 1997.

[20] Y. Kamotani and S. Ostrach. Theoretical analysis of thermocapillary flow in cylindrical columns of high Prandtl number fluids. *Transactions of the ASME*, 120: 758 - 764, August 1998.

[21] V. A. Batischev, V. V. Kuznetsov, and V. V. Pukhnachov. Marangoni boundary layers. *Prog. Aerospace Sci.*, 26: 353 - 370, 1989.

[22] V. V. Pukhnachov. Boundary layers near free surface. In *Computational and asymptotic methods for boundary and interior layers*, Bool Press, Dublin, pp. 97 - 110, 1982.

[23] L. G. Napolitano. Marangoni boundary layers. In *Proceedings of the IIIrd European symposium on materials science in space*, ESA SP-142: 349, 1979.

[24] S. Ostrach. Motion induced by capillarity. In *Physico-chemical hydrodynamics*, Spalding (ed.), V. G. Levich Festschrift, Advance Publications, London, Vol 2, 1977.

[25] M. Strani, R. Piva, and G. Graziani. Thermocapillary convection in a rectangular cavity: asymptotic theory and numerical simulation. *J. Fluid Mech.*, 130: 347 - 376, 1983.

[26] M. R. Huber. *An investigation of low Marangoni number fluid flow in a cold corner.* ADA271317, Master's Thesis, The Naval Postgraduate School, June 1993.

[27] L. Prandtl. *Motion of fluids with very little viscosity.* NACA Technical Memorandum No. 452, March 1928 (translation of *Über Flüßigkeitsbewegung bei sehr kleiner Reibung*, Verh. III. Int. Math. Kongr., Heidelberg, pp.484-491, 1904).

[28] K. Pohlhausen. Zur näherungsweisen Integration der Differentialgleichung der laminaren Grenzschicht. *Z. angew. Math. Mech.*, 1: 252 - 268, 1921.

[29] L. Rosenhead. *Laminar Boundary Layers*, Oxford University Press, New York, 1963.

[30] H. Schlichting. *Boundary-Layer Theory*, translated by J. Kestin, 7th edition, McGraw-Hill, Inc., New York, 1979.

[31] R. Timman. A one-parameter method for the calculation of laminar boundary layers. *Rep. Trans. nat. LuchtvLab., Amsterdam*, 15: F29 - F45, 1949.

[32] M. Van Dyke. Higher-Order Boundary-Layer Theory. *Ann. Rev. Fluid Mech.*, 1: 265 - 292, 1969.

[33] D. Zwillinger. *Handbook of Differential Equations*, Academic Press, Inc., New York, 1989.

[34] E. Kamke. *Differentialgleichungen*, Akademische Verlagsgesellschaft Becker & Erler Kom.-Ges., Leipzig, 1943.

[35] G. M. Murphy. *Ordinary Differential Equations and Their Solutions*, Van Nostrand Reinhold Company, New York, 1960.

[36] M. B. Glauert. The wall jet. *J. Fluid Mech.*, 1: 625 - 643, 1956.

[37] G. K. Batchelor. *Fluid Dynamics*, Cambridge University Press, Cambridge, 1967.

[38] D. A. Anderson, J. C. Tannehill, and R. H. Pletcher. *Computational Fluid Mechanics and Heat Transfer*, Hemisphere Publishing Corporation, New York, 1984.

[39] V. I. Polezheav. Numerical solution of the system of two-dimensional unsteady navier-stokes equations for a compressible gas in a closed region. *Fluid Dyn.*, 2: 70 - 74, 1967.

[40] A. Plotkin. A second-order correction to the Glauert wall jet solution. *AIAA J.*, 8: 189 - 190, January 1970.

[41] C. M. Bender and S. A. Orszag. *Advanced Mathematical Methods for Scientists and Engineers*, McGraw-Hill, Inc., New York, 1978.

THIS PAGE INTENTIONALLY LEFT BLANK

INITIAL DISTRIBUTION LIST

1. Defense Technical Information Center 2
   8725 John J. Kingman Road., Ste 0944
   Ft. Belvoir, VA 22060-6218

2. Dudley Knox Library 2
   Naval Postgraduate School
   411 Dyer Rd.
   Monterey, CA 93943-5101

3. David Canright 3
   Naval Postgraduate School
   Department of Mathematics
   Code MA/Ca
   Monterey, CA 93943-5101

4. Chris Frenzen 1
   Naval Postgraduate School
   Department of Mathematics
   Code MA/Fr
   Monterey, CA 93943-5101

5. Guillermo Owen 1
   Naval Postgraduate School
   Department of Mathematics
   Code MA/On
   Monterey, CA 93943-5101

6. Wei Kang 1
   Naval Postgraduate School
   Department of Mathematics
   Code MA/Kw
   Monterey, CA 93943-5101

7. Indranath Dutta 1
Naval Postgraduate School
Department of Mechanical Engineering
Code ME/Du
Monterey, CA 93943-5101

8. Michael Morgan, Chairman 1
Naval Postgraduate School
Department of Mathematics
Code MA/Mw
Monterey, CA 93943-5101

9. COL David C. Arney, Chairman 1
Department of Mathematical Sciences
United States Military Academy
West Point, NY 10996

10. MAJ Michael R. Huber 5
Department of Mathematical Sciences
United States Military Academy
West Point, NY 10996